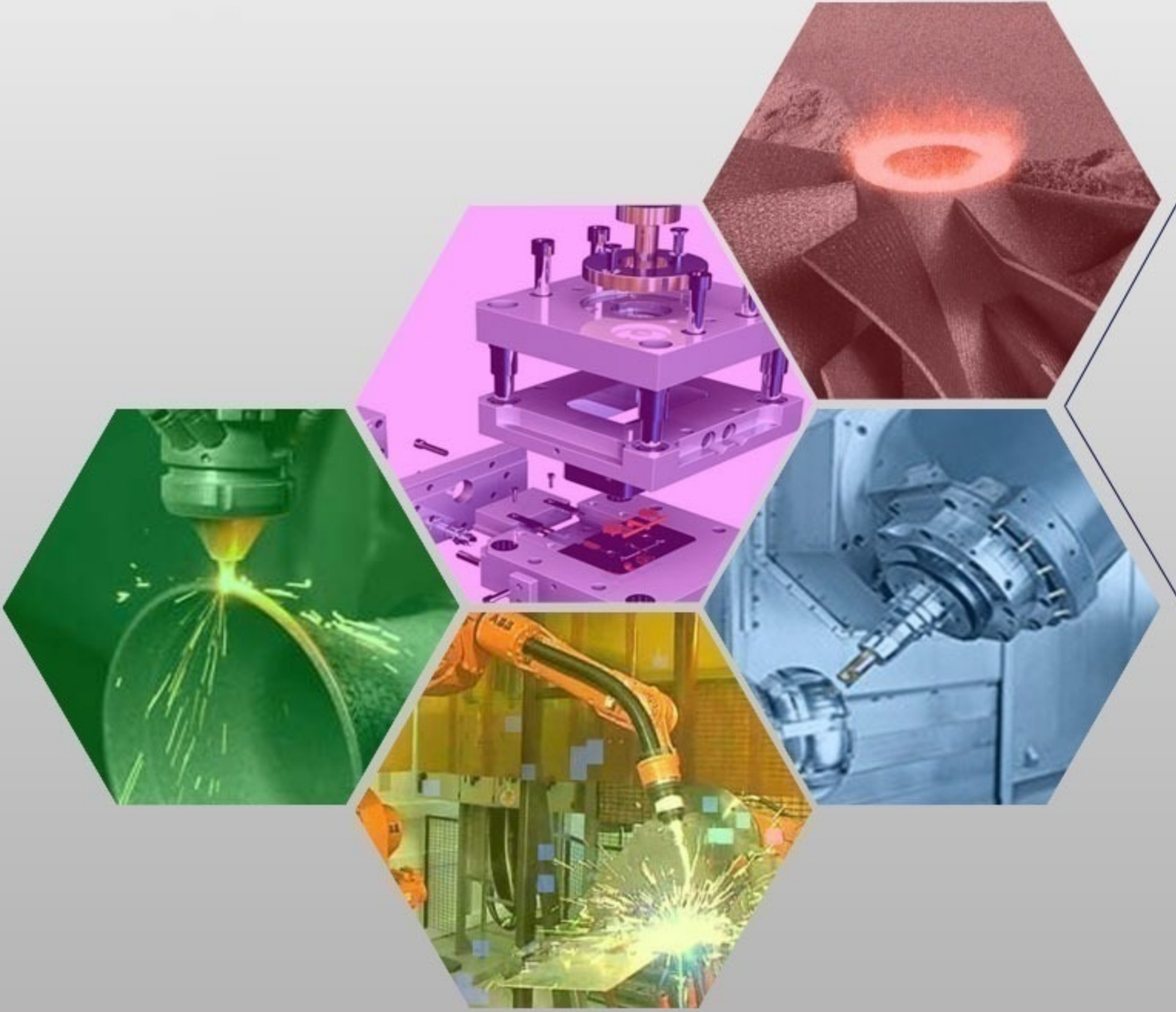




İMİLAT TEKNOLOJİLERİ VE UYGULAMALARI

CİLT:4 SAYI:1 YIL: 2023

e-ISSN: 2717-7475



MANUFACTURING TECHNOLOGIES AND APPLICATIONS

VOLUME:4 ISSUE:1 YEAR:2023



İmalat Teknolojileri ve Uygulamaları Manufacturing Technologies and Applications (MATECA)

<https://dergipark.org.tr/tr/pub/mateca>

Honoray Editör (Honorary Editor)

Prof. Dr. Ulvi Şeker, Gazi Üniversitesi

Baş Editor (Editor in Chief)

Prof. Dr. Mustafa Günay, Karabük Üniversitesi

Yardımcı Editör (Associate Editor)

Prof. Dr. Alaattin Kaçal, Kütahya Dumlupınar Üniversitesi

Alan Editörleri (Editors)

Prof. Dr. Turgay Kıvak, Düzce Üniversitesi
Prof. Dr. Murat Sarıkaya, Sinop Üniversitesi
Doç. Dr. Yakup Turgut, Gazi Üniversitesi
Dr. Munish Kumar Gupta, Opole University of Technology
Dr. Öğr. Üyesi Serkan Apay, Düzce Üniversitesi

Dil Editörü (Language Editor)

Doç. Dr. Mehmet Erdi Korkmaz, Karabük Üniversitesi

Teknik Editörler (Technical Editors)

Doç. Dr. Ramazan Çakıroğlu, Gazi Üniversitesi
Dr. Öğr. Üyesi Ramazan Özmen, Karabük Üniversitesi

Danışma Kurulu (Advisory Board)

Prof. Dr. Can Çoğun, Çankaya Üniversitesi
Prof. Dr. Serdar Salman, Marmara Üniversitesi
Prof. Dr. Grzegorz M. Królczyk, Opole University of Technology
Prof. Dr. Mustafa Cemal Çakır, Uludağ Üniversitesi
Prof. Dr. Teyfik Demir, TOBB Ekonomi ve Teknoloji Üniversitesi
Prof. Dr. İhsan Korkut, Gazi Üniversitesi
Prof. Dr. Oğuzhan Yılmaz, Gazi Üniversitesi
Prof. Dr. İlyas Uygur, Düzce Üniversitesi
Prof. Dr. Ramazan Kaçar, Karabük Üniversitesi
Prof. Dr. Ulaş Çaydaş, Fırat Üniversitesi
Prof. Dr. Ayhan Erol, Afyon Kocatepe Üniversitesi
Prof. Dr. İbrahim Çiftçi, Çankırı Üniversitesi
Doç. Dr. Mohd Fathullah Ghazali, University of Malaysia Perlis
Doç. Dr. Gültekin Uzun, Gazi Üniversitesi
Doç. Dr. Çağrı Vakkas Yıldırım, Erciyes Üniversitesi
Doç. Dr. Nafiz Yaşar, Karabük Üniversitesi
Dr. Mozammel Mia, Imperial College London
Dr. Catalin Pruncu, University of Strathclyde
Dr. Ferhat Yıldırım, Çanakkale Onsekiz Mart Üniversitesi
Dr. Selçuk Yağmur, Gazi Üniversitesi



Cilt (Volume) : 4
Sayı (Issue) : 1
Yıl (Year) : 2023
e-ISSN: 2717-7475

Yayıncı (Publisher)
Mustafa GÜNAY

Web Sayfası (Web Page)
<http://dergipark.gov.tr/pub/mateca>

Yayın Tarihi (Publication Date)
Nisan 2023 (April 2023)

Yayın Dili (Publication Language)
Türkçe / İngilizce (Turkish/English)

Yayın Aralığı (Publication Frequency)
Yılda üç kez yayınlanır (Tri-annual)

Yayın Türü (Publication Type)
Sürekli yayın (Periodical)

Kapak Tasarımı (Cover Design)
Ozan YETKİN

İletişim

Prof. Dr. Mustafa Günay (Editör)
Telefon: +90 370 4187400
E-posta: matecajournal@gmail.com, mgunay@karabuk.edu.tr

<https://dergipark.org.tr/tr/pub/mateca> adresinden dergiye ilişkin bilgilere ve makalelerin tam metnine ulaşılabilir.

Contact

Prof. Dr. Mustafa Günay (Editor)
Phone: +90 370 4187400

E-mail: matecajournal@gmail.com, mgunay@karabuk.edu.tr

Instructions for authors and all articles in this journal can be reached at
<https://dergipark.org.tr/en/pub/mateca>

İÇİNDEKİLER (CONTENTS)

Araştırma Makalesi (Research Article)	Sayfa (Page)
<p>Bilgisayarların Sıvı Soğutma Sistemlerinde Kanatçıklar Arası Mesafenin (KAM) Ortalama Mikro Kanatçık Sıcaklığına (OMKS) Etkisinin Sonlu Hacimler Analizi ile Optimizasyonu (<i>Optimization of the Effect of Distance Between Fins (DBF) on Average Heatsink Temperature (AHT) in Liquid Cooling Systems of Computers by Finite Volume Analysis</i>) Furkan ÖZSARI, Burak ÖZCAN, Ulvi ŞEKER</p>	1-10
<p>Mathematical Modelling and Multiresponse Optimization to Minimize Surface Roughness in Drilling Custom 450 Stainless Steel (<i>Custom 450 Paslanmaz Çeliğinin Delinmesinde Yüzey Pürüzlülüğünü Minimize Etmek İçin Matematiksel Modelleme ve Çok Yanıtlı Optimizasyon</i>) Hüseyin GÖKÇE, İbrahim ÇİFÇİ</p>	11-24
<p>Comparison of Strength, Surface Quality and Cost of Different Additive Manufacturing Methods (<i>Farklı Katkılı Üretim Yöntemlerinin Dayanım, Yüzey Kalitesi Ve Maliyetlerinin Karşılaştırılması</i>) Mehmet Mahir SOFU, Hatice VAROL ÖZKAVAK, Selim BACAK, Mehmet FENKLİ</p>	25-36
<p>Investigation of the Effect of Vulcanization Time on Belt Strength (<i>Vulkanize Kaynak Süresinin Bant Mukavemetine Etkisinin Araştırılması</i>) Tuğçe DANIŞMAN ÇEBİ, Recep DEMİRSÖZ, Mehmet Tayyip ÖZDEMİR, Ahmet Emrah ERDOĞDU</p>	37-48
<p>Investigation of The Effect of Reduced Shank Thickness of Friction Welded Yoke Shaft on Strength (<i>Sürtünme Kaynaklı Çatallı Milin Boğaz Cidar Kalınlığındaki Azaltmanın Dayanım Üzerindeki Etkisinin İncelenmesi</i>) Onur ŞEN, Mert Can KAHYALAR</p>	49-58

Bilgisayarların Sıvı Soğutma Sistemlerinde Kanatçıklar Arası Mesafenin (KAM) Ortalama Mikro Kanatçık Sıcaklığına (OMKS) Etkisinin Sonlu Hacimler Analizi ile Optimizasyonu

Furkan ÖZSARI¹ , Burak ÖZCAN¹ , Ulvi ŞEKER² 

¹ Simunes İleri Teknoloji A.Ş., 100. Yıl Blv. No:99, 06374 Ostim OSB, Ankara

² Gazi Üniversitesi, Teknoloji Fakültesi, İmalat Mühendisliği ABD, 06500-Teknikokullar, Ankara

MAKALE BİLGİSİ

Alınma: 17.11.2022

Kabul: 05.03.2023

Anahtar Kelimeler:

Bilgisayar

Sıvı soğutma

Mikro kanatçık

Sonlu hacimler analizi

Simülasyon

ÖZET

Teknolojinin ilerlemesiyle birlikte hemen her alanda kullanılan bilgisayarların yüksek performansta uzun süre çalışması oldukça önem arz etmektedir. Bilgisayar sistemlerinde performansı en çok etkileyen birimlerden biri olan merkezi işlem biriminin çalışma sıcaklığı performansına doğrudan etki etmektedir. Artan soğutma ihtiyaçlarına geleneksel hava soğutma sistemlerinin cevap verememesinden dolayı sıvı soğutma tabanlı sistemler endüstride yaygınlaşmaktadır. Gelişen simülasyon yazılımları, tasarlanan ürünün prototipini üretmeden sanal ortamda testlerini zamandan ve prototip maliyetlerinden tasarruf ederek gerçekleştirme olanağı sunmaktadır. Bu çalışma kapsamında merkezi işlem birimlerinin soğutulması için kullanılan sıvı soğutma sistemlerinin bir bileşeni olan mikro kanatçığın sanal ortamda sonlu hacimler yöntemi kullanılarak akış simülasyonları gerçekleştirilmiştir. Bu simülasyonlar gerçekleştirilirken mikro kanatçığın soğutma performansını doğrudan etkileyen kanatçıklar arası mesafe (KAM: 0.1mm, 0.2mm, 0.3mm) parametresi referans alınmıştır. Gerçekleştirilen sonlu hacimler analizi sonucunda ortalama mikro kanatçık sıcaklığı (OMKS) incelenmiştir. Akış simülasyonları sonucunda KAM'ın artmasıyla birlikte OMKs'nin de arttığı görülmüştür. Bu kapsamda, KAM 0.1mm, 0.2mm ve 0.3mm olduğunda OMKs'nin sırasıyla 28.93°C, 29.39°C, 30.24°C olduğu gözlemlenmiştir.

Optimization of the Effect of Distance Between Fins (DBF) on Average Heatsink Temperature (AHT) in Liquid Cooling Systems of Computers by Finite Volume Analysis

ARTICLE INFO

Received: 17.11.2022

Accepted: 05.03.2023

Keywords:

Computer

Liquid cooling

Heatsink

Finite volume analysis

Simulation

ABSTRACT

With the advancement of technology, it is very important for computers used in almost every field to work at high performance for a long time. The operating temperature of the central processing unit (CPU), which is one of the units that most affect performance in computer systems, directly affects its performance. Liquid cooling-based systems are becoming widespread in the industry due to the inability of traditional air-cooling systems do not respond to increasing cooling needs. Developing simulation software offers the opportunity to perform tests in a virtual environment without producing a prototype of the designed product, saving time and prototype costs. In the scope of this study, flow simulations were carried out using finite volume analysis method in virtual environment of heatsink which is a component of liquid cooling systems used for cooling processors. While performing these simulations, the distance between the fins (DBF: 0.1mm, 0.2mm, 0.3mm) parameter, which directly affects the cooling performance of the heatsink, was taken as reference. As a result of the finite volume analysis performed, the average heatsink temperature (AHT) was investigated. As a result of flow simulations, it was seen that AHT increased with the increase of DBF. It was observed that when the DBF was 0.1mm, 0.2mm and 0.3mm, the AHT were 28.93°C, 29.39°C, 30.24°C, respectively.

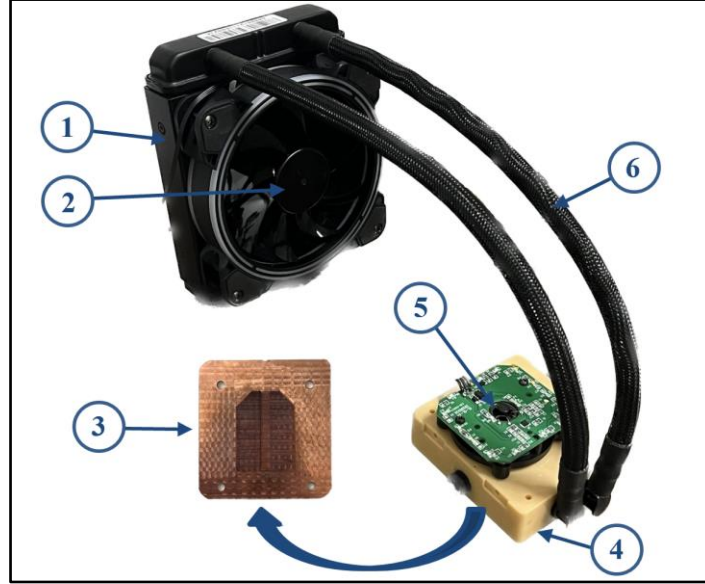
* Sorumlu yazar, e-posta: furkanozsari97@gmail.com

To cite this article: F. Özşarı, B. Özcan, U. Şeker, Optimization of the Effect of Distance Between Fins (DBF) on Average Heatsink Temperature (AHT) in Liquid Cooling Systems of Computers by Finite Volume Analysis, Manufacturing Technologies and Applications, 4(1),1-10, 2023.

<https://doi.org/10.52795/mateca.1206042>, This paper is licensed under a CC BY-NC 4.0

1. GİRİŞ (INTRODUCTION)

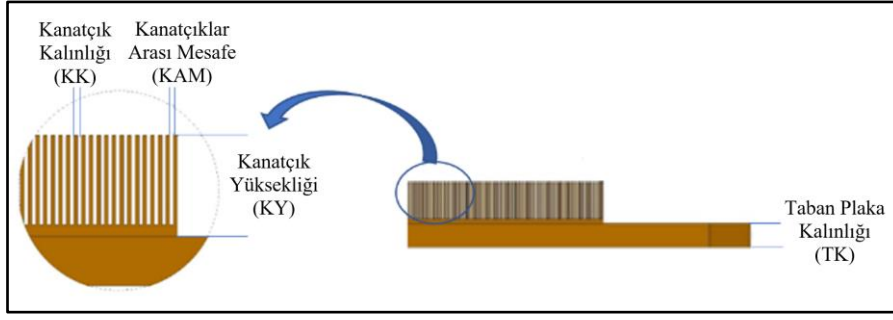
Elektronik teknolojinin hızla gelişmesiyle birlikte, elektronik cihazlar günlük hayatımızda önemli bir yer almıştır. Bu cihazlardan maksimum verimi alabilmek için bileşenlerinde oluşan sıcaklık değerlerini optimum düzeyde tutmak gerekir. Elektronik bileşenlerin çalışma sıcaklığı istenen sıcaklık seviyesini aşabilir. Bu nedenle, ısı transfer hızını arttırmak ve bileşen sıcaklığını istenen çalışma seviyesinde tutmak, elektronik bileşenlerin güvenilir bir şekilde çalışmasını sağlamada önemli bir rol oynar.



Şekil 1. Sıvı soğutma sistem bileşenleri (Liquid cooling system components)

Elektronik sistemleri soğutmada çeşitli yöntemler vardır. Bu yöntemler geleneksel hava soğutma sistemi ve sıvı soğutma sistemidir. Sıvı soğutma sistemleri Şekil 1’de görüldüğü üzere radyatör (1), fan (2), mikro kanatçık (3), akış odası (4), pompa (5) ve sıvı aktarma hortumları (6) olmak üzere toplamda 6 temel bileşenden (all-in-one) oluşmaktadır [1].

Mikro kanatçıklar soğutma sistemlerinde ısı kaynağı (CPU) ile temas halinde olan, oluşan ısıyı emen bakır veya alüminyum malzemeden üretilen yapılardır. Mikro kanatçıklar ısı kaynağında oluşan ısıyı, iletim ve zorlanmış taşınım ısı transferi mekanizmalarıyla ekipmanlardan uzaklaştırır. Böylece ekipmanların çalışma ömrünün ve performansının artmasını sağlar [2]. Endüstride yaygın olarak bakır ve alüminyum malzemelerden üretilen mikro kanatçıklar kullanılmaktadır. Uygulama alanlarına göre bu malzemelerden üretilen mikro kanatçıklar birbirine göre farklı avantaj sağlamaktadır. Bu avantajlar şunlardır; alüminyumun yoğunluğu (2700kg/m^3) bakıra (8900kg/m^3) göre düşük olduğu için hafiftir. Alüminyumun termal iletkenliği (90W/mK) diğer metallerle göre (demir: 55W/mK , çelik: 36W/mK , kalay: 50W/mK) daha yüksektir. Alüminyum mikro kanatçıklar, fotovoltaik endüstrisinde, elektrikli araçlarda, invertörlerde, led ışıklarda, iletişim ürünlerinde ve benzeri alanlarda yaygın olarak kullanılmaktadır [3]. Bakır (385W/mK), alüminyumdan (90W/mK) daha iyi ısı iletkenliğine sahiptir. Dezavantajı ise ağırlık ve maliyettir. Bakır ısı iletkenliğinin ve korozyon direncinin öneminin, ağırlık tasarrufundan daha ağır bastığı yerlerde, genellikle işlemcilerde, yüksek özellikli çiplerde ve sunucularda (server) kullanılır [4].



Şekil 2. Mikro kanatçık tasarım parametreleri (Heatsink design parameters)

Mikro kanatçık tasarımında termal iletkenlik önemli bir faktördür. Şekil 2’de gösterilen kanatçıklar arası mesafe (KAM), kanatçık kalınlığı (KK), kanatçık yüksekliği (KY) ve taban plaka kalınlığı (TK) gibi parametreler mikro kanatçık tasarımı yapılırken dikkat edilmesi gereken hususlardır [5]. Aşağıda mikro kanatçık parametreleri üzerine yapılmış çalışmaların genel bir özeti verilmiştir.

R.Mohan ve arkadaşları [6], kanatçık yüksekliği (15mm, 30mm, 50mm) kanatçıklar arası mesafe (1.5mm, 2.5mm, 4.5mm) ve kanatçık sayısı parametrelerini dikkate alarak; hesaplamalı akışkanlar dinamiği simülasyonları yardımıyla bu parametrelerin mikro kanatçık üzerindeki ısı dağılımını farklı kombinasyonlarla incelemiştir. Aynı zamanda fan, mikro kanatçık, ısıtıcı ve termokupl ekipmanlarını kullanarak bir deney düzeneği hazırlamışlardır. R. Mohan ve arkadaşının bir diğer çalışmasında [7], taban plaka kalınlığı (2.5mm, 5mm), kanatçık geometrisi (silindirik ve ince levha) ve mikro kanatçık malzemesi (bakır, alüminyum) parametrelerini dikkate alarak; hesaplamalı akışkanlar dinamiği simülasyonları sonucunda elde ettikleri çıktılar ile kurmuş oldukları deney düzeneğinde yaptıkları çalışmaların çıktılarını karşılaştırmışlardır. Freegah ve arkadaşları [8], kanatçıklar arasına radyus vererek ve kanatçık yüzeylerine radyuslu ek parça ekleyerek ısı transfer yüzeyini artırmayı amaçlamışlardır. Öztürk ve arkadaşları [9], 3 farklı kanatçık tasarımı yaparak ve farklı ısı kaynakları tanımlayarak (50W, 100W) mikro kanatçıklar üzerindeki sıcaklık dağılımını incelemiştir.

Daha önce gerçekleştirilen çalışmalarda boyutsal olarak büyük kanatçık yapıları üzerinde simülasyon çalışmaları gerçekleştirilmiştir. Bu çalışma kapsamında, bilgisayarlarda kullanılan sıvı soğutma sistemlerinin bir bileşeni olan mikro kanatçık yapısı özelinde mikro analiz çalışmaları yapılarak KAM – OMKS ilişkisi incelenmiştir.

2. TEORİK TEMELLER (THEORETICAL FOUNDATION)

2.1. Hesaplamalı Akışkanlar Dinamiği (Computational Fluid Dynamics)

Hesaplamalı akışkanlar dinamiği (HAD), akışkan fizikini bilgisayar tabanlı ticari bir yazılım kullanarak simüle eden ve ilgili olayları tahmin eden mühendislik yöntemidir. Bu tahminleri yapabilmek için çeşitli korunum denklemlerinden (süreklilik denklemi, momentum denklemleri, enerji denklemi) yararlanır [10].

İlk olarak 1930’larda A.Thom [11], bir silindir etrafındaki akış üzerine çalışmalar yapmıştır. 1950’li yıllarda M. Kawaguti [12], Reynold sayısını dikkate alarak bir silindir etrafındaki akış üzerine çalışmış, önemli sayısal yöntemler elde etmiştir. 1990’larda teknolojinin ilerlemesiyle beraber birçok ticari yazılım geliştirilmiştir. Ölçülmesi veya gözlemlenmesi zor, ölçülme imkânı olup pahalı deney düzenekleri gerektiren uygulamalar HAD sayesinde incelenir. HAD, sonlu hacimler yöntemi, sonlu farklar yöntemi veya sonlu elemanlar yöntemlerinden birini kullanarak analitik çözümü sayısal çözüme çevirir. Bu çalışma kapsamında sonlu hacimler yöntemi kullanılmıştır.

2.1.1. Süreklilik denklemi (Continuity equation)

Giren akışkanın kütleli debisi ile çıkan akışkanın kütleli debisi aynıdır [13].

$$\rho A_1 V_1 = \rho A_2 V_2 \quad (1)$$

Eş. (1)'de yoğunluk (ρ), kesit alanı (A_1, A_2), akışkan hızı (V_1, V_2) ile ifade edilmiştir.

2.1.2. Momentum denklemleri (Momentum equations)

Newton'un ikinci yasasına göre uzaydaki hızlanmış bir cismin üzerine herhangi bir etki olmadığı takdirde hızını korumaya devam edecektir [13].

$$\frac{\partial(\rho u)}{\partial t} + \frac{\partial(\rho u^2)}{\partial x} + \frac{\partial(\rho uv)}{\partial y} + \frac{\partial(\rho uw)}{\partial z} = -\frac{\partial p}{\partial x} + \frac{1}{Re_r} + \left[\frac{\partial \tau_{xx}}{\partial x} + \frac{\partial \tau_{xy}}{\partial y} + \frac{\partial \tau_{xz}}{\partial z} \right] \quad (2)$$

$$\frac{\partial(\rho v)}{\partial t} + \frac{\partial(\rho uv)}{\partial x} + \frac{\partial(\rho v^2)}{\partial y} + \frac{\partial(\rho vw)}{\partial z} = -\frac{\partial p}{\partial y} + \frac{1}{Re_r} + \left[\frac{\partial \tau_{xy}}{\partial x} + \frac{\partial \tau_{yy}}{\partial y} + \frac{\partial \tau_{yz}}{\partial z} \right] \quad (3)$$

$$\frac{\partial(\rho w)}{\partial t} + \frac{\partial(\rho uw)}{\partial x} + \frac{\partial(\rho vw)}{\partial y} + \frac{\partial(\rho w^2)}{\partial z} = -\frac{\partial p}{\partial z} + \frac{1}{Re_r} + \left[\frac{\partial \tau_{xz}}{\partial x} + \frac{\partial \tau_{yz}}{\partial y} + \frac{\partial \tau_{zz}}{\partial z} \right] \quad (4)$$

Eş. (2), Eş. (3) ve Eş. (4)'te yoğunluk (ρ), x eksenindeki hız (u), y eksenindeki hız (v), z eksenindeki hız (w), kinematik viskozite (μ), zaman (t) ve Reynolds sayısı (Re) ile ifade edilmiştir.

2.1.3. Enerji denklemi (Energy equation)

Termodinamiğin birinci kanununa göre bir sistemin iç enerjisindeki değişim miktarı, o sisteme ilave edilen ısı miktarı ile sistemin çevresine uyguladığı iş arasındaki farka eşittir. Bir radyatör içerisindeki akışın ürettiği enerji ya da dışarıya aktarılmakta olan enerji havaya toplamda aynı miktarda aktarılmaktadır. Kısacası, iki taraftaki entalpiler birbirine eşittir [13].

$$W = \Delta U + \Delta K = \Delta E \quad (5)$$

Eş. (5)'te iç enerji (ΔU), kinetik enerji (ΔK), toplam enerji (ΔE) ve yapılan iş (W) ile ifade edilmiştir.

3. MALZEME VE YÖNTEM (MATERIAL AND METHOD)

Bu çalışma kapsamında KAM'ın OMKS'ye etkisini incelemek için ticari bir yazılım kullanılarak sonlu hacimler analizi gerçekleştirilmiştir. Mikro kanatçık tasarımında dikkat edilmesi gereken diğer parametreler sabit tutulmuştur.

3.1. Mikro Kanatçık Parametreleri (Heatsink Parameters)

Çalışma kapsamında incelenen mikro kanatçık parametreleri Tablo 1'de verilmiştir.

Tablo 1. Mikro kanatçık parametreleri (Heatsink parameters)

KAM (mm)	0.1, 0.2, 0.3
Mikro kanatçık malzemesi	Bakır

3.2. Parametrik Tasarım (Parametric Design)

Tablo 1'de belirtilen parametreler dikkate alınarak parametrik tasarım yapılmıştır. Yapılan tasarım konfigürasyonları Tablo 2'de verilmiştir.

Tablo 2. Tasarım konfigürasyonları (Design configurations)

Konfigürasyon	TK (mm)	KK (mm)	KAM (mm)	KY (mm)
1	1.5	0.15	0.1	2.5
2	1.5	0.15	0.2	2.5
3	1.5	0.15	0.3	2.5

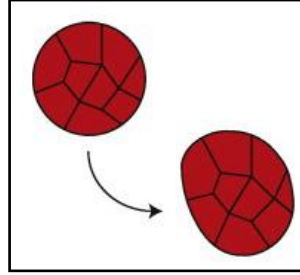
3.3. Sonlu Hacim Yöntemi (Finite Volume Method)

Hesaplamalı akışkanlar dinamiği yazılımları sonlu elemanlar yöntemiyle veya sonlu hacimler yöntemi ile çalışırlar. Bu yöntem kısmi diferansiyel denklemlerin cebirsel denklemler ile çözülmesidir. Kısmi diferansiyel denklemlerde sapma terimi içeren hacim integralleri, sapma teoremi ile yüzey integrallerine dönüştürülmektedir [14].

3.3.1. Lagrange yaklaşımı (Lagrange approach)

Her bir akışkan parçacığının hareketini ayrı ayrı izleme yöntemidir. Her bir partikülün uzaydaki hızının, ivmesinin ya da yer değiştirmesinin incelenmesini sağlar. Partiküller çok yol almıyorsa bu yöntem ile çalışmak avantaj sağlayabilir [15, 16, 17].

Lagrange yaklaşımında Şekil 3'te görüldüğü üzere düğümlerin geçici olarak malzemeye sabitlendiği ve elemanların malzeme ile birlikte şekil değiştirdiği varsayılmaktadır [18].



Şekil 3. Lagrange yaklaşımı (Lagrange approach)

3.3.2. Euler yaklaşımı (Euler approach)

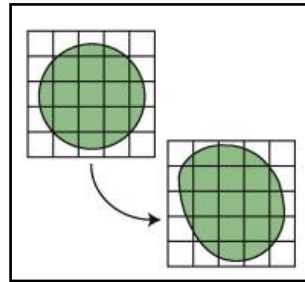
Euler yaklaşımı ile akışkanın hareket ettiği bir akış bölgesi veya kontrol hacmi belirlenir (Şekil 4). Böylece sabit kütleli akışkan parçacıklarının konum ve hızlarının takibine gerek duyulmaz. Bunun yerine kontrol hacmi içerisinde yer alan basınç alanı, hız alanı ve ivme alanı gibi alan değişkenleri tanımlanır [15, 16, 17].

Euler yaklaşımı ile gerçekleştirilen analizler büyük deformasyonlar içeren akış problemlerinde tercih edilir.

$$P = P(x, y, z, t) \quad (6)$$

$$\vec{V} = \vec{V}(x, y, z, t) \quad (7)$$

$$\vec{a} = \vec{a}(x, y, z, t) \quad (8)$$



Şekil 4. Euler yaklaşımı (Euler approach)

Eş. (6), Eş. (7) ve Eş. (8)'de basınç alanı (P), hız alanı (V), ivme alanı (a) ile gösterilmiş olup (x,y,z) kartezyen koordinatı, (t) zamanı ifade etmektedir.

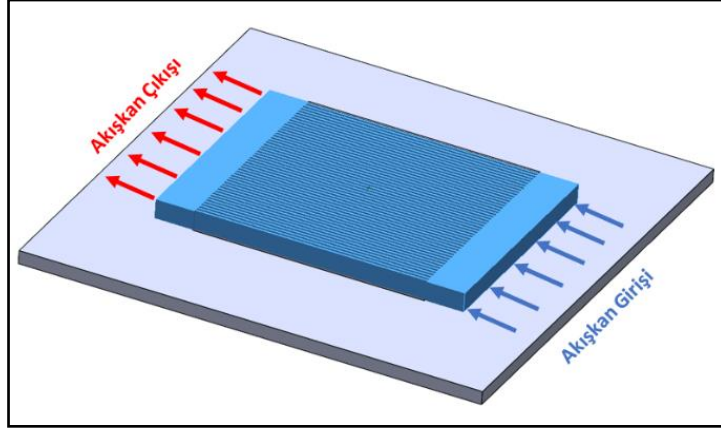
Bu yaklaşımda, lagrange yaklaşımındaki gibi her bir partikül tek tek incelenmediği için analiz süresi açısından bir kazanç sağlamaktadır [18].

3.4. Sınır Şartları ve Yükler (Boundary Conditions and Loads)

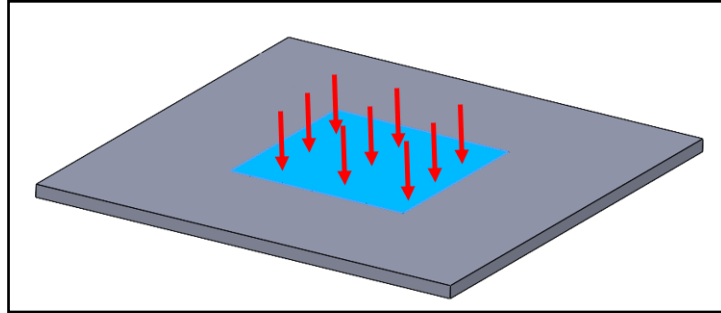
Çalışma kapsamında KAM-OMKS ilişkisi incelendiği için basitleştirilmiş bir akış hacmi oluşturulmuş olup iç akış analizi gerçekleştirilmiştir (Şekil 5). Akışkan sıvı olarak su seçilmiştir

(Tablo 6). Akış tipi türbülanslı olarak tanımlanmıştır. Akış alanı kanatçık duvarlarına yakın olduğu için türbülans modeli $k-\omega$ olarak seçilmiştir. Giriş debisi 0.005kg/sn ve ilk sıcaklık 26°C olarak tanımlanmıştır. Mikro kanatçık işlemci ile temas alanına 105W 'lık bir ısı tanımlaması yapılmıştır (Şekil 6). Mikro kanatçık malzemesi bakır olarak belirlenmiştir (Tablo 3, Tablo 4, Tablo 5).

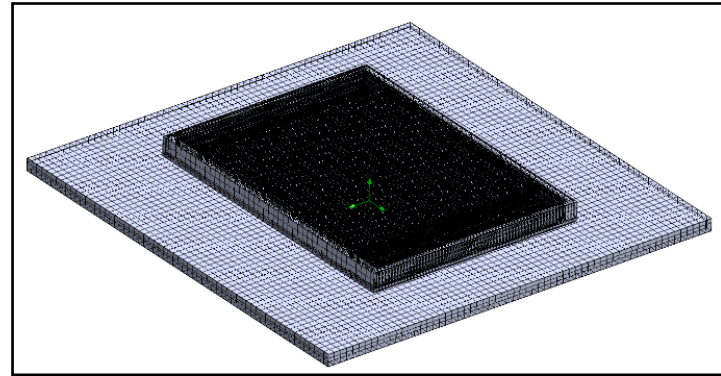
Yapıda bulunan kanatçıklardan dolayı bir mikro akış analiz çalışması yapılmıştır. Bu yüzden gelişmiş kanal iyileştirme aktif hale getirilip minimum mesh boyutu 0.02 olarak belirlenmiştir. Analizler sonucunda en doğru sonucu alabilmek için çözüm ağı bağımsızlığı (mesh independent) dikkate alınmıştır. Toplam element sayısı parametrik tasarımlardan (3 adet) dolayı $450.000-550.000$ arasında değişmektedir (Şekil 7). Tüm tanımlamalar yapıldıktan sonra mikro kanatçık yapıya sıcaklık sensörü atanmış olup sonuçlar incelenmiştir.



Şekil 5. Sıvı alan tanımlaması (Fluid area identification)



Şekil 6. Isı tanımlaması (Heat identification)



Şekil 7. Katı-akışkan mesh görünümü (Solid-fluid mesh appearance)

Tablo 3. Bakırın sıcaklığa bağlı özgül ısı değerleri (Specific heat values of copper depending on temperature)

Sıcaklık (K)	Özgül Isı (J/(kg·K))	Sıcaklık (K)	Özgül Isı (J/(kg·K))
1	0.0116	40	58.76
2	0.0278	80	202.6
3	0.053	150	322.6
4	0.0916	250	373.3
5	0.1482	298.1	384
8	0.4729	400	397.5
10	0.8709	600	416.7
15	2.907	1000	451.1
20	7.29	1356.2	475

Tablo 4. Bakırın sıcaklığa bağlı ısı iletkenlik değerleri (Thermal conductivity values of copper depending on temperature)

Sıcaklık (K)	Isıl İletkenlik (W/(m·K))
4	16200
10	24000
20	10800
40	2170
80	560
150	429
200	413
300	401
400	393
600	379
800	366
1000	352
1356.2	327

Tablo 5. Bakırın yoğunluk ve erime sıcaklık değerleri (Density and melting temperature values of copper)

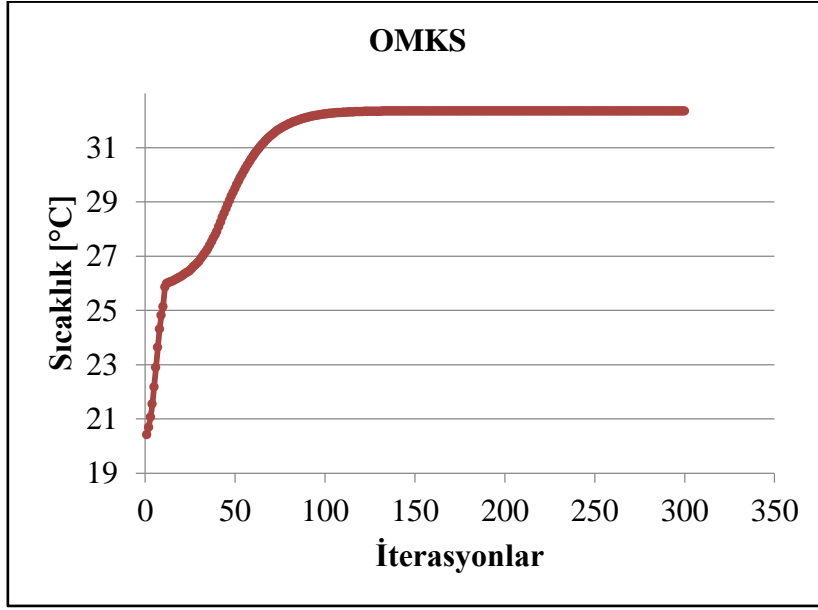
Yoğunluk (kg/m ³)	8960
Erime Sıcaklığı (K)	1356.2

Tablo 6. Soğutucu akışkan (su) termal özellikleri (Thermal properties of coolant (water))

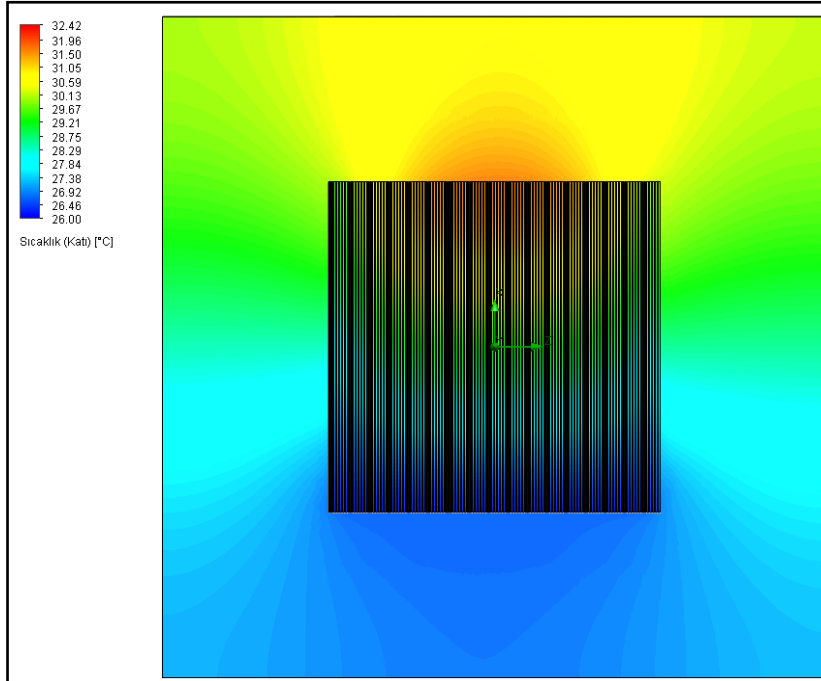
Sıcaklık (K)	Yoğunluk (kg/m ³)	Dinamik Viskozite (Pa·sn)	Isıl İletkenlik (W/(m·K))	Özgül Isı (J/(kg·K))
273.16	999.79	0.00179	0.56104	4219.9
303.16	995.6	0.000797	0.61547	4180.1
343.16	977.73	0.00044038	0.6631	4190.2
403.16	934.83	0.0002129	0.6837	4261.5
458.16	881.59	0.0001458	0.67114	4425.5
496.16	833.73	0.0001187	0.6456	4649.9
518.16	806.21	0.0001084	0.62667	4819.2

4. BULGULAR VE TARTIŞMA (FINDINGS AND DISCUSSION)

KAM parametresi ve sınır şartlarına göre 3 adet analiz gerçekleştirilmiş olup OMKS değerleri incelenmiştir. Analizler 300 iterasyonda çözdürülmüş olup yakınsama grafiği Şekil 8’de verilmiştir. Soğutucu akışkanın mikro kanatçığa ilk temas ettiği bölgede minimum sıcaklık değerleri görülürken, mikro kanatçıktan çıkış bölgesinde maksimum sıcaklık değerleri görülmektedir. Optimum tasarımın sıcaklık kontur dağılımı incelendiğinde maksimum sıcaklık 32.42°C’dir (Şekil 9). Mikro kanatçık yapının soğutma performansına birincil dereceden etki eden faktör ısı transfer yüzey alanıdır. Bu kapsamda, katılarla temas eden akışkan hücreler; KAM 0.1mm iken 235.000, KAM 0.2mm iken 200.000 ve KAM 0.3mm iken 160.000 olduğu görülmüştür.



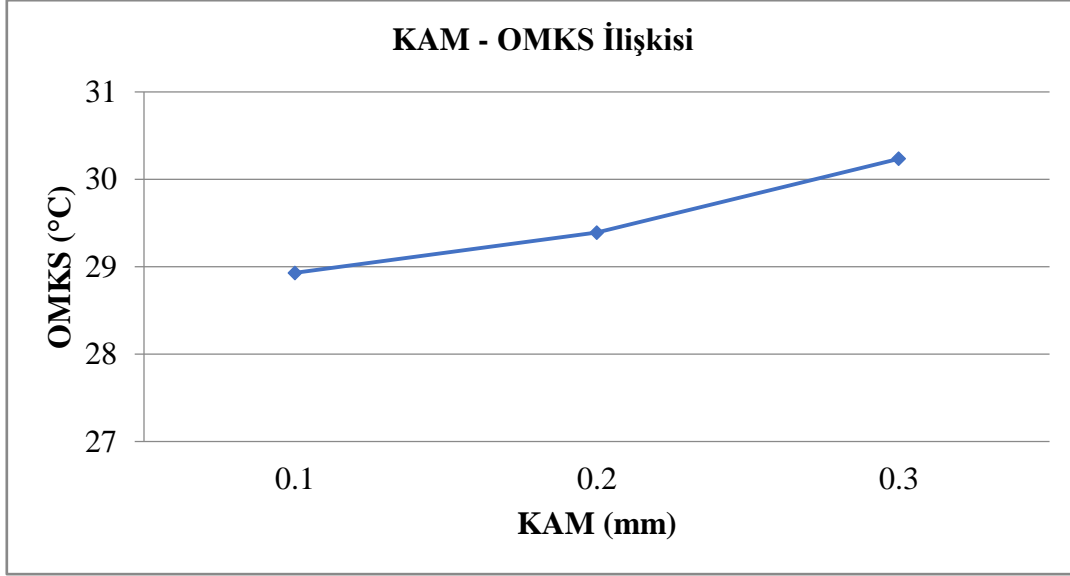
Şekil 8. Optimum tasarımın ortalama mikro kanatçık sıcaklığı yakınsama grafiği (Average heatsink temperature convergence graph of optimum design)



Şekil 9. Optimum tasarımın sıcaklık dağılım konturu (Temperature distribution contour of optimum design)

4.1. Ortalama Mikro Kanatçık Sıcaklığı (OMKS) (Average Heatsink Temperature (AHT))

Yapılan analiz çalışmalarına göre KAM'ın OMKs'ye etkisi Şekil 10'da grafik halinde verilmiştir. Belirli bir alandaki kanatçık sayısı artırılınca ısı transfer yüzey alanı artar. Kanatçık sayısı ve KAM arasında ise ters bir ilişki bulunmaktadır. KAM düşük (kanatçık sayısı fazla) olduğu zaman ısı transfer yüzey alanı artmaktadır. Bu durum ısı transferini artırmaktadır. Gerçekleştirilen sonlu hacimler analizi sonuçları dikkate alındığında KAM'ın artmasıyla birlikte OMKs'nin de arttığı görülmüştür. KAM 0.1mm, 0.2mm ve 0.3mm olduğunda OMKs'nin sırasıyla 28.93°C, 29.39°C, 30,24°C olduğu gözlemlenmiştir. Bu kapsamda KAM değeri 0.1mm olduğunda mikro kanatçık yapının en yüksek soğutma performansına sahip olacağı görülmüştür. Elde edilen sonuçlar R.Mohan ve arkadaşının yapmış olduğu çalışmayı destekler niteliktedir.



Şekil 10. KAM'ın OMKs'ye etkisi (Effect of KAM on OMKs)

5. SONUÇLAR (CONCLUSION)

Analiz çalışmalarını sonucunda elde edilen veriler aşağıda özetlenmiştir;

- Yapılan analiz çalışmaları ile elde edilen OMKs, bilgisayar ortamında sonlu hacimler paket programlarıyla yapılabileceği ortaya koyulmuştur.
- Deneylerde elde edilmesi zor ya da mümkün olmayan verilerin (katılarla temas eden akışkan hücreler gibi) elde edilmesi ve bu verilere bağlı olarak tasarım iyileştirmelerinin mümkün olabileceği görülmüştür.
- Katılarla temas eden akışkan hücreler KAM arttıkça azalmaktadır. Bu yüzden KAM arttıkça OMKs'nin de arttığı görülmüştür.
- KAM'ın artmasıyla beraber ısı transfer yüzey alanının azalacağı, bu durumun OMKs'yi arttıracığı görülmüştür.

6. ÖNERİLER (SUGGESSTIONS)

Bu çalışma kapsamında KAM 0.1mm olduğunda en iyi soğutma performansı görülmüştür. Ancak KAM'ın 0.1mm olması üretilebilirliği zor ve maliyetli bir hale getirmektedir. Bundan sonra yapılacak olan çalışmalarda üretilebilirliği göz önüne alarak KAM parametresinin soğutma performansına etkisinin incelenmesi önerilmektedir. Buna ek olarak, mikro kanatçık yapısının soğutma performansına etki eden KAM parametresi ile diğer tasarım parametreleri (kanatçık geometrisi, kanatçık yüksekliği ve kanatçık kalınlığı) beraber değerlendirilerek bir çalışma yapılması önerilmektedir.

TEŞEKKÜR (ACKNOWLEDGEMENTS)

Bu çalışmamın gerçekleşmesinde, yüksek lisans eğitimim boyunca değerli bilgilerini bizlerle paylaşan saygıdeğer danışman hocam; Prof. Dr. Ulvi ŞEKER'e ve şirket altyapısını kullanmama olanak sağlayan Simunes İleri Teknoloji A.Ş. ve çalışanlarına sonsuz teşekkürlerimi sunarım.

KAYNAKLAR (REFERENCES)

1. S. H., Wang, G. Y. Lee, W. Z. Wang, Z. Y. Wang, C. S. Tsai, An innovative active liquid heat sink technology for CPU cooling system, 8th International Conference on Electronic Packaging Technology, IEEE, 2007.
2. J. Choi, M. Jeong, J. Yoo, M. Seo, A new CPU cooler design based on an active cooling heatsink combined with heat pipes, Applied Thermal Engineering, 44: 50-56, 2012.
3. J.Khan, S.A. Momin, M. Mariatti, A review on advanced carbon-based thermal interface materials for electronic devices, Carbon, 168: 65-112, 2020.
4. S. Lee, Optimum design and selection of heat sinks, IEEE Transactions on Components, Packaging, and Manufacturing Technology: Part A, 18: 812-817, 1995.
5. A. Bar-Cohen, M. Iyengar, A.D. Kraus, Design of optimum plate-fin natural convective heat sinks, Journal of Electronic Packaging, 125 (2): 208-216, 2003.
6. R. Mohan, P. Govindarajan, Experimental and CFD analysis of heat sinks with base plate for CPU cooling, Journal of Mechanical Science And Technology, 25(8): 2003-2012, 2011.
7. R. Mohan, P. Govindarajan, Thermal analysis of CPU with variable heat sink base plate thickness using CFD, International Journal of the Computer, The Internet and Management, 18: 27-36, 2010.
8. B. Freegah, A.A. Hussain, A.H Falih, H. Towsyfyhan, CFD analysis of heat transfer enhancement in plate-fin heat sinks with fillet profile: Investigation of new designs, Thermal Science and Engineering Progress, 17: 100458, 2020.
9. E.Ozturk, I. Tari, Forced air cooling of CPUs with heat sinks: A numerical study, IEEE Transactions on Components and Packaging Technologies, 31(3): 650-660, 2008.
10. H.H. Hu, Computational fluid Dynamics, Fluid Mechanics. Academic Press, 421-472, 2012.
11. A. Thom, The flow past circular cylinders at low speeds, Proceedings of the Royal Society of London. Series A, Containing Papers of a Mathematical and Physical Character, 141(845): 651-669, 1933.
12. M. Kawaguti, Numerical solution of the Navier-Stokes equations for the flow around a circular cylinder at Reynolds number 40, Journal of the Physical Society of Japan, 8(6): 747-757, 1953.
13. D. Kuzmin, Introduction to computational fluid Dynamics, University of Dortmund, Dortmund, 2004.
14. F. Moukalled, L. Mangani, M. Darwish, The finite volume method, The Finite Volume Method in Computational Fluid Dynamics, 103-135, 2016.
15. Y.A. Çengel, J.M. Cimbala, Akışkanlar Mekaniği Temelleri ve Uygulamaları, Palme Yayıncılık, 122-123, 2004.
16. W.M. Silver, On the equivalence of Lagrangian and Newton-Euler dynamics for manipulators, The International Journal of Robotics Research, 1(2): 60-70, 1982.
17. G. Qiu, S. Henke, J. Grabe, Application of a Coupled Eulerian-Lagrangian approach on geomechanical problems involving large deformations, Computers and Geotechnics, 38(1): 30-39, 2011.
18. E. Gücüyen, R.T. Erdem, Kompozit deniz yapısının dalga kuvvetleri altında incelenmesi, Dicle Üniversitesi Mühendislik Fakültesi Mühendislik Dergisi, 10(3): 1125-113, 2019.

Mathematical Modelling and Multiresponse Optimization to Minimize Surface Roughness in Drilling Custom 450 Stainless Steel

Hüseyin GÖKÇE¹ , İbrahim ÇİFTÇİ¹ 

¹Çankırı Karatekin University, Faculty of Engineering, Çankırı, Turkey

ARTICLE INFORMATION

Received: 23.01.2023

Accepted: 27.03.2023

Keywords:

Stainless steel
Drilling
Surface roughness
Adhering workpiece
Optimization

ABSTRACT

In the present study, drilling tests were carried out on Custom 450 stainless steel workpieces. The influences of control factors (cutting speed-Vc, feed rate-f and drill bit geometry-D) on the drilled holes' surface roughness (Ra) and on the size of adhering workpiece (AW) to the drill bit was examined. The results obtained from tests designed based on the Taguchi's L16 orthogonal array were analysed using ANOVA and grey relational analyses (GRA). Therefore, the control factors and their levels were optimised simultaneously for the quality characteristics (Ra and AW). In addition, mathematical models were also developed using Response Surface Methodology (RSM) in order to estimate the quality characteristics. The used drill bits were examined under digital and scanning electron microscopes and EDX analysis was also carried out on the drill bits. The experimental results showed that the Ra and AW increased with increasing the f. It was also seen that increasing the Vc resulted in decrease in the size of adhering layer and that the drill bit wear became clear at the highest Vc of 60 m/min. According to the ANOVA results, the most effective control factor on Ra was f with 93.11% and Vc with 58.14% on AW. GRA analysis revealed that the most influential control factor was the f and that the optimum levels were 60 m/min Vc, 0.005 m/min f and drill bit 4.

Custom 450 Paslanmaz Çeliğinin Delinmesinde YüzeY Pürüzlülüğünü Minimize Etmek için Matematiksel Modelleme ve Çok Yanıtlı Optimizasyon

MAKALE BİLGİSİ

Alınma: 23.01.2023

Kabul: 27.03.2023

Anahtar Kelimeler:

Paslanmaz çelik
Delme
YüzeY pürüzlülüğü
Yığıntı talaş
Optimizasyon

ÖZET

Bu çalışmada, Custom 450 paslanmaz çelik iş parçaları üzerinde delme testleri yapılmıştır. Kontrol faktörlerinin (kesme hızı-Vc, ilerleme miktarı-f ve matkap ucu geometrisi-D) delinen deliklerin yüzeY pürüzlülüğü (Ra) ve matkap ucuna yapışan iş parçasının boyutu (AW) üzerindeki etkileri incelenmiştir. Taguchi'nin L16 ortogonal dizisine dayalı olarak tasarlanan testlerden elde edilen sonuçlar, ANOVA ve Gri İlişkisel Analizler (GRA) kullanılarak analiz edilmiştir. Kalite karakteristikleri (Ra ve AW) kontrol faktörleri ve seviyelerine bağlı olarak eş zamanlı optimize edilmiştir. Ayrıca, kalite karakteristiklerini tahmin etmek için Tepki YüzeY Metodolojisi (RSM) kullanılarak matematiksel modeller geliştirilmiştir. Kullanılan matkap uçları dijital ve taramalı elektron mikroskoplarında incelenmiş ve EDX analizleri yapılmıştır. Deneysel sonuçlar, Ra ve AW'nin f arttıkça arttığını göstermiştir. Ayrıca Vc'nin artması AW boyutunda azalmaya neden olduğu ve matkap ucu aşınmasının en yüksek Vc olan 60 m/dak'da belirginleştiği görülmüştür. ANOVA sonuçlarına göre Ra üzerinde en etkili kontrol faktörü %93.11 ile f ve AW üzerinde ise %58.14 ile Vc olmuştur. GRA analizi, en etkili kontrol faktörünün f olduğunu ve optimum seviyelerin 60 m/dk kesme hızı, 0.005 m/dk ilerleme ve 4 numaralı matkap ucu olduğunu belirlenmiştir.

*Corresponding author, E-mail: huseyingokce@karatekin.edu.tr

To cite this article: H. Gökçe, İ. Çiftçi, Mathematical Modelling and Multiresponse Optimization to Minimize Surface Roughness in Drilling Custom 450 Stainless Steel, Manufacturing Technologies and Applications, 4(1), 11-24, 2023.

<https://doi.org/10.52795/mateca.1238328>, This paper is licensed under a CC BY-NC 4.0

1. INTRODUCTION (GİRİŞ)

Stainless steels, which have high corrosion resistance and mechanical properties, are indispensable materials in all areas of the industry [1-3]. Feature of stainless steels can be altered by heat treatments and/or addition of various alloying elements [4]. Custom 450 is a type of martensitic stainless steel. It is especially suitable for the applications requiring corrosion resistance at high temperatures (650 °C) and used for making components used in submarine applications, nuclear power plants and defense industry [5]. It is stated that Custom 450 is resistant to pitting and corrosion even in salt water atmospheres [5, 6]. The high tensile strengths, low heat transfer coefficient and relatively high ductility of the Custom 450 alloy make it difficult to machine [1-3, 7, 8]. During machining of stainless steel, high cutting forces, strongly adhered chips to the cutting tool and relatively long chips adversely affect the process. Effective machining of these difficult-to-machine materials including Custom 450 is of crucial importance for cost effective manufacturing and sustainability [5].

Drilling with drill bits, which is used with a high rate of approximately 35% among machining methods, is the most important hole drilling method with its economy and simple structure [9-12]. Therefore, many researchers have focused on understanding and solving the potential problems encountered during drilling [13]. The process is influenced by the factors including drilling parameters, workpiece to be drilled and machine tool used. In addition, cutting action in drilling takes place inside the hole and therefore it is not easy to observe the process when compared to other machining processes [14].

Good dimensional accuracy and good surface quality are essential for the mating parts to serve efficiently for a long time. [15-17]. Although it is usually difficult and costly to obtain good surface quality, surface quality of a manufactured product influences its fatigue strength, wear resistance and friction properties significantly [16-18]. During machining, the cutting tools are subjected to high stresses and temperatures. These stress and temperatures cause rapid tool wear. The worn tool adversely affects the surface quality and dimensional accuracy of the workpiece [17, 19]. Poor dimensional accuracy causes the parts to be out of the specified dimensional tolerances.

Parts with good surface quality and close tolerances are often aimed to be produced at reasonable cost [12, 18]. For this reason, various optimization techniques have recently been utilized to determine the optimum machining conditions [20, 25]. Öktem et al. used the Genetic Algorithm (GA) to determine the optimum cutting conditions for minimum surface roughness in milling die steel surfaces, and the RSM to obtain the analytical model. Their methodology was capable of reducing the surface roughness (Ra) by about 10% [26]. Suresh et al. used the RSM to estimate the roughness value of the surface machined by turning steel materials with carbide cutting tools. In addition, the optimum values of the cutting variables were determined by GA. [27]. Günay and Meral developed the analytical model with the RSM depending on the Vc (cutting speed) and f (feed rate) on the Fc (cutting force), AW and Ra in the drilling process, and optimized the variables with the GRA. In their study on ferritic stainless steel, they stated that the Fc and Ra value decreased with the increase in Vc, and the Aw and Vc are directly proportional [20]. Zhang et al. used the Taguchi method to optimize the surface quality in the drilling process. Spindle speed, f, pecking amount and drill bit type were determined as control factors. They explained that the optimization was valid with the verification experiments they performed with the optimum control factor and levels they obtained [28]. Abbas et al. estimated the machining time, Ra and machining cost in CNC machines depending on the Vc, cutting depth and f. They made their predictions using AN. They stated that the predictive values they obtained were consistent and the model could be used with confidence [29]. Toulfatzis et al. realized turning tests on three lead-free brass alloys based on Taguchi's L16 series. ANOVA was utilized to state the effects of Vc, depth of cut, f, and workpiece material on Fc and Ra [30]. Çaydaş et al. examined the performances of different drill bit materials (HSS, carbide and coated HSS) in drilling of AISI 304 steel. The drilling experiments were achieved based on Taguchi's L9 series. The influence of spindle speed, f, drill point angle and number of holes on the Ra, drill bit wear, burr height and hole diameter were evaluated. Their experimental results showed that coated HSS drill bits performed best state of affairs of tool life,

hole quality and Ra [31]. Çiçek et al. performed drilling tests on AISI 304 workpieces for the purpose of investigating the effects of the drill bit cryogenic process and drilling parameters on Ra and hole quality. The tests were done based on Taguchi's L27 full factorial design with a series (mixed type). They used ANOVA to determine the most significant experiment variable. In addition, they developed a model by RSM to obtain the best Ra and ovality [32]. Mavi investigated the effects of drilling parameters on deviation from geometric and dimensional tolerances when drilling a stainless steel. The experimental design was based on L18 orthogonal array. The results were analyzed using grey relational analyses (GRA) [33]. Orak et al. optimized the cutting parameters in the turning process in terms of surface roughness, noise and tool wear using a hybrid decision making algorithm using Artificial Neural Networks (ANN) – TOPSIS. They emphasized that the method they developed will be used successfully in reducing vibrations [34]. Benefit et al. they subjected the AA7075 alloy tempered under different conditions to a series of drilling tests at different drilling parameters. They used the Response Surface Method (RSM) to evaluate the experimental results [35].

Work to date shows that considerable studies were carried on drilling of various grades of stainless steel. Custom 450 is an important martensitic stainless-steel grade and work on drilling this material is limited. The purpose of this study is to investigate the influence of f , V_c and drill bits geometry on Ra and adhering workpiece size (AW) when drilling Custom 450 stainless steel. Optimum drilling conditions and their levels were aimed to be determined using GRA. In addition, analytical models of Ra and AW were also aimed to be developed using RSM.

2. MATERIAL AND METHOD (MATERYAL VE YÖNTEM)

2.1. Material, Equipment and Experimental Conditions (Malzeme, Ekipman ve Deney Koşulları)

Ingredient and various properties of Custom 450 martensitic stainless steel are given in Table 1. Workpieces were cut off from Ø60 cylindrical Custom 450 billet for drilling test. These workpieces were machined to 14 mm height so that the drilling depth was at least three times the drill bit diameter of 4.5 mm. Four different solid carbide twist drill bits were used. Drill geometry and coating details are given in Table 2. 3 factors (V_c , f and drill bit geometry) and four levels were determined for Taguchi's L16 in experimental design (Table 3). Taguchi experimental design is an experimental design method developed to determine the most appropriate combination of the levels of control factors that cause variability in the product or process, and to minimize the variability in the product and process. Considering the most effective machining parameters and levels that will affect the relevant experiments, the experiments should be carried out in accordance with the L16 orthogonal experiment design. In the Taguchi experimental design, which was used to obtain accurate results in a short time and at low cost, the experiments were not repeated.

The catalog numbers given in Table 2 give the international codes of the manufacturer, and the grade gives the applied coating class. KCPK15 refers to multilayered TiN+MT+TiCN+Al₂O₃ CVD coating, KC7315 and KC7325 refers to TiAlN-PVD coating, and MG10 refers to nACo coating. The drilling parameters were selected based on the manufacturer's suggestions and previous studies. In addition, before starting the experiments, a preliminary experiment was carried out at the highest cutting speed and feed rate determined with each drill bit.

Table 1. Ingredient and various properties of Custom 450 (Custom 450'nin içeriği ve çeşitli özellikleri) [36]

Density - 20 °C (g/cm^3)	7.75
Brinell (Ball) Hardness (HB)	278
Yield Strength (N/mm^2)	814
Ultimate Strength (N/mm^2)	979
Elasticity Modulus (GPa)	200
Poisson's Ratio	0.29
Thermal Conductivity - 20 °C ($W/(mK)$)	15
Composition	Fe:75%, Cu:1.25%-1.75%, Ni:5%-7%, Cr:14%-16%, Mo:0.5%-1%

Table 2. Manufacturer codes of drill bits and its coating details (Matkap uçlarının üretici kodları ve kaplama detayları)

Drill bits	1	2	3	4
Manufacturer	Kennametal	Kennametal	Kennametal	Toolex
ISO Catalogue Number and Grade	B221A04500HP-KCPK15	B966A04500-KC7315	B042A04500CPG-KC7325	BE0450X2C24AS6N058-MG10

Table 3. Drilling parameters and levels (Delme parametreleri ve seviyeleri)

Experimental factors	Vc (m/min)	f (mm/rev)	D
Code	A	B	C
Levels	15 – 30 – 45 – 60	0.005 – 0.020 – 0.035 – 0.050	1 – 2 – 3 – 4

The drilling tests were conducted dry on an Arion IMM-600 CNC machine. The cylindrical workpieces were clamped rigidly using a four-jaw precision chuck. Solid carbide drill bits were clamped to the spindle of the machining center using a suitable collet. The tool overhang was kept constant for all drilling tests, because changing the tool overhang will affect the test results. Through holes were drilled on the workpieces.

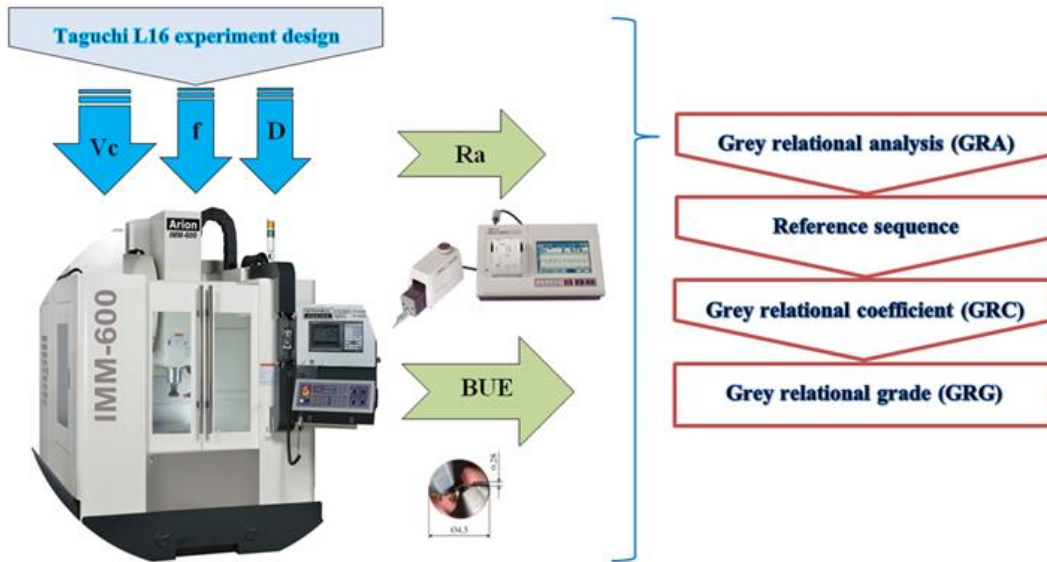


Figure 1. The experimental setup and statistical sequence (Deneysel kurulum ve istatistiksel sıra)

Surface roughness is a sensitive quality criterion that is effective on properties such as the actual contact area, fatigue and corrosion resistance of the manufactured parts. When the surface is examined from a micro point of view, it is seen that it consists of many crack, crater, waviness, intrusion and hill recesses and protrusions. There are several measuring points that define the surface roughness. Except for special applications and ultra-sensitive surfaces, it is very difficult, time consuming and far from economical to examine the entire surface in terms of these measuring points. Measurements are made with a stylus-tipped profilometer on the sample lines that will best show the roughness value of the whole surface. Movement of the stylus tip along the sample line creates a curve that represents the roughness depending on the radius of the stylus tip. A straight line is formed from the middle of the sum height of this curve (mean line). The curve creates a field and another line is obtained that cuts this area in the middle. The difference between the mean line and this line gives the mean surface roughness (R_a). R_a is the surface roughness definition that gives the most general information about the whole surface.

R_a values were obtained with a Mitutoyo SJ-410 profilometer with a cut-off wavelength (cut length) of 0.8 mm and a gauge length of 5.6 mm (ISO 4288:2000). R_a values at different angles (120°) for each hole were measured three times and averaged. The images of AW to drill bit's were obtained using a Dinolite AM7115MZT digital microscope. The digital microscope used is LED-illuminated, 5 megapixels with 2592×1944 resolution, with brightness reduction feature and digital

220 magnification features. The AW was defined using AutoCAD software. In addition, At the end of the experiment, the drill bits were detailed with Carl Zeiss scanning electron microscope (SEM). EDX analyses were also performed. Figure 1 shows the experimental setup and statistical sequence.

2.2. Statistical Methods (İstatistiksel Yöntemler)

Grey system theory can be useful to make decision and to carry out analyses in the case of poor, incomplete and uncertain information [37-39]. Various methods under grey relational analysis such as grey modelling, grey prediction and grey decision making have been applied to various fields. Scientists have often used these methods to make decision [40, 41]. In grey relational analysis, best fit values of the controlling factors and their levels for multiple quality characteristics are determined simultaneously [42].

Table 4. Steps and equations in GRA optimization (GRA optimizasyonundaki adımlar ve eşitlikler) [20, 40]

Steps	Definition	Equation	
		No	Equation
1	Definition of reference series	1	$Y_0 = (Y_{0,1}, Y_{0,2}, \dots, Y_{0,n})$
		2	$Y_{i,k} = \frac{Y_{i,k}^0 - \min(Y_{i,k}^0)}{\max(Y_{i,k}^0) - \min(Y_{i,k}^0)}$
		The larger - the better	
2	Data normalisation	3	$Y_{i,k} = \frac{\max(Y_{i,k}^0) - (Y_{i,k}^0)}{\max(Y_{i,k}^0) - \min(Y_{i,k}^0)}$
		The smaller-the better	
		4	$Y_{i,k} = 1 - \frac{ Y_{i,k}^0 - Y^0 }{\max(Y_{i,k}^0 - Y^0)}$
		The nominal-the better	
		$y_{i,k}^0$: Original series, $Y_{i,k}$: Series after pre-processing, $\max(Y_{i,k}^0)$: The maximum value of $Y_{i,k}^0$, $\min(Y_{i,k}^0)$: The minimum value of $Y_{i,k}^0$, Y^0 : Intended value.	
3	Comparison of series	5	$Y_i = (Y_{i,1}, Y_{i,2}, \dots, Y_{i,n}) i = 1, 2, \dots, m$ $i = 1 \dots m$ and $k = 1 \dots n$: The measurement data and their responses, respectively.
		6	$\xi_{i,k} = \frac{\Delta_{min} + \xi \Delta_{max}}{\Delta_{0,i,k} + \xi \Delta_{max}}$
4	GRC	$\Delta_{0,i,k}$: Deviation series $\Delta_{0,i,k} = x_{0,k}^* - x_{i,k}^* $ Δ_{min} and Δ_{max} : Minimum and maximum values of all series. ξ : Identification or distinguishing coefficient ($\xi = 0.5$ is used in experimental studies).	
5	GRG	7	$\gamma_i = \frac{1}{n} \sum_{k=1}^n \xi_{i,k}$
		n: The number of response properties	
6	Determination of optimum control factors: The strongest relation is related to the level having the largest GRG value.		

In this study, the Ra and AW to the drill bit were defined as the quality characteristic. These characteristics were optimised simultaneously based on Vc, f and D in drilling Custom 450 stainless steel using GRA. Table shows the steps in the optimisation and the equations used.

3. EXPERIMENTAL RESULTS AND DISCUSSION (DENEYSSEL SONUÇLAR VE TARTIŞMA)

The experimentally measured Ra and AW to the drill bit's cutting edges (D) are given in Table 5. As can be seen from Table 5, the lowest and highest values for Ra are 0.246 μm and 2.064 μm , respectively, while the lowest and highest values for AW are 0.13 mm and 0.56 mm, respectively. It is seen that the differences between these values are quite high, which indicates that the

experimental parameters (quality characteristic) and the results (control factors) are highly correlated with each other.

Table 5. The experimentally obtained Ra and AW values (Deneysel olarak elde edilen Ra ve AW değerleri)

Test	Vc (m/min)	f (mm/rev)	D	Ra (μm)	AW (mm)
1	15	0.005	1	0.246*	0.38
2	15	0.020	2	1.087	0.44
3	15	0.035	3	1.252	0.48
4	15	0.050	4	1.724	0.56**
5	30	0.005	2	0.506	0.20
6	30	0.020	1	1.114	0.28
7	30	0.035	4	1.284	0.41
8	30	0.050	3	2.006	0.36
9	45	0.005	3	0.536	0.19
10	45	0.020	4	1.147	0.21
11	45	0.035	1	1.310	0.28
12	45	0.050	2	2.027	0.39
13	60	0.005	4	0.775	0.13*
14	60	0.020	3	1.148	0.23
15	60	0.035	2	1.644	0.25
16	60	0.050	1	2.064**	0.34
Average				1.242	0.32

* The lowest value, ** The highest value

3.1. Surface Roughness – Ra (Yüzey Pürüzlülüğü – Ra)

The lowest Ra value of 0.246 μm is obtained at Vc: 15 m/min and f: 0.005 mm/rev with drill bit 1, while the highest Ra of 2.064 μm is obtained at Vc: 60 m/min and f: 0.050 mm/rev with drill bit 1 control factors and levels. ANOVA was applied to find the effect (percent contribution) of Vc, F and D on Ra and the results are presented in Table 6. In terms of F ratios and P values, Vc and f seem to be effective and statistically significant on quality characteristics (F ratio > Fa: 0.05: 5.99 and P value < 0.05). The percentage contributions (PCR) of the quality characteristics (Vc, f and D) are 4.80%, 93.11% and 1.30%, respectively.

Based on variance analysis (ANOVA), the highest percentage contribution rates belong to f and Vc. Figure 2 gives the influence of variations in f and Vc on Ra. It can be seen from Figure 2 that increasing f significantly increases Ra. Increasing f values increases the cross-sectional zone of undeformed material and therefore the amount of plastic deformation also increases [39]. High amount of plastic deformation, in turn, increases the required forces and vibration in drilling. In addition, the high ductility of workpiece material causes some of the deformed material to adhere to the drill bit. This adhered material is also considered to increase the Ra [4, 43-46].

Table 6. Variance analysis results of Ra (Ra'nın varyans analizi sonuçları)

Source	DF	Seq SS	Adj MS	F ratios	P values	PCR
Vc	3	0.22017	0.07339	7.36	0.020	4.80
f	3	4.26916	1.42305	142.72	0.000	93.11*
D	3	0.03598	0.01199	1.20	0.386	0.78
Error	6	0.05982	0.00997			1.30
Total	15	4.58514				100.00
R ²		98.70%				

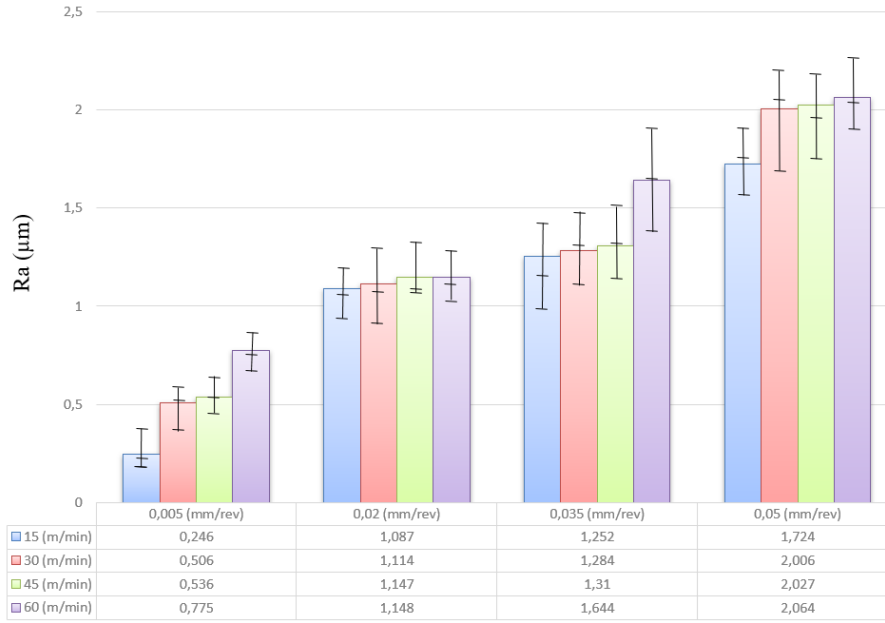


Figure 2. Vc - f interactions of Ra values (Ra değerlerinin Vc - f etkileşimi)

3.2. Adhering Workpiece to The Drill Bit's Cutting Edges – AW (İş Parçasının Matkap Ucu Kesici Kenarlarına Yapışması – AW)

The measured AW to the D used in drilling Custom 450 workpiece are given in Table 5. The lowest AW of (0.13 mm) is obtained at 60 m/min Vc and 0.005 mm/rev f with drill bit 4, while the highest size of 0.56 mm is obtained at 15 m/min Vc and 0.050 mm/rev f with drill bit 4. Based on the ANOVA results given in Table 7, it can be said that Vc and f are statistically significant on the AW (P value < 0.05, F ratio > F α : 0.05: 5.99).

Table 7. ANOVA for the AW (AW için ANOVA)

Source	DF	Seq SS	Adj MS	F ratios	P values	PCR
Vc	3	0.122006	0.040669	22.58	0.001	58.14*
f	3	0.076855	0.025618	14.22	0.004	36.63
D	3	0.000163	0.000054	0.03	0.992	0.08
Error	6	0.010808	0.001801			5.15
Total	15	0.209833				100.00
R²						94.85%

These results and higher coefficient of determination values (94.85%) indicate a strong correlation between the variation of control factors and results. The PCR of the control factors on the AW are also given in Table 7. Accordingly, the contributions of Vc, f and D are 58.14%, 36.63% and 0.08%, respectively. In the surface graph in Figure 3, it is seen that the changes in Vc and f values have a significant effect on AW (especially affected by Vc changes).

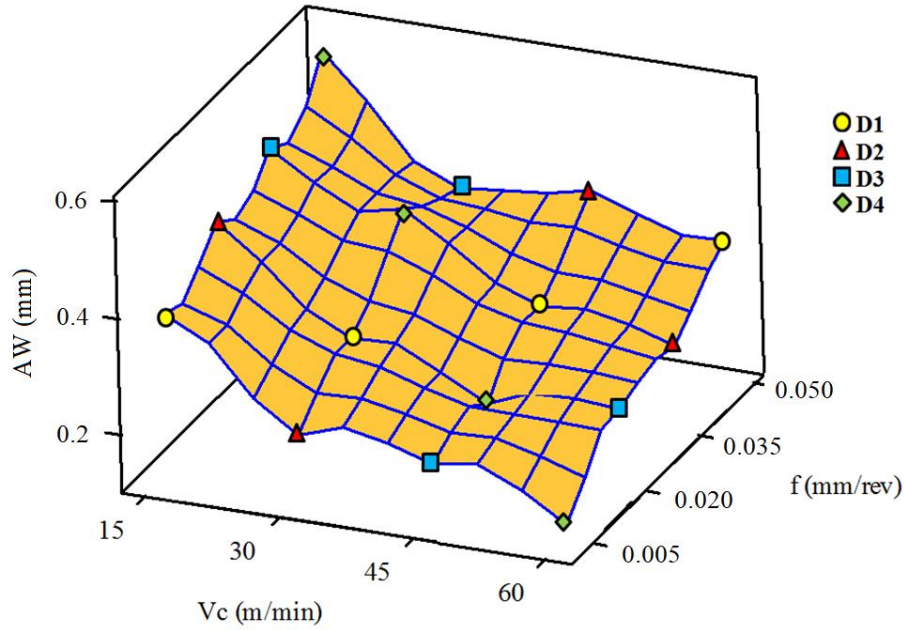


Figure 3. Influence of Vc, f and D on the AW values (AW değerlerinin Vc, f ve D üzerindeki etkisi)

Workpiece material tends to adhere strongly to the drill bit's cutting edges due to the high temperature and high stresses during drilling. This is the case especially in machining of austenitic stainless steel [43, 47] and is not desirable. This adhered workpiece usually causes rapid tool wear and poor surface quality.

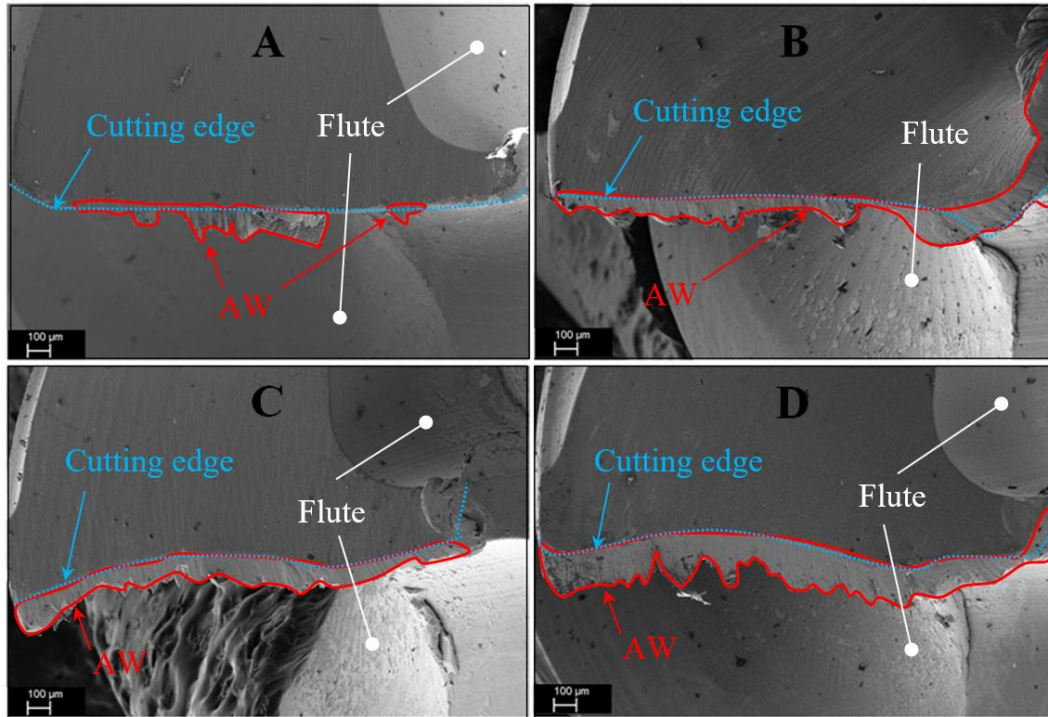


Figure 4. SEM images of the drill bits used at 15 m/min Vc at various f: A: 0.005 mm/rev, B: 0.0020 mm/rev, C: 0.0035 mm/rev and D: 0.050 mm/rev (Vc=15 m/dk'de matkap uçlarının SEM görüntüleri, A: 0,005 mm/dev, B: 0,0020 mm/dev, C: 0,0035 mm/dev ve D: 0,050 mm/dev)

Figure 4 shows the SEM images of the D used at 15 m/min Vc and various f, while Figure 5 shows the SEM images of the D used at 0.050 m/min f and various Vc. In Figure 4, it is seen that increasing the f increases the size of adhered workpiece. This increase can be attributed to increased forces and temperatures during drilling due the increasing cross-sectional area of uncut chip thickness with increasing f. However, increasing the Vc decreases the size of adhered workpiece, Figure 5. Moreover, no adhered workpiece is seen at the highest Vc of 60 m/min, Figure 5D.

However, Figure 5D also shows the worn and locally fractured cutting edges of the D. Further increase in the temperature with the increasing V_c decreases the bonding force between the drill bit's cutting edges and adhered workpiece and this, in turn, leads to detachment of the adhered workpiece [43].

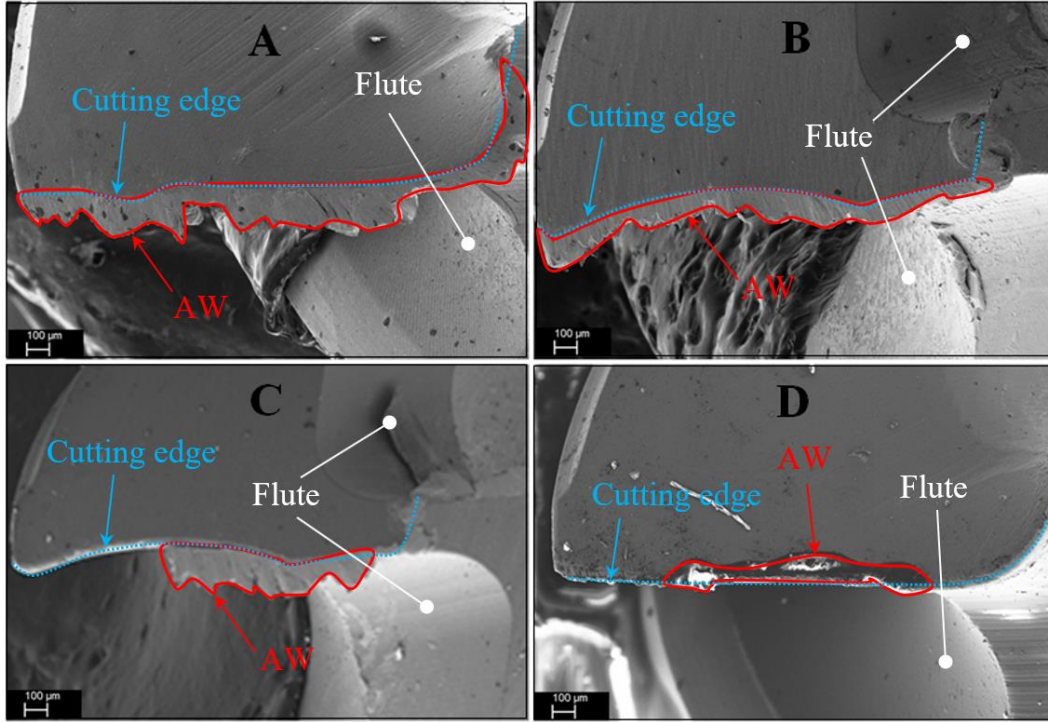


Figure 5. SEM images of the drill bits used at $f=0.050$ mm/rev and at various V_c : A: 15 m/min, B: 30 m/min, C: 45 m/min and D: 60 m/min ($f=0,050$ mm/dev'de matkap uçlarının SEM görüntüleri, A: 15 m/dk, B: 30 m/ dk, C: 45 m/ dk ve D: 60 m/ dk)

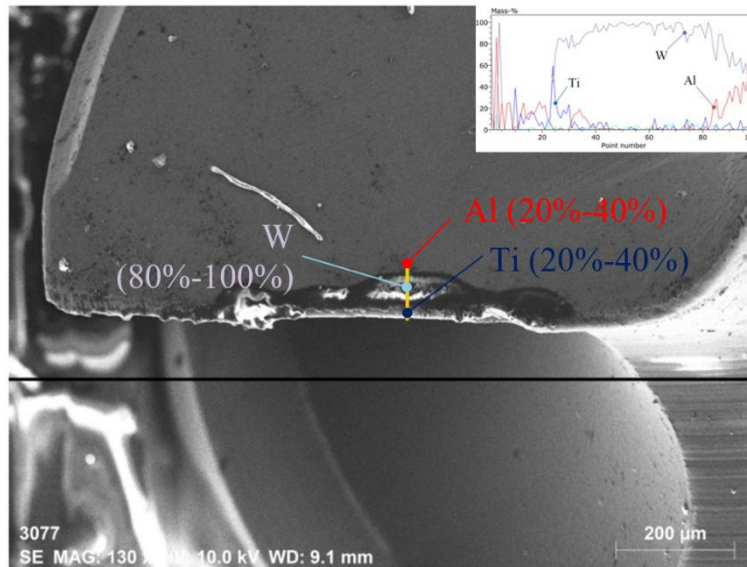


Figure 6. EDX analysis result of the used drill bit (Kullanılan matkap ucunun EDX analiz sonucu)

From Figure 5D, it is also considered that adhesive wear is the dominant wear mechanism in the drill bit wear. When there is an adhered workpiece material on the cutting tool, it is likely that the particles of the cutting tool wear away through workpiece seizure and pull-out process during machining [45-49]. EDX analysis result given in Figure 6 reveals that AlTiN coating on the drill bit was detached and the main element (W) of the drill bit's substrate came out.

3.3. Optimization with GRA (GRA optimizasyonu)

The obtained Ra and AW values in the drilling of Custom 450 stainless steel and ANOVA results show the presence of different control factors and levels for optimum drilling conditions. For drilling efficiency, simultaneous optimization for the both quality characteristics of Ra and AW is of crucial importance. For this purpose, the first step in GRA is normalization of the experimental results. For the quality characteristics, lower values of the experimental results are desired. Equation 3 is applied to the experimental results and normalized values are calculated. The second step is to find the GRC values using the normalized values and Equation 6. Finally, GRC values and GRG values (using Equation 7) are calculated. The calculated GRA values are given in Table 8.

Table 8. Experimentally obtained results and calculated GRA values (Deneyssel olarak elde edilen sonuçlar ve hesaplanan GRA değerleri)

Test	Experimental results		Normalized values		GRC		GRG	Order
	Ra (μm)	AW (mm)	Ra	AW	Ra	AW		
1	0.246	0.38	1.0000	0.4186	1.0000	0.4624	0.7312	4
2	1.087	0.44	0.5374	0.2791	0.5194	0.4095	0.4645	10
3	1.252	0.48	0.4466	0.1860	0.4747	0.3805	0.4276	12
4	1.724	0.56	0.1870	0.0000	0.3808	0.3333	0.3571	16
5	0.506	0.20	0.8570	0.8372	0.7776	0.7544	0.7660	3
6	1.114	0.28	0.5226	0.6512	0.5115	0.5890	0.5503	7
7	1.284	0.41	0.4290	0.3488	0.4669	0.4343	0.4506	11
8	2.006	0.36	0.0319	0.4651	0.3406	0.4831	0.4119	14
9	0.536	0.19	0.8405	0.8605	0.7581	0.7818	0.7700	2
10	1.147	0.21	0.5044	0.8140	0.5022	0.7288	0.6155	5
11	1.310	0.28	0.4147	0.6512	0.4607	0.5890	0.5249	8
12	2.027	0.39	0.0204	0.3953	0.3379	0.4526	0.3953	15
13	0.775	0.13	0.7090	1.0000	0.6321	1.0000	0.8161	1
14	1.148	0.23	0.5039	0.7674	0.5019	0.6825	0.5922	6
15	1.644	0.25	0.2310	0.7209	0.3940	0.6418	0.5179	9
16	2.064	0.34	0.0000	0.5116	0.3333	0.5059	0.4196	13

Table 9. Response table for GRG (GRG için yanıt tablosu)

Control factors	Levels				Delta (max-min)
	1	2	3	4	
Vc	0.4951	0.5447	0.5764	0.5865**	0.0914
f	0.7708**	0.5556	0.4802	0.3960	0.3748*
Drill bit	0.5565	0.5359	0.5504	0.5598**	0.0239

Mean GRG: 0.5507

* The most important control factor, ** Optimum level

In GRG response table (Table 9) built using averages of GRG values belonging to the same levels of each control factor, the highest values among the levels determine the optimum level, while the highest difference among the levels indicates the most important control factor. By taking into these definitions, level 4 is for the cutting speed (60 m/min), level 1 is for the feed rate and level 4 is for the drill bit (D:4) are determined as the optimum levels (Run: 13). In addition, the most important control factor is seen to be f with a value of 0.3748.

3.4. Mathematical Modelling with RSM (RSM ile Matematiksel Modelleme)

Response surface methodology (RSM) is used to develop analytical models of the quality characteristics by carrying out full quadratic regression model (Equation 8) of control factors. In Equation 8, η is the predicted response (Ra and AW), β_0 is the constant in regression equation, β_i and β_{ii} are the regression coefficients, X_i are the values of independent variables and k is the number of parameters. The developed models for the Ra and AW are given in Equations 9 and 10. The predicted values through Equations 9 and 10 and the experimental results are given in Figures 7 and 8 comparatively. In addition, determination coefficients (R-Sq) are also given in Figures 7 and

8 for the analytical models. Accordingly, R-Sq values of the mathematical models for the Ra and AW are 96.9% and 94.7%, respectively. These results indicate the reliability and can be used effectively.

$$\eta = \beta_0 + \sum_{i=1}^k \beta_i X_i + \sum_{i=1}^k \beta_{ii} x_i^2 \quad (8)$$

$$Ra = 0.115086 - 0.00415593 Vc + 42.662 f + 0.0916951 D + 2.91667 \times 10^{-6} Vc^2 - 0.0339646 Vc \times f + 0.00380417 Vc \times D - 27.6389 f^2 - 2.39811 f \times D - 0.0337188 D^2 \quad (9)$$

$$BUE = 0.543205 - 0.0154486 Vc + 2.88547 f + 0.0135245 D + 0.000133186 Vc^2 + 0.0490007 Vc \times f - 0.000310768 Vc \times D - 14.2436 f^2 - 0.0365091 f \times D + 0.0019548 D^2 \quad (10)$$

The values obtained as a result of drilling experiments and calculations are quite close. These results prove that the variables used in the experiments (control factors) are highly effective variables on surface roughness and adhesion to the cutting tool, which are determined as quality characteristics [20, 41, 50]. However, it is seen that there is a difference of 3.1% in the surface roughness and 5.3% in the amount of adhesion to the cutting tool. Although these values are small, they show that the results are also affected by factors other (such as machine tool, environment, ambient temperature, measuring device) than the determined quality characteristics [45, 51].

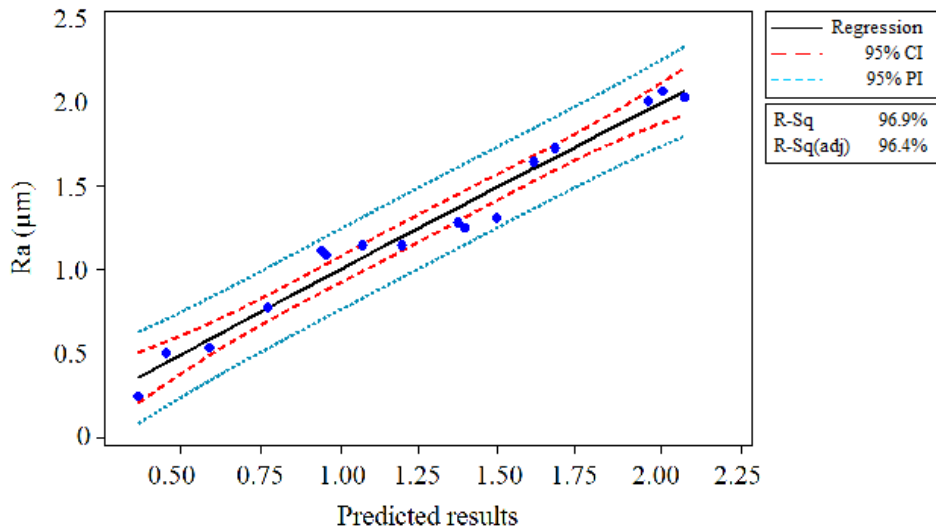


Figure 7. Comparison of experimentally obtained and calculated results for Ra (Ra için deneysel olarak elde edilen ve hesaplanan sonuçların karşılaştırılması)

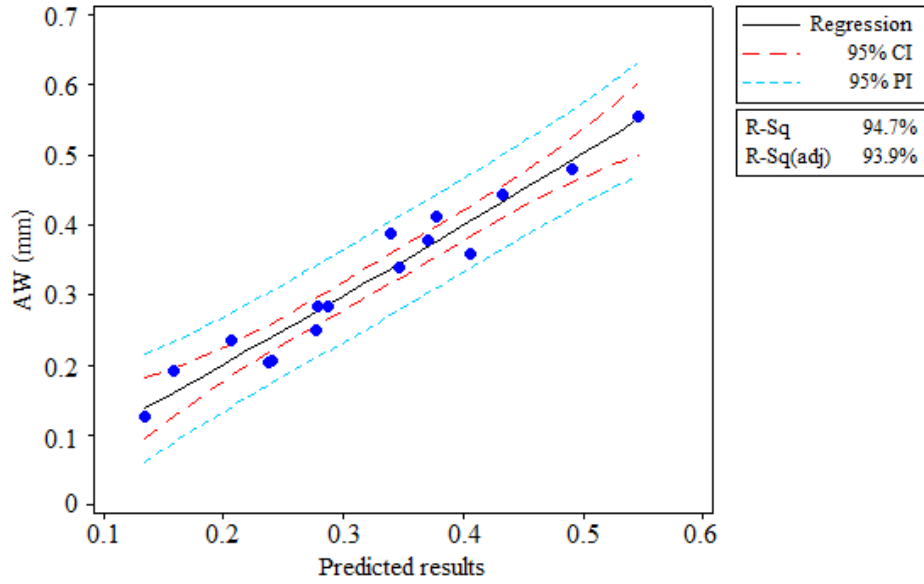


Figure 8. Comparison of experimentally obtained and calculated results for AW (AW için deneysel olarak elde edilen ve hesaplanan sonuçların karşılaştırılması)

4. CONCLUSIONS (SONUÇLAR)

In this study, drilling tests were carried out on a Custom 450 austenitic stainless steel workpiece. The surface roughness (Ra) and size of adhering workpiece (AW) to the drill bit's cutting edges were determined. Based on the control factors, simultaneous optimisation was performed through grey relational analysis (GRA) method. In addition, mathematical models for the Ra and AW were obtained through response surface methodology (RSM). The following conclusions can be drawn from the present work:

- Increasing the feed rate values increased the Ra and AW to the drill bits' cutting edges.
- AW decreased significantly with increasing the cutting speed. This decrease was considered to be result of increased temperature.
- From ANOVA, the feed rate and cutting speed were found to be the most influential control factors on the Ra and AW. The influence of feed rate on the Ra was 93.11%, while the influence of the cutting speed on the AW was 58.14%.
- At the highest cutting speed, adhesive wear mechanism was seen to be dominant on the drill bit wear.
- The simultaneous optimisation through grey relational grade (GRG) revealed that the feed rate was the most important control factor with a value of 0.378.
- High R^2 values of the developed mathematical models indicated that these models can be used effectively (Ra: 96.9% and AW: 94.7%).

ACKNOWLEDGMENTS (TEŞEKKÜR)

This study was supported by the Scientific Research Projects of Çankırı Karatekin University (Project no: MYO801202B33).

REFERENCES (KAYNAKLAR)

1. G. Basmacı, Optimization of processing parameters of AISI 316 Ti stainless steels, Academic Platform Journal of Engineering and Science, 6(3): 01-07, 2018.
2. J.D. Darwin, D.M. Lal, G. Nagarajan, Optimization of cryogenic treatment to maximize the wear resistance of 18%Cr martensitic stainless steel, Journal of Materials Processing Technology, 195: 241-247, 2008.
3. J.C. Outeiro, D. Umbrello, R. M'Saoubi, Experimental and numerical modelling of the residual stresses induced in orthogonal cutting of AISI 316L steel, International Journal of Machine Tools and Manufacture, 46: 1786-1794, 2006.

4. Ö. Tekaslan, N. Gerger, U. Şeker, AISI 304 östenitik paslanmaz çeliklerde kesme parametrelerine bağlı olarak yüzey pürüzlülüklerinin araştırılması, Balıkesir Üniversitesi FBE Dergisi, 10(2): 3-12, 2008.
5. H. Gökçe, Optimization of cutting tool and cutting parameters in face milling of Custom 450 through the Taguchi method, Advances in Materials Science and Engineering, 1-11, 2019.
6. Internet:<https://www.spacematdb.com/spacemat/manudatasheets/custom%20450.pdf>
7. A. Uysal, Investigation of cutting temperature in minimum quantity lubrication milling of ferritic stainless steel by using multi wall carbon nanotube reinforced cutting fluid, Journal of the Faculty of Engineering and Architecture of Gazi University, 32(3): 645-650, 2017.
8. N.A. Özbek, A. Çiçek, M. Gülesin, O. Özbek, AISI 304 ve AISI 316 östenitik paslanmaz çeliklerin işlenebilirliğinin değerlendirilmesi, Journal of Polytechnic, 20(1): 43-49, 2017.
9. S. Kalpakjian, S. Schmid, Manufacturing Engineering and Technology, 7th ed., Pearson Education Inc, Singapore, 625–665, 2014.
10. M. Yavuz, H. Gökçe, İ. Çiftçi, H. Gökçe, Ç. Yavaş, U. Şeker, Investigation of the effects of drill geometry on drilling performance and hole quality, The International Journal of Advanced Manufacturing Technology, 106(9): 4623-4633, 2020.
11. M. Kurt, Y. Kaynak, B. Bakır, U. Köklü, G. Atakök, L. Kutlu, Experimental investigation and Taguchi optimization for the effect of cutting parameters on the drilling of Al 2024-t4 alloy with diamond like carbon (DLC) coated drills, 5. Uluslararası İleri Teknolojiler Sempozyumu (IATS'09), 2009, Karabük.
12. H.L. Tonshoff, W. Spintig, W. König, A. Neises, Machining of holes developments in drilling technology, Annals of the CIRP, 43(2): 551-560, 1994.
13. A. Çakır, O. Bahtiyar, U. Şeker, Farklı soğutma şartları ile farklı kesme parametrelerinin AA7075 ve AA2024 alüminyum alaşımlarında delik delme işlemlerine etkisinin deneysel olarak incelenmesi, 16. Uluslararası Makina Tasarım ve İmalat Kongresi, 30 Haziran – 03 Temmuz 2014, İzmir, Türkiye.
14. S. Yağmur, A. Acır, U. Şeker, M. Günay, An experimental investigation of effect of cutting parameters on cutting zone temperature in drilling, J. Fac. Eng. Archit. Gazi Univ, 28(1): 1-6, 2013.
15. M. Sekmen, M. Günay, U. Şeker, Effect on formations of built-up edge and built-up layer, surface roughness of cutting speed and rake angle in the machining of aluminum alloys, Journal of Polytechnic, 18(3): 141-148, 2015.
16. İ. Çiftçi, H. Gökçe, Ti6Al4V titanyum alaşımının delinmesinde delme yönteminin aşınmaya etkisinin incelenmesi, Journal of Polytechnic, 22:3, 627-631, 2019.
17. S. Kalpakjian, S.R. Schmid, Manufacturing Engineering and Technology 6th ed., Pearson Education, 2009.
18. H. Gökçe, Investigation of drilling performance of copper material in terms of cutting force and tool temperature, El-Cezerî Journal of Science and Engineering, 7(3): 1039-1053, 2020.
19. H. Gökçe, M. Yavuz, İ. Çiftçi, An investigation into the performance of HSS drills when drilling commercially pure molybdenum, Sigma Journal of Engineering and Natural Sciences, 38(1): 61-70, 2020.
20. M. Günay, T. Meral, Modelling and multiresponse optimization for minimizing burr height, thrust force and surface roughness in drilling of ferritic stainless steel, Indian Academy of Sciences - Sadhana, 45, 275, 2020.
21. V.N. Gaitonde, S.R. Karnik, B.T. Achyutha, B. Siddeswarappa, GA applications to RSM based models for burr size reduction in drilling, J. Sci. Ind. Res. (India) 64, 347–353, 2005.
22. S. Kumar, Y. Rizvi, R. Kumar, A review of modelling and optimization techniques in turning processes, Int. J. Mech. Eng. Technol., 9, 1146–56, 2018.
23. N. Mondal, S. Mandal, M.C. Mandal, FPA based optimization of drilling burr using regression analysis and ANN model, Measurement, 152, 1-10, 2020.
24. M. Dörterler, İ. Şahin, H. Gökçe, A grey wolf optimizer approach for optimal weight design problem of the spur gear, Engineering Optimization, 51(6): 1013-1027, 2019.
25. D. Özyürek, A. Kalyon, M. Yıldırım, T. Tuncay, İ. Çiftçi, Experimental investigation and prediction of wear properties of Al/SiC metal matrix composites produced by thixomoulding method using Artificial Neural Networks, Materials & Design, 63, 270-277, 2014.
26. H. Öktem, T. Erzurumlu, H. Kurtaran, Application of response surface methodology in the optimization of cutting conditions for surface roughness, Journal of Materials Processing Technology, 170(1–2): 1-16, 2005.
27. P.V.S. Suresh, P.V. Rao, S.G. Deshmukh, A genetic algorithmic approach for optimization of surface roughness prediction model, International Journal of Machine Tools and Manufacture, 42(6): 675-680, 2002.

28. J.Z. Zhang, J.C. Chen, Surface roughness optimization in a drilling operation using the taguchi design method, *Materials and Manufacturing Processes*, 24(4): 459-467, 2009.
29. A.T. Abbas, D.Y. Pimenov, I.N. Erdakov, M.A. Taha, M.S. Soliman, M.M. El Rayes, ANN surface roughness optimization of AZ61 magnesium alloy finish turning: minimum machining times at prime machining costs, *Materials*, 11(5): 808, 2018.
30. A.I. Toulfatzis, G.A. Pantazopoulos, C.N. David, D.S. Sagris, A.S. Paipetis, Machinability of eco-friendly lead-free brass alloys: cutting-force and surface-roughness optimization, *Metals*, 8(4): 250, 2018.
31. U. Çaydaş, A. Hasçalık, Ö. Buytoz, A. Meyveci, Performance evaluation of different twist drills in dry drilling of AISI 304 austenitic stainless steel, *Mater. Manuf. Process.* 26, 951–960, 2011.
32. A. Çiçek, T. Kıvak, E. Ekici, Optimization of drilling parameters using Taguchi technique and response surface methodology (RSM) in drilling of AISI 304 steel with cryogenically treated HSS drills, *Journal of Intelligent Manufacturing*, 26, 295-305, 2015.
33. A. Mavi, Determination of optimum cutting parameters affecting the surface form properties in the ductile stainless steels with gray relational analysis method, *Gazi University Journal of Science Part C: Design and Technology*, 6, 634–643, 2018.
34. S. Orak, R.A. Arapoğlu, M.A. Sofuoğlu, Development of an ANN-based decision-making method for determining optimum parameters in turning operation. *Soft Comput* 22, 6157–6170, 2018.
35. E. Yazar, A.T. Ertürk, F.G. Koç, Comparative Analysis in Drilling Performance of AA7075 in Different Temper Conditions. *J. of Materi Eng and Perform*, 2022.
36. <https://www.ulbrich.com/uploads/data-sheets/Custom-450-Stainless-Steel-Wire-UNS-S45000.pdf>
37. Y. Kuo, T. Yang, G.W. Huang, The use of grey relational analysis in solving multiple attribute decision-making problems, *Computers & Industrial Engineering*, 55(1): 80-93, 2008.
38. E. Yılmaz, F. Güngör, S. Hartomacıoğlu, Determining the appropriate tool holder selection by using grey relational analysis on machining process of AISI 4340 steel, *Beykent Üniversitesi Fen ve Mühendislik Bilimleri Dergisi*, 12(2): 7-13, 2019.
39. S. Gurgen, M.A. Sofuoglu, F.H. Cakir, S. Orak, M.C. Kushan, Multi response optimization of turning operation with self-propelled rotary tool, *Procedia - Social and Behavioral Sciences*, 195: 2592-2600, 2015.
40. N. Yaşar, Thrust force modelling and surface roughness optimization in drilling of AA-7075: FEM and GRA, *J. Mech. Sci. Technol.*, 33: 4771–4781, 2019.
41. M.A. Amran, S. Salmah, N.I.S. Hussein, R. Izamshah, M. Hadzley, M.S. Kasim, M.A. Sulaiman, Effects of machine parameters on surface roughness using response surface method in drilling process, *Procedia Engineering*, 68: 24–29, 2013.
42. İ. Çiftçi, Tool wear during machining of aisi 304 austenitic stainless steel using a coated cemented carbide tool, *Teknoloji*, 7(3): 489-495, 2004.
43. E.O. Ezugwu, S.K. Kim, The performance of cermet cutting tools when machining an Ni-Cr-Mo (En 24) steel, *Lubrication Engineering*, 51(2): 139-145, 1995.
44. *Material-Removal Process and Machine Tools*, Mark Standart Handbook for Mechanical Engineers, 9th ed., New York, Mc Graw Hill, 1996.
45. Z. Tekiner, S. Yeşilyurt, Investigation of the cutting parameters depending on process sound during turning of AISI 304 austenitic stainless steel, *Materials & Desing*, 25(6): 507-513, 2004.
46. E.M. Trent, *Metal Cutting*, Butterworths Pres, London, 1989.
47. İ. Çiftçi, M. Turker, U. Şeker, CBN cutting tool wear during machining of particulate reinforced MMCs, *Wear*, 257: 1041-1046, 2004.
48. H. Gökçe, Investigation of the effect of the tap geometry on the Al 5083 aluminium material in tapping, *Gazi Journal of Engineering Sciences (GJES)*, 6(3): 242-247, 2020.
49. C. Relvas, A. Ramos, New methodology for product development process using structured tools, *Proceedings of the Institution of Mechanical Engineers Part B-journal of Engineering Manufacture*, 235(3): 378-393, 2021.
50. H. Gökçe, M.A. Biberici, Mathematical modeling and multiresponse optimization to reduce surface roughness and adhesion in Al 5083 H116 alloys used in ammunition propulsion actuators, *Multidiscipline Modeling in Materials and Structures*, 19(2): 341-359, 2023.
51. N. Bhople, S. Mastud, R. Mittal, Metallurgical and machining performance aspects of cryotreated tungsten carbide micro-end mill cutters, *Proceedings of the Institution of Mechanical Engineers, Part B: Journal of Engineering Manufacture*, 237(3):492-502, 2023.

Comparison of Strength, Surface Quality and Cost of Different Additive Manufacturing Methods

Mehmet Mahir SOFU¹, Hatice VAROL ÖZKAVAK¹, Selim BACAĞ², Mehmet FENKLİ³

¹ Suleyman Demirel University, Faculty of Engineering, Department of Automotive Engineering, Isparta, 32260, Turkey

² Isparta University of Applied Sciences Technical Sciences Vocational School, Department of Mechanical and Metal Technology, Isparta, 32260, Turkey

³ Isparta University of Applied Sciences, Faculty of Technology, Department of Civil Engineering, Isparta, 32260, Turkey

ARTICLE

INFORMATION

Received: 15.03.2023

Accepted: 03.04.2023

Keywords:

Additive manufacturing

Cost analysis

Strength

Surface quality

ABSTRACT

Additive manufacturing is a manufacturing method that includes systems that produce using many different methods. The most widely used and accessible methods of additive manufacturing can be listed as Fused Deposition Modeling (FDM), Selective Laser Sintering (SLS) and UV light assisted Stereolithography (SLA). Today, it is quite easy to produce thermoplastic products suitable for direct use in low quantities with these three methods. In addition, the production success of the parts produced in geometric difficulties also increases this demand. The most important problem is the lack of sufficient studies and information about the strength limits, surface quality and costs of the parts produced for additive manufacturing methods with such advantages. In this study, the comparison of three different production methods in terms of surface roughness, strength and cost is discussed in order to eliminate this deficiency in the literature. For this purpose, the tensile strength and surface roughness values of the samples produced using FDM, SLS and SLA methods were determined. In addition, cost analyzes were made depending on the production time of the produced samples. In the study, the lowest cost was obtained in the SLA material with a value of \$ 0.19. Again, the lowest values were obtained for the samples produced from SLA material, with a production time of 17 minutes and a surface roughness of 1.96 μ m compared to other methods. However, when evaluated in terms of strength, the highest strength value was obtained as 57.67 N/mm² in the FDM method.

Farklı Katkılı Üretim Yöntemlerinin Dayanım, Yüzey Kalitesi Ve Maliyetlerinin Karşılaştırılması

MAKALE BİLGİSİ

Alınma: 15.03.2023

Kabul: 03.04.2023

Anahtar Kelimeler:

Ekleme İmalat

Maliyet analizi

Mukavemet

Yüzey kalitesi

ÖZET

Katmanlı imalat, birçok farklı yöntem kullanılarak üretim yapan sistemleri içeren bir imalat yöntemidir. Katmanlı imalat yöntemlerinden en yaygın kullanılan ve erişilebilir yöntemler Fused Deposition Modeling (FDM), Selective Laser Sintering (SLS) ve UV ışık destekli Stereolitografi (SLA) olarak sıralanabilir. Günümüzde bu üç yöntem ile düşük miktarlarda doğrudan kullanıma uygun termoplastik ürünler üretmek oldukça kolaydır. Bunun yanında geometrik zorluklarda üretilen parçaların üretim başarısı da bu talebi arttırmaktadır. Bu kadar avantaja sahip katmanlı imalat yöntemleri için üretilen parça dayanım limitleri, yüzey kalitesi ve maliyetleri hakkında yeterli çalışma ve bilgi olmaması en önemli sorun olarak karşımıza çıkmaktadır. Bu çalışmada literatürdeki bu eksikliği gidermek amacıyla üç farklı üretim yöntemi yüzey pürüzlülüğü, mukavemet ve maliyet açısından karşılaştırılması ele alınmıştır. Bu amaçla FDM, SLS ve SLA yöntemleri kullanılarak üretilen numunelerin çekme dayanımları, yüzey pürüzlülük değerleri belirlenmiştir. Ayrıca üretilen numunelerin üretim süresine bağlı olarak maliyet analizleri yapılmıştır. Çalışmada en düşük maliyet 0.19 \$ değer ile SLA malzemede elde edilmiştir. Yine SLA malzemenin üretilen numuneler için 17 dakika üretim süresi ve 1.96 μ m yüzey pürüzlülük değerleri diğer yöntemlere nazaran en düşük değerler elde edilmiştir. Ancak dayanım açısından değerlendirildiğinde en yüksek dayanım değeri FDM yönteminde 57.67 N/mm² olarak elde edilmiştir.

* Corresponding author, E-mail: mehmetsofu@isparta.edu.tr

To cite this article: M. M. Sofu, H. Varol Özkavak, S. Bacak, M. Fenkli, Comparison of Strength, Surface Quality and Cost of Different Additive Manufacturing Methods, Manufacturing Technologies and Applications, 4(1), 25-36, 2023.

<https://doi.org/10.52795/mateca.1265509>

1. INTRODUCTION (GİRİŞ)

Additive manufacturing (AM), also known as 3D printing, is a technology used in many fields such as aerospace, biomedical, automotive and turbomachinery in the industry. In addition, the AM method is also used in the production of auxiliary elements such as tools, gauges and fasteners used in manufacturing [1]. AM has many advantages such as prototyping for new designs, enabling the manufacturer to be more agile, reducing the time required for innovation, taking direct physical outputs from the digital form, and thus revealing new design ideas. Although many AM techniques have been developed since the 1980s, this technology, whose commercialization has been delayed, has become an important place in the material and service sector after 2016 [2]. The AM method is used in many areas such as sports and musical instruments, lightweight prosthetic legs, dental splints and injection molding. with AM, significant changes are expected in the automotive, aerospace and medical industries [3]. While AM causes a significant decrease in fuel consumption due to the production of complex and light parts for the aviation industry, the patient-specific production with the AM method in the medical industry and the rapidity of this production have made the costs affordable. This is particularly effective in hearing aids, prostheses and surgical guides and models [3]. In the automotive industry, it provides advantages such as shortening the production time of special parts in small groups, increasing the delivery time and saving costs. In addition, many chemical companies and research industries have started to use the AM method for the production of special materials [4]. With the increasing demand for AM manufacturing, AM equipment companies have started to invest heavily in technological innovations. The best example of the innovations made is printing more than one material at the same time using multiple print heads [5,6].

There are many polymer AM techniques for rapid prototyping in industry. These techniques have been examined by ASTM in 7 groups and these are 1. Material extrusion, 2. Powder bed fusion, 3. Vat photopolymerization, 4. Binder spraying, 5. Material spraying, 6. Directed energy deposition and 7. Layer lamination. The common theme between these methods is to produce the 3D part by producing the materials layer by layer. When the methods are considered in general, while the filament is used as the feeding material in the FFF (Fused Filament Fabrication) method; 20-150 μm powder material in SLS (Selective Laser Sintering) method; Liquid resins are preferred in SLA (Steriolithography) method. The comparison for each method is given in Table 1. Figure 1 provides a comparison of technical capabilities for various AM methods.

Table 1. Comparison of different AM techniques [1] (Farklı AM tekniklerinin karşılaştırılması)

Technology	SLS	FDM	MJF	SLA
Category	Powder bed fusion	Materials extrusion	Powder bed fusion	Vat photopolymerization
Feed Stock	Powder	Filament	Powder	Liquid resin
Materials	Metals,thermoplastics,glass,ceramics	Large variety of thermoplastics	Nylon 11 and 12, TPU	Photopolymers
Resolution(microns)	60-150	50-500	21	25
Support (for complex printing)	Not required	Required	Not required	Required
Recyclability	Manual	N/A	Automatic	N/A
Machine Price (USD)	> 250.000	> 200	> 300.000	> 3500

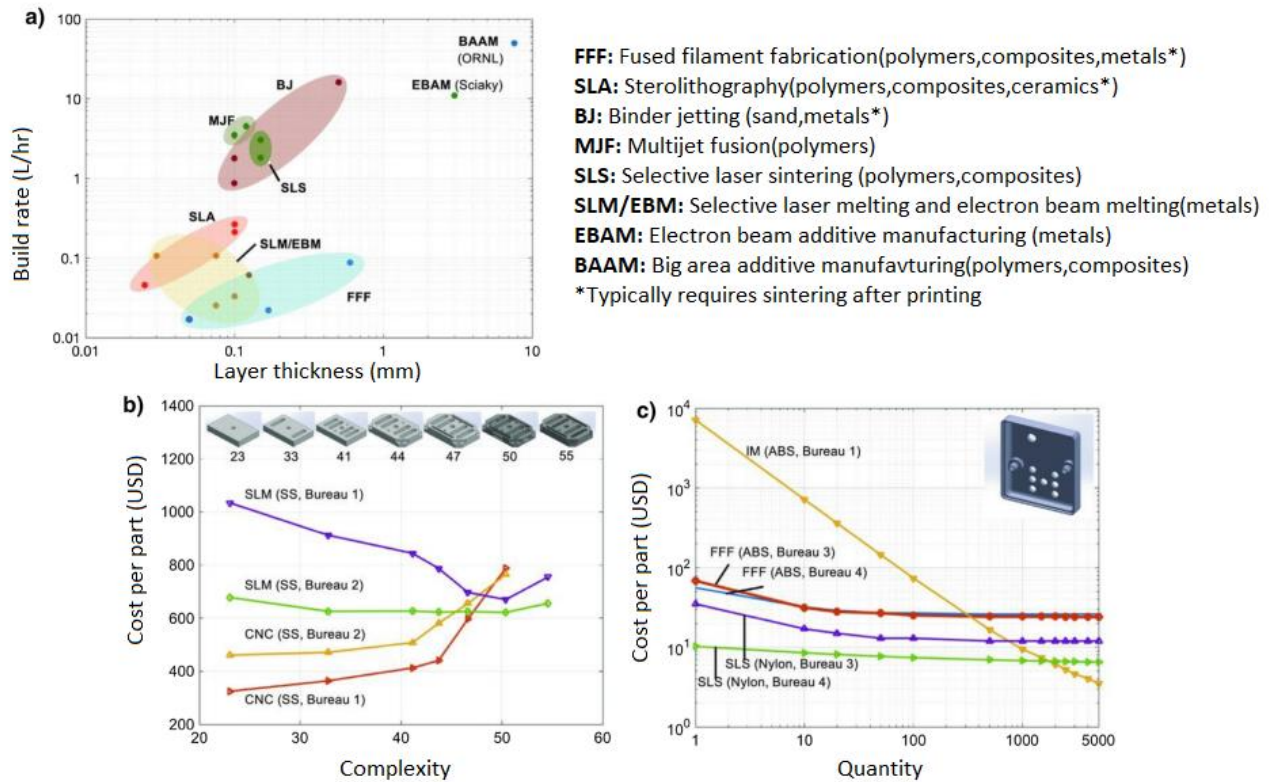


Figure 1. A comparison of technical capabilities for various AM methods [1] (Çeşitli AM yöntemleri için teknik yeteneklerin karşılaştırılması)

Although many materials have been developed for each AM method, certain materials are commonly preferred for each method. For this reason, developing materials for the AM method is currently the subject of studies. FDM rapid prototyping is a widely used AM method for composite component design due to its many superior features such as rapid production and low cost [7]. Compared to other traditional methods, the FDM method has lower mechanical properties due to the porosity that occurs during the printing process. However, for applications in tissue engineering, such as skeletal design, high porosity may provide some advantages. In addition, thanks to the space density control and filament orientation, the customization of the mechanical properties is provided by the FDM method. Considering all these, it is clearly observed that there are many parameters that affect the quality and properties of the part in the FDM method. In the FDM method, the mechanical properties depend on parameters such as filament material property, space density and fiber-to-fiber bond strength [8]. When the studies on the FDM method are examined, the parameters affecting the process quality are determined as nozzle temperature, layer thickness, and raster and structure direction [9]. Es-Saeid et al. In their study, they examined the effect of sheet orientation on mechanical properties. In this Study, it was determined that the best features were obtained at 0° orientation, and the lowest features were obtained at 45° orientation. In addition, it was determined that the breaks were obtained along the layer interface in the study [10]. Maloch et al. They discussed the effect of extrusion nozzle and layer thickness on the mechanical properties of the samples produced from ABS material by the FDM method. The authors concluded in this study that the best properties are obtained at low thicknesses, and that good melting is achieved between adjacent layers with increasing nozzle temperature [11]. Radriquez-Panez et al. examined the mechanical properties of PLA and ABS thermoplastic materials produced by the FDM method. At the end of the study, it was determined that the mechanical properties of the samples produced from PLA material were higher than the samples produced from ABS. It was also determined that ABS showed lower variability [12]. Examining the tensile properties of ABS and PC parts, Cantrell et al. determined that the structure and raster orientation have significant effects on Young's Modulus and Poisson's Ratio. PC samples showed anisotropic behavior [13]. Warnung et al. in their study, used 8

different materials in the FDM method. The authors concluded that the strongest material was obtained in the case of using PA wire, while the hardest material was obtained in the case of using wire made of PET material reinforced with carbon fiber [14]. Valean et al. investigated the effect of process parameters (print direction, layer thickness/size effect) on the tensile properties of PLA material produced by FDM method. In their study, they reached the following results: While the Young's modulus changes 1.8% according to the compression direction; tensile strength changed by more than 8%. In addition, both tensile strength and Young's modulus decreased with increasing layer thickness [15].

Production with SLA is the widely used AM method for polymer materials due to its wide range of properties [16]. Production of parts with high resolution and precision can be expressed as the main advantage of SLA technology [17]. In the SLA method, the pieces are formed by the adhesion of the polymer layers to the previous layer. This situation causes no weakness to occur at the junction of the layers [18]. Jacobs discussed inhomogeneous mechanical properties of SLA models in his work. Through this work, the author determined that the mechanical properties of SLA depend on the function of the laser opener and will reduce the shrinkage that occurs during part fabrication [19]. Mahan and Bayly applied the impact test to SLA samples produced in different directions (XY, YZ, ZX) and the authors obtained the highest strength in the samples produced in the XY plane [20]. Benerjee et al. investigated the effect of post-curing time and layer thickness on the tensile strength of SLA samples. At the end of the study, the authors determined that the tensile strength primarily depends on the layer thickness and the effect of curing time on small parts such as test specimens is low [21]. Chackaligam and Jawahar investigated the effect of layer thickness on mechanical properties in their study. And with these studies, they found that an increase in tensile strength occurs when low layer thickness is selected [22].

Wohlers in this report, SLS is a 3D technology that has found application in many sectors such as hearing aids and Formula 1 vehicles. In addition, in some aircraft, parts produced with the SLS method are used. However, the parts used are limited due to low mechanical properties. For this reason, studies have focused on improving the mechanical properties of the parts produced by the SLS method [23]. Zarringhalam et al. They conducted research on the reproducibility and improvement of the mechanical properties of Nylon 12 material using the SLS method. And at the end of their research, they determined that while an increase in tensile strength was observed with some machine parameters, there was no change in Young's modulus [24].

When the literature is examined, 3D technology has become a technology used in many sectors. It is observed that this technology will be used more widely with the further improvement of mechanical properties. It is seen that literature studies focus on determining the effect of process parameters of SLS, SLA, FDM methods used in 3D technology on strength values. When the reasons for the preference of 3D technology are examined, it is also noteworthy that the costs are low. It is clearly seen that this feature has not been evaluated in the studies carried out. For this reason, one of the focal points of the study has been material cost analysis. For this purpose, samples were produced with SLS, SLA and FDM methods by choosing the optimum process parameters (100 % occupancy rate and low layer thickness) determined in the literature. Manufacturing times were also measured during the production of the samples. Surface roughness and tensile strength of the samples obtained after production were determined. In addition, material cost analysis was performed for each sample. After the experimental studies, strength-cost-production time and surface roughness comparisons were made. Thus, the selection of the method to be used for the part planned to be produced becomes more efficient.

2. MATERIAL AND METHOD (MATERYAL VE YÖNTEM)

2.1. Production of Samples (Numunelerin Üretimi)

In this study, it is aimed to select the appropriate production method by comparing the samples produced using FDM, SLS and SLA methods in terms of strength, surface roughness and material cost. For this purpose, the samples used for mechanical experiments in the study were prepared in

the form of solid models in accordance with ASTM D638-IV standard and then saved in a file with STL extension in a format suitable for slicing software. In all three methods, two samples were produced on each printer at a time in order to calculate and compare the time spent while performing more than one production at the same time. In order to compare the strength values in all three methods, 100% fill density was used. In addition, for each method, the software developed by the manufacturers of the devices belonging to that method was preferred as the slicing software. When placing the samples on the printer table, the same positioning was made for each method in order not to create an imbalance in production time. In addition, the time spent between the start and the finish of production of the printer was recorded in order to determine the production time of the samples in all methods.

2.2. Production by FDM Method (FDM Yöntemiyle Üretim)

In the study, Makerbot brand 5th generation Replicator model three-dimensional printer was used for production by FDM method. The feature of this printer is the use of a special head system with a nozzle diameter of 0.4 mm, which is launched as a smart extruder. Smart extruder provides contact control with a special sensor structure and height optimization in layer thicknesses. In this way, it can reduce the layer thickness to 0.05 mm. Two samples were produced in Makerbot print slicing software with a 0.05 mm layer thickness and 95% (maximum setting) fill density (Figure 2). 1.75 mm diameter PLA+ filament material was used in the production made by FDM. The maximum stress value for the filament of the FDM manufacturer is given as 33 MPa.

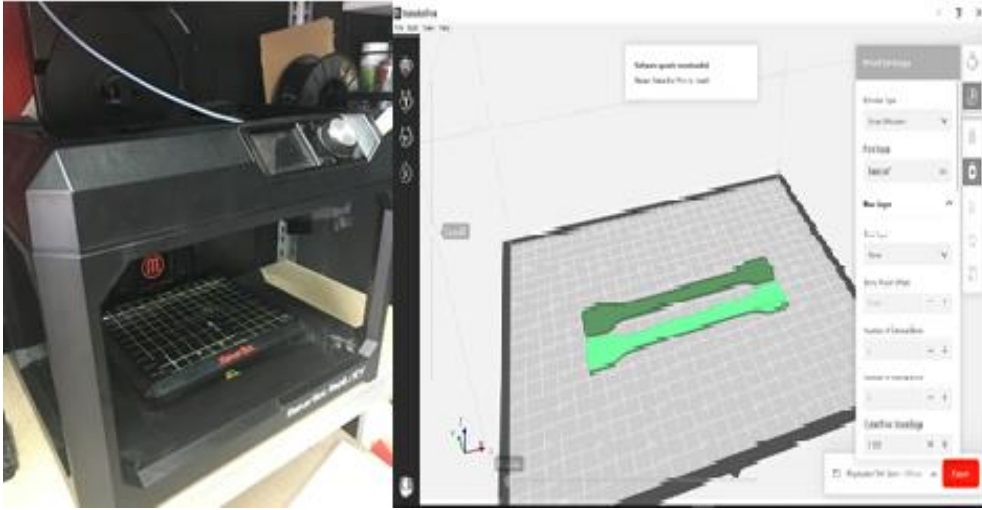


Figure 2. Makerbot printer and MaketBot Print slicing software used in the FDM method (FDM yönteminde kullanılan Makerbot yazıcı ve MaketBot Print dilimleme yazılımı)

2.3. Production with SLA Method (SLA Yöntemiyle Üretim)

Another method used in sample production is the SLA method. For the method, Anycubic brand Photon s model, a three-dimensional printer using 405 nm UV matrix light was preferred (Figure 3). A white photopolymer resin of Anycubic Company was used as the material, which reacts in UV light at a wavelength of 405nm.

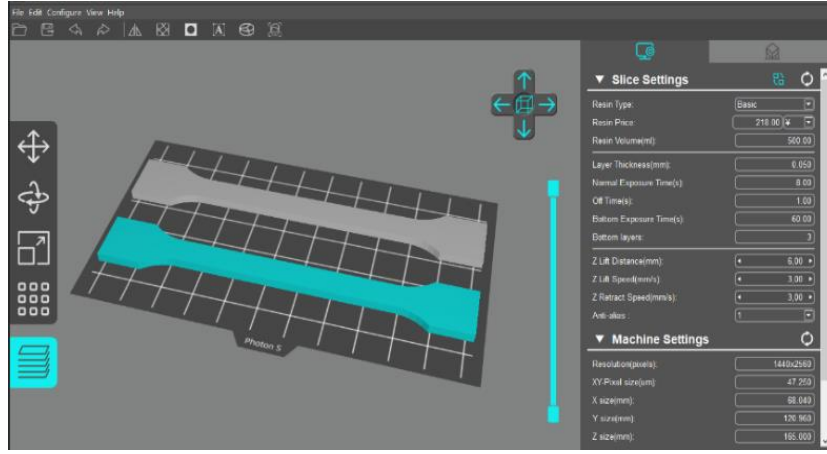


Figure 3. Preparation of samples for the SLA method (SLA yöntemi için numunelerin hazırlanması)

2.4. Production by SLS Method (SLS Yöntemiyle Üretim)

A Sinterit brand Lisa model desktop printer was chosen for the SLS method used in the study (Figure 4). The laser power of the printer is IR Laser Diode 5 W, 808 nm. For production, the temperature of the powder chamber is increased up to 178°C with halogen heaters. In this way, the printer can reach instant melting temperature by using 8W power. The minimum layer thickness of the printer is 0.075 mm.



Figure 4. Sinterit lisa brand printer and production area used in SLS method (SLS yönteminde kullanılan Sinterit lisa marka yazıcı ve üretim alanı)

The material used in the SLS printer is highly nylon; PA 12 is a nylon-based powder sold in smooth form. The tensile strength of the polyamide powder is 32 MPa, the breaking elongation is 10 %, the melting point is 185 °C and the grain size of the powder is between 18 – 90 µm. Two samples in ASTM D638-IV standard were produced with 0.075 mm layer thickness with Sinterit studio slicing software in Figure 5. Not all of the powder was used as new powder during production. In accordance with the process proposed by the company, the production was carried out by mixing 26% new powder with the previously used powder mixture.

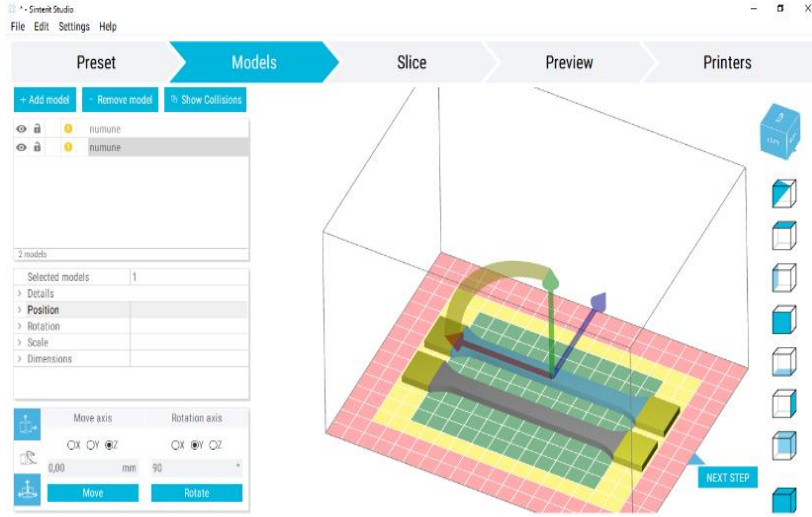


Figure 5. Positioning of samples in Sinterit studio slicing software (Sinterit studio dilimleme yazılımında örneklerin konumlandırılması)

2.5. Surface Roughness Measurement (Yüzey Pürüzlülüğü Ölçümü)

The surface roughness measurements of the samples produced horizontally on the table in three different methods selected for the study were determined by measuring from three different regions perpendicular to the layer formation directions. The measurement was made at two different points on the surface with the Hommel Verke Tester T500 device. The sampling length (L_c) was taken as 0.25 mm, the measuring length (L_m) 1.25 mm ($5.L_c$) and the traverse length (L_t) 1.5 mm. The measuring device gives the roughness values (R_a) in μm . This device measures R_a surface roughness parameter according to ISO 4287/1 standard.

2.6. Tensile test (Çekme testi)

In the study, it is aimed to compare the tensile strength values of the samples produced separately using three methods. Tensile tests were applied to the samples produced for this purpose as in Figure 6.



Figure 6. Tensile test and deformation (Çekme testi ve deformasyon)

Tensile tests applied to the samples were carried out in a 10KN capacity Shimadzu AGS-X brand electromechanical static test device at a tensile speed of 1 mm/min and at room temperature. The dimensions of the tensile test specimens produced in the ASTM D638-IV standard for the study are given in Figure 7.

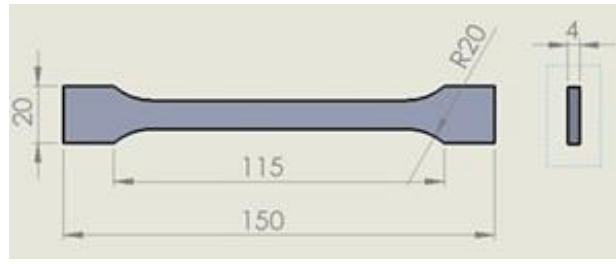


Figure 7. Tensile specimens produced in accordance with ASTM D638-IV standard used in the study (Çalışmada kullanılan ASTM D638-IV standardına uygun olarak üretilmiş çekme numuneleri)

3. RESULTS (SONUÇLAR)

In the study, it is aimed to compare the strength, surface roughness and cost of the samples produced using SLA, SLS and FDM methods, and thus to choose the most efficient method.

Surface roughness is a key property for additive manufacturing methods. The preparation of the product according to its finish properties is important for the surface roughness value. Selecting the appropriate material, working conditions and method for rapid prototyping technology has a significant effect on achieving the targeted surface roughness and extending the service life during operation. It is expected that the surface roughness of the post-production parts will be low as in other methods. Since it is a key feature for additive manufacturing and affects the service life of the produced part, surface roughness examinations of the samples produced for each method were made in the study. The results obtained as a result of the measurements are given in Table 2. When Table 2 is examined, the lowest roughness values are 1.97 μm and 2.16 μm in SLA samples; the highest roughness values were obtained as 14.68 μm and 15.63 μm in the samples produced using the FDM method.

Table 2. Surface roughness measurement results (Yüzey pürüzlülüğü ölçüm sonuçları)

Measurement (μm)	FDM	SLA	SLS
1.	14.68	1.97	8.73
2.	15.63	2.16	6.8

Sample weight is important in terms of sample cost. For this reason, the weights of the produced samples were measured using precision balances and the obtained values are given in Table 3.

Table 3. Weights of manufactured parts (Üretilen parçaların ağırlıkları)

PLA +	PA 12 smooth	Resin
9.518 gr	6.992gr	9.642gr

In the parts manufactured with the additive manufacturing method, it is required to have high strength values, as in the production using other methods. Many studies have been carried out in order to obtain the desired strength values and are still in progress. In this study, it is aimed to compare the methods in terms of tensile strength as well as material cost analysis. For this purpose, samples with 100% filling ratio were produced by PA12 for SLS method; using PLA for the FDM method and resin material for the SLA method. The produced samples were subjected to tensile test. The maximum stress, elongation and breaking elongation values of the samples after the test are given in Table 4 and the graphics are given in Figure 8. When the table is examined, the highest maximum stress value of 56.67 MPa was obtained in the FDM method using PLA material. The lowest stress value was determined as 21.45 MPa in the samples produced by the SLA method. The maximum tensile value of the samples produced by the SLS method was obtained (21.78 MPa), which is very close to the SLA samples. However, the maximum elongation values of the samples produced by the SLS method are approximately 4.7 times that of the samples produced using the SLA method. This is an expected result and is a result of the characteristics of PA12 material. PA12 material exhibits high straining specialty in tensile strength.

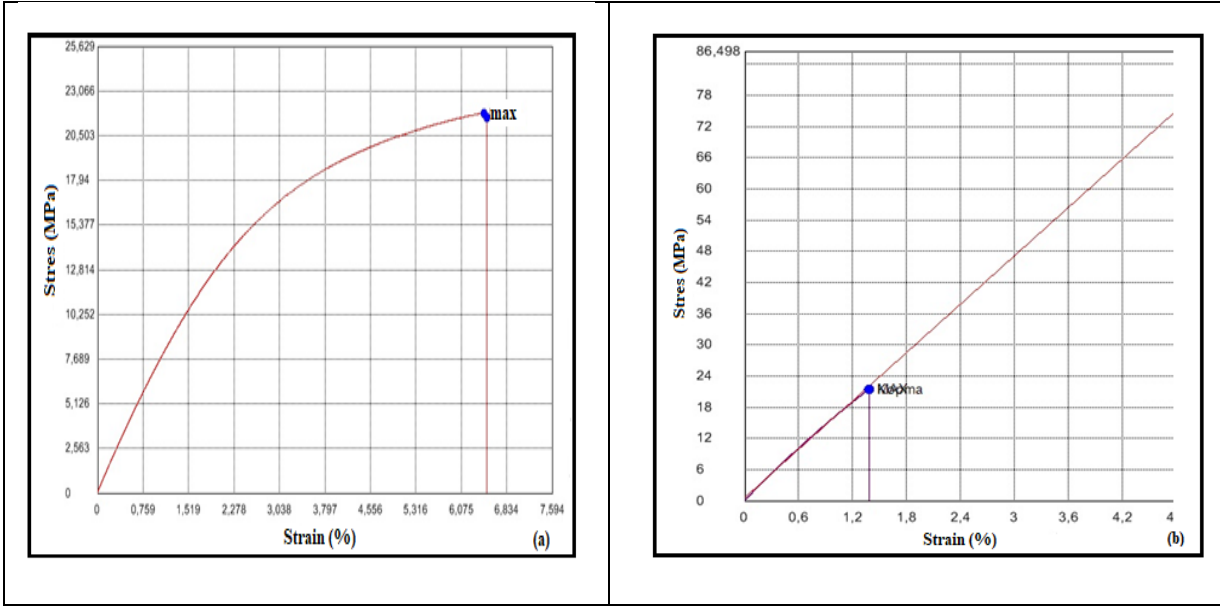


Figure 8. Stress-strain graphs of test specimens (a) PA12sample (b) resin sample (Test numunelerinin gerilim-uzama grafikleri (a) PA12 numunesi (b) reçine numunesi)

Table 4. Tensile test values obtained from the samples (Numunelerden elde edilen çekme testi değerleri)

Production Method (Material)	Maximum Stress (N/mm ²)	Maximum Elongation (mm)	Breaking Sensitivity (%)
SLS (PA12)	21.78	5.81	6.5
FDM (PLA+)	57.67	2.96	4.16
SLA (Rosin)	21.45	1.24	1.38

3.1. Comparison in terms of cost and time (Maliyet ve zaman açısından karşılaştırma)

3.1.1. SLA

The production time for the UV light sourced SLA printer took 17 minutes in total. And a total of 6.930 ml of liquid resin was consumed. The price of Anycubic brand resin (1000 ml white material) on amazon.com was determined as \$ 28.09, and the unit price was calculated as \$0.028 /ml in ml. The weight of the sample prepared for the test is 9.642 gr. However, the value of the material used in ml determined by the software is 6.930 ml. According to this result, the price of the test sample was found to be \$ 0.19.

3.1.2. FDM

The production time in the FDM method took 2 hours and 59 minutes. The production temperature was realized at 205 °C. Esun brand red 1kg 1.75 mm filament value is sold on amazon.com for \$ 22.99. The unit price of the filament is calculated as \$ 0.023 /gr. Sample total weight was measured as 9.518 g. According to this result, the material cost of the sample produced with filament is calculated as \$ 0.22.

3.1.3. SLS

Total production time is 5 hours 56 minutes. The printer took approximately 2 hours and 15 minutes to preheat the powder in the powder chamber (175°C). The manufacturing time took 2 hours and 32 minutes. 1 hour and 12 minutes of cooling time was spent. A total volume of 16.5 cm³ powder was used. Sinterit PA12 Smooth V2 Fresh Powder 2 kg powder can be accessed from the commercial site called imakr for \$ 340. According to this price, the unit price is \$ 0.17/gr. Since the weight of the test sample that came out of production is 6.992 gr, the cost of only this test sample was calculated as \$ 1.188.

4. CONCLUSIONS (SONUÇLAR)

When the materials produced with three different methods are evaluated in terms of tensile strength, breaking elongation, surface roughness and material cost. Comparative preparation of the data of all results is given in Table 5.

Table 5. Comparative results of additive manufacturing methods (Eklemeli imalat yöntemlerinin karşılaştırmalı sonuçları)

Feature	FDM	SLA	SLS
Material	PLA +	UV resin 405nm	PA 12 smooth
Weight (g)	9.518	9.642	6.992
Surface roughness (μm)	14,68 - 15,63	1,97-2,16	8,73 - 6,8
Production time	2 hours 59 minutes	17 minutes	5 hours 56 minutes
Fullness	% 100	% 100	% 100
Strength (N/mm²)	57.67	21.45	21.78
Production cost (material)\$	0,22	0,19	1,188
Machine Price	\$ 1999	\$ 239	Desktop SLS \$ 8568

In this study, the fastest printing method is the SLA method. The ability of the system using UV light curing technique to print more than one part in the same time on the same layer causes it to be quite good at printing speed. On the other hand, in the SLS method, there is no bad surface formation due to the support of the parts produced thanks to manufacturing in powder without the need for support. In addition, in the SLS method, movable mechanisms can be produced as assembled very easily.

The highest tensile strength was measured at 57.67 MPa in the sample produced from PLA+ material, while the values were close to each other (21.45 MPa, 21.78 MPa) in the samples produced from resin and PA12 materials.

While the highest value of elongation at break was 6.5% in the samples produced from PA12 material, the lowest value was observed in the samples produced from Resin with 1.38 %.

The order of the surface roughness from the lowest to the highest was obtained from the samples produced from Resin - PA12 - PLA+ materials and their average values are respectively measured 2.06-7.76-15.15 μm . Burke et al., as a result of their work to obtain the best surface quality printing with PLA material, obtained the best surface roughness value of 12.4 μm (0.2 mm) by printing in a flat direction using a 0.2mm nozzle diameter with a 5% core fill rate [25]. M. Launhardt et al., used the optical measurement method on the parts printed with the SLS method using PA12 material and found the best result as 13 μm [26]. Pazhamanil et al., using vegetable-based liquid resin, measured the surface roughness on different samples printed with a DLP printer and obtained Ra values in the range of 0.67 μm to 2.7 μm [27]. This shows us that it coincides with the surface roughness values obtained in the literature. Even better results were obtained for parts produced for SLS.

In terms of material cost, the most affordable sample was obtained from resin material with \$ 0.19, and the most expensive one was obtained from PA12 material with \$ 1.88. The results obtained are in agreement with the literature [28].

Although the production with the SLS method seems more disadvantageous when evaluated in terms of all parameters, it is one of the advantages of this method to be able to produce without the need for support staff during manufacturing.

In production with the SLA method, partially unsupported manufacturing is also carried out. In addition, the production of the parts on the workbench, regardless of the number of pieces, can be realized in the same time and low surface roughness are among the advantages of production.

Considering the weights in the study, it also sheds light on studies involving specific strength, also known as strength-to-weight ratio or strength-to-weight ratio or strength-to-mass ratio. Specific strength is widely used in other applications, particularly in aerospace, where the weight savings are worth the higher material cost.

REFERENCES (KAYNAKLAR)

1. H. Wu, W.P. Fahy, S. Kim, H. Kim, N. Zhao, L. Pilato, A. Kafi, S. Bateman, J.H. Koo, Recent developments in polymers/polymer nanocomposites for additive manufacturing, *Progress in Materials Science*, 111:100638, 2020.
2. X. Wei, D. Li, W. Jiang, Z. Gu, X. Wang, Z. Zhang, Z. Sun, 3D Printable Graphene Composite, *Scientific Reports*, 5(1):11181, 2015.
3. D. Küpper, W. Heising, G. Corman, M. Wolfgang, C. Knizek, V. Lukic, Get ready for industrialized additive manufacturing, *Digit. Bost. Consult. Gr.* 1–15, 2019.
4. S. Gantenbein, K. Masania, W. Woigk, J.P.W. Sesseg, T.A. Tervoort, A.R. Studart, Three-dimensional printing of hierarchical liquid-crystal-polymer structures, *Nature*, 561: 226–230, 2018.
5. Gnanasekaran, K., Heijmans, T., van Bennekom, S., Woldhuis, H., Wijnia, S., de With, G., Friedrich, H., 3D printing of CNT- and graphene-based conductive polymer nanocomposites by fused deposition modeling. *Appl. Mater. Today*, 9: 21–28, 2017.
6. K. Kim, J. Park, J. Suh, M. Kim, Y. Jeong, I. Park, 3D printing of multiaxial force sensors using carbon nanotube (CNT)/thermoplastic polyurethane (TPU) filaments, *Sensors Actuators, A Phys.* 263:493–500, 2017.
7. T.D. Ngo, A. Kashani, G. Imbalzano, K.T.Q. Nguyen, D. Hui, Additive manufacturing (3D printing): A review of materials, methods, applications and challenges, *Composite Part B: Engineering*, 143:172-196, 2018.
8. S. Garzon-Hernandez, D. Garcia-Gonzalez, A. Jérusalem, A. Arias, Design of FDM 3D printed polymers: An experimental-modelling methodology for the prediction of mechanical properties, *Materials and Design*, 188, 108414, 2020.
9. D.I. Stoia, E. Linul, L. Marsavina, Influence of manufacturing parameters on mechanical properties of porous materials by selective laser sintering, *Materials (Basel)*, 12 (6):871, 2019.
10. Es-Said, O.S., Foyos, J., Noorani, R., Mendelson, M., Marloth, R., Pregarer, B.A., Effect of layer orientation on mechanical properties of rapid prototyped samples. *Mater. Manuf. Process*, 15: 107–122, 2000.
11. J. Maloch, E. Hnátková, M. Žaludek, P. Krátký, Effect of processing parameters on mechanical properties of 3D printed samples, *Mater. Sci. Forum*, 919: 230–235, 2018.
12. A. Rodríguez-Panes, J. Claver, A.M. Camacho, The influence of manufacturing parameters on the mechanical behaviour of PLA and ABS pieces manufactured by FDM: A comparative analysis, *Materials (Basel)*, 11(8), 1333, 2018.
13. S. Rohde, J. Cantrell, A. Jerez, C. Kroese, D. Damiani, R. Gurnani, L. DiSandro, J. Anton, A. Young, D. Steinbach, P. Ifju, Experimental Characterization of the Shear Properties of 3D-Printed ABS and Polycarbonate Parts, *Exp. Mech.*, 58: 871–884, 2018.
14. L. Warnung, K. Landsteiner, S.E. Karl, L. Privatuniversität, A. Reisinger, K. Landsteiner, Mechanical Properties of Fused Deposition Modeling (FDM) 3D Printing Materials, *RTEjournal-Fachforum für Rapid Technologien*, 1–18, 2018.
15. Vălean, C., Marşavina, L., Mărghitaşl, M., Linul, E., Razavi, J., Berto, F., Effect of manufacturing parameters on tensile properties of FDM printed specimens, *Procedia Structural Integrity*, 313–320, 2020.
16. J.R.C. Dizon, A.H. Espera, Q. Chen, R.C. Advincula, Mechanical characterization of 3D-printed polymers, *Additive Manufacturing*, 20:44-67, 2018.
17. X. Wang, M. Jiang, Z. Zhou, J. Gou, D. Hui, 3D printing of polymer matrix composites: A review and prospective, *Composites Part B: Engineering*, 110: 442-458, 2017.
18. J.S. Saini, L. Dowling, J. Kennedy, D. Trimble, Investigations of the mechanical properties on different print orientations in SLA 3D printed resin, *Proc. Inst. Mech. Eng. Part C J. Mech. Eng. Sci.*, 234: 2279-2293, 2020.
19. P.F. Jacobs, *Rapid Prototyping and Manufacturing, Fundamentals of Stereolithography*, Society of Manufacturing Engineers, Dearborn, MI, 1992.
20. Mahn, J.P., Bayly, P. V., Impact testing of stereolithographic models to predict natural frequencies, *Journal of Sound and Vibration*, 224(3): 411-430, 1999.
21. Benerjee A. Sinha., Shekar K. P. Roy, Benerjee M.K., A study of SLA process parameter over strength of built model, National level symposium on Rapid Prototyping & Tooling, Vol 1, Proceedings of the 2nd National Symposium on Rapid Prototyping & Rapid Tooling Technologies, 2002.
22. Chockalingam, K., Jawahar, N., Chandrasekhar, U., Influence of layer thickness on mechanical properties in stereolithography, *Rapid Prototyping Journal*, 12(2): 106–113, 2006.

23. T. Wohlers, Wohlers report, Wohlers Associates. Inc. Fort Collins, CO, USA, 2007.
24. H. Zarringhalam, N. Hopkinson, N.F. Kamperman, J.J. Vlieger, Effects of processing on microstructure and properties of SLS Nylon 12. *Mater. Sci. Eng. A*, 435-436: 172-180, 2006.
25. Burke, C., Dalal, A., Abukhalaf, A., Noorani, R., Effects of process parameter variation on the surface roughness of Polylactic acid (PLA) materials using design of experiments (DOE). In *IOP Conference Series: Materials Science and Engineering*, 897(1): 012003, 2020.
26. M. Launhardt, A. Wörz, A. Loderer, T. Laumer, D. Drummer, T. Hausotte, M. Schmidt, Detecting surface roughness on SLS parts with various measuring techniques, *Polymer Testing*, 53: 217-226, 2016.
27. R.V. Pazhamannil, H.M. Hadidi, G. Puthumana, Development of a low-cost volumetric additive manufacturing printer using less viscous commercial resins, *Polym. Eng. Sci.*, 63(1):65, 2023.
28. D. Thomas, W.G. Stanley, Costs and Cost Effectiveness of Additive Manufacturing A Literature Review and Discussion, NIST Special Publication, 2014.

Investigation of the Effect of Vulcanization Time on Belt Strength

Tuğçe DANIŞMAN ÇEBİ^{1,2} , Recep DEMİRSÖZ² , Mehmet Tayyip ÖZDEMİR² , Ahmet Emrah ERDOĞDU¹ 

¹Karabük University, Faculty of Engineering, Mechanical Engineering Department, Karabük, Turkey
²KARDEMİR Karabük Iron Steel Industry Trade & Co. Inc., Karabük, Türkiye

ARTICLE INFORMATION

Received: 03.04.2023
Accepted: 24.04.2023

Keywords:

Vulcanization
Splicing
Conveyor belt
Strength

ABSTRACT

In today's technology, the power of mechanization has emerged in places where manpower is insufficient in order to meet the increasing needs at many facilities. With belt conveyor systems, it has become much easier to transport the material from one site to another in the facilities in terms of time, distance, and capacity. Since belt conveyors are a reliable and cost-effective system in material handling, the quality of the belt used should be carefully determined. It is important that the wear and tear that occurs on the belt over time is repaired quickly and effectively in order not to prolong the downtime in the plant. A small damage detected needs to be repaired immediately so that it does not cause bigger problems. In this study, vulcanization time, which is one of the parameters affecting the belt strength in belt splice made by vulcanization method, is discussed. By studying the effect of time on belt strength, it is aimed to extend the life of the belt splicing area. According to the test results, it has been observed that the increase in vulcanization time has a positive effect on the tape strength and the usage of welding machine saves time in terms of faster use of the tape in the facility.

Vulkanize Kaynak Süresinin Bant Mukavemetine Etkisinin Araştırılması

MAKALE BİLGİSİ

Alınma: 03.04.2023
Kabul: 24.04.2023

Anahtar Kelimeler:

Vulkanizasyon
Birleştirme
Konveyör bandı
Mukavemet

ÖZET

Günümüz teknolojisinde birçok tesiste artan ihtiyaçları karşılamak amacıyla insan gücünün yetersiz kaldığı yerlerde makineleşmenin gücü ortaya çıkmıştır. Konveyör sistemleri ile tesislerde malzemenin bir noktadan diğer bir noktaya taşınması zaman, mesafe ve kapasite yönüyle çok daha kolay hale gelmiştir. Bantlı konveyörler, malzeme taşımada güvenilir ve maliyet açısından da avantajlı bir sistem olduğundan kullanılan bandın kalitesinin itina ile seçilmesi gerekmektedir. Zamanla bantta meydana gelen yıpranma ve aşınmaların, tesiste duruş süresini uzatmamak adına çabuk ve etkili bir şekilde tamir edilmesi ve tespit edilen küçük bir hasarın daha büyük sıkıntılara yol açmaması için derhal onarım yapılması önemlidir. Bu çalışmada, vulkanize kaynak yöntemi ile yapılan bant birleştirmelerinde bant dayanımına etki eden parametrelerden biri olan vulkanizasyon süresi ele alınmıştır. Sürenin, mukavemete olan etkisi incelenerek bant ek yerlerinin ömrünü uzatmak amaçlanmıştır. Yapılan çalışmada, bantlı konveyörlerin genel özellikleri, bantlı konveyör çeşitleri, bant yapısı ve özellikleri, vulkanizasyon tanımı, vulkanize kaynak yöntemi ile birleştirme işlem adımları ve farklı sürelerde uygulanan vulkanizasyonun etkisini incelemek amacıyla yapılan deney çalışmalarından bahsedilmiştir. Test sonuçlarına göre vulkanizasyon süresindeki artışın bant mukavemetine olumlu etki yaptığı ve kaynak makinesi kullanımının bandın tesiste daha hızlı kullanılması açısından zamandan tasarruf sağladığı gözlemlenmiştir.

* Corresponding author, E-mail: aemraherdogdu@karabuk.edu.tr

To cite this article: T.D. Çebi, R. Demirsöz, M.T. Özdemir, A.E. Erdoğan, Investigation of the Effect of Vulcanization Time on Belt Strength, Manufacturing Technologies and Applications, 4(1),37-48, 2023.

<https://doi.org/10.52795/mateca.1276153>, This paper is licensed under a CC BY-NC 4.0

1. INTRODUCTION (GİRİŞ)

The endless belt conveyor system is one of the most important systems that English engineer Lyster found in 1868 and is still used in material handling today. Conveyors are continuous transfer systems that can operate in a closed loop, allowing the materials to be transported from the air or from the ground, and the continuity of the material transmission is one of the most effective parameters in the business economy [1,2]. Today, belt systems can generally operate up to distances of 20-30 km, and the longest operating system since 1970 is 100 km long [3].

Belt conveyors represent an endless belt between two tensioned pulleys, fixed with rollers. Belt conveyors provide the most suitable and economical solution when material transport is carried out over long distances and at large capacities. These conveyors, which play a role in the transport of all kinds of dry and wet materials, have an important application area, especially in the transport of bulk materials such as ore, grain, sand, and coal. The conveyed material is carried by a belt driven by one or more drums [1]. Conveyor belts are equipment that wraps the entire facility like blood vessels in the human body and delivers the needed material to the desired location at the desired time [4].

The weakest points of belt conveyors operating at long distances and high capacities are splice. For the long-lasting use of the belts, high quality and correctly applied splice are important [5]. The costliest component in conveyor belts is the belt itself. Correct operation of the system is important for reliability. During the operation of the conveyor, the belt is exposed to many varying loads. Materials carried along the conveyor line while in the loading and unloading cycle cause wear on belt covers, roller assemblies and cleaning systems. Another factor in the wear of rubber and belt is environmental conditions. All the factors mentioned cause natural wear and tear of the belt. The wear process varies depending on the working conditions and the selection of the belt suitable for these conditions. Belt wear is also affected by compliance with operating conditions. In order to prevent wear, it is necessary to follow the operating conditions of the conveyor (especially loading the belt along the axis of the conveyor, not overloading, ensuring sufficient initial tension). The strength of the splice should be suitable for the working conditions since the wear can occur mostly at the belt splice, which is the weakest point of the belt conveyors. The strength of the splice depends on the splicing method used and the quality of the attached part. Belt bonding or hot-cold bonding with the vulcanization method is the most suitable solution to provide the best strength and durability [6,7]. Today, mechanical splicing (attachment) method, cold splicing method, and hot splicing (vulcanization) methods are used in the splicing process of rubber conveyor belts. If the tensile strength of these belts is 100 %, this value decreases to 35-45 % when fixed with mechanical attachment, to 65-75 % when fixed with cold splicing, and to 75-80 % when bonded with vulcanization. As can be seen, the weakest point of the belt is the junction points [8-10]. Vulcanization and mechanical attachment methods are applied all over the world. Especially in North America, mechanical attachment of the belt is more common, while vulcanization is more common outside of North America.

Soyubol investigated the parameters affecting the static and dynamic properties of elastomer materials and revealed that parts with different properties can be obtained by changing the vulcanization parameters. In the measurements obtained by changing the vulcanization times, it was observed that the change in elongation at break with the increase of the firing time and the elastomer type were an important factor for this change. The rupture and elongation values of EPDM and NR raw material specimens cured at 175 °C for 6 and 8 minutes were investigated [11]. Hardygora et al., in their study on the analysis of splice in conveyor belts, showed that the strength loss can vary between 30 % and 45 % depending on the coefficient, that the strongest splice can be made between belts with the same strength characteristics, and that the tests performed at the Wrocław University of Technology Belt Transport Laboratory (LTT) showed that by reducing the layers spliced by hot vulcanization, the middle layers can be shorter than the outer splice without losing the strength of the splice [6]. Şahbaz, when examining the test specimens taken from the same points of the conveyor belts after the hot press bonding and cold vulcanized bonding process, determined that the shear stress values were 2070 N in the hot press bonding process and 2920 N in

the cold vulcanized bonding process, with the obtained result, it has been shown that the cold vulcanized bonding developed can be applied to the hot press bonding zone [12]. Zhaoxiang et al., in their study, to examine the effects of vulcanization on the rubber gasket, a modeling showing the stress-strain relationship taking into account thermal expansion, cold shrinkage and shrinkage was created. A temporary analysis method was developed for the thermal-mechanical-chemical bonding of the process from rubber gasket vulcanization to mold opening, and dimensional changes of the rubber gasket in the mold and after cooling were predicted. The research results showed that an increase in the vulcanization temperature causes an increase in the dimensional shrinkage of the gasket. As the vulcanization temperature increased from 165 °C to 185 °C, the dimensional shrinkage rate increased non-linearly from 3.2 % to 3.8 %. The vulcanization molding time causes a greater seal shrinkage, which may be associated with the high elastic modulus of the rubber, which limits the release of thermal stress, for example, for the curing temperature of 175 °C, the dimensional shrinkage rate increased by 0.206 % for every 1 % increase in shrinkage caused by the vulcanization reaction [13]. Chen et al., prepared the ZnS (Zinc Sulfide) film by vulcanization at 440 °C for 2, 4, 6 and 8 hours in a sulfur vapor atmosphere. The crystal structure, surface morphology, microscopic defects and optical properties of the specimens were measured retrospectively by XRD, SEM, slow positron beam, Doppler expansion spectroscopy and UV visible spectrophotometer. The results showed that the vulcanization time had a significant effect on the crystallinity and optical properties of the specimens, and the crystallinity of the specimens increased as the vulcanization time increased. However, excessive vulcanization time weakened the crystallinity of the specimen. It was determined that the crystallinity of the specimens was the best and the belt gap value was 3.49 eV (electronvolts) during the vulcanization period of 6 hours. The optimum vulcanization time at 440 °C was found by investigating the vulcanization time, and the properties of the ZnS film prepared by low temperature vulcanization were optimized and potentially used in various optoelectronic devices [14].

In this study, it was aimed to examine in detail the splicing steps of the belt conveyors used in industrial facilities with the vulcanization method in the belts that break as a result of the wear that occurs over time. Unlike the literature, a vulcanized welding machine with different properties was used and the splicing effect of vulcanization time was investigated. In addition, it was objective to determine the most appropriate time to be applied in the facilities by investigating the effect of the vulcanization time on the belt strength.

2. EXPERIMENTAL STUDIES (DENEYSSEL ÇALIŞMALAR)

In our study, the effect of the welding time on the belt strength during the assembly of the conveyor belts used in the Kardemir A.Ş Sinter Directorate facility with the vulcanized welding method is examined. EP800-1000-5-6/3 mm A-type wear-resistant belt is used as the conveyor belt. This belt with a capacity of 1000 t/h is used during the transmission of material transfer between facilities at the facility and carries sinter, coke powder, lime powder and ore materials. The TS EN ISO 283 standard is used in the vulcanized welding method for the conveyor belt we use. This standard describes the test method to determine the elongation at break of textile fabric conveyor belts. It is desired that the tensile test device is capable of elongation at a constant rate of (100 ± 10) mm/min uninterrupted. In addition, as can be seen in Figure 1, it is recommended to use transverse serrated jaws in the device [15].

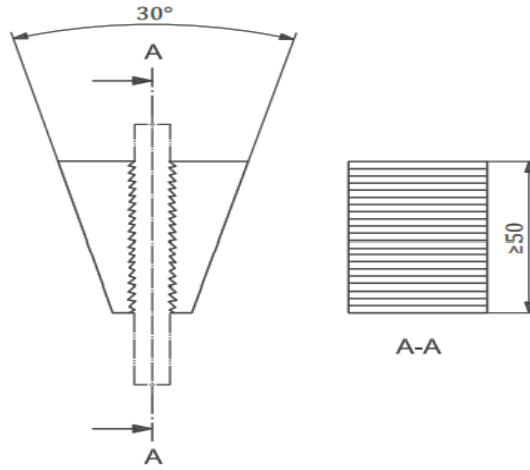


Figure 1. The serrated jaws of the tensile tester device [10] (Çekme test cihazının tırtıklı çeneleri).

2.1. Specimen Preparation (Numune Hazırlama)

In order to prepare the vulcanization specimens (Figure 2), first of all, belt cutting was performed. After the belt was cut, the opening process was applied and the cleaning process was carried out on the opened floors. Adhesive vulcanized belt solution was applied to the cleaned surfaces. After this process, intermediate rubber is positioned between the stages. This promotes better adhesion of the rubber belt to each other. Then, the sleepers were divided into two parts and the lower part of the belt was placed on the upper part of the lower sleeper, and the other part of the belt was placed on the upper sleeper. In the last stage, two belts were pressed by applying force at the determined pressure and temperature value, during the planned time.

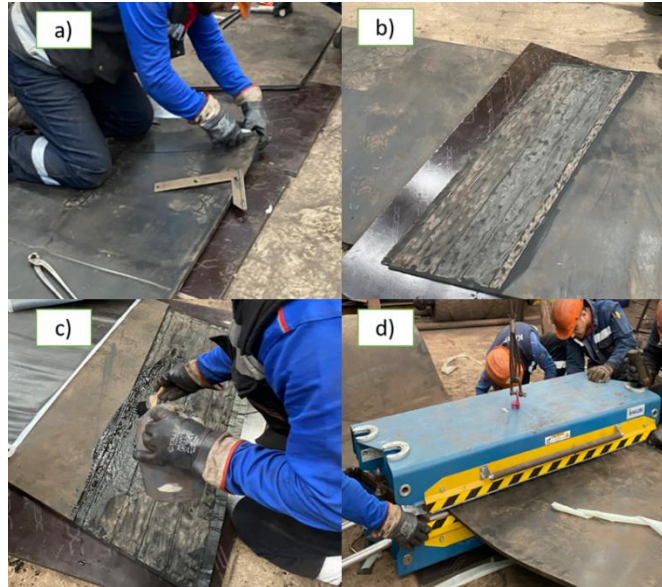


Figure 2. Preparation of vulcanization specimen processes, a) Cutting b) Opening c) Solution coating d) Pressing.

The vulcanization process was carried out on the belt specimens, which will be subjected to tensile testing, at the times given in Table 1. A total of 12 specimens were prepared, 3 specimens each for 15, 30, 45 minutes, and 3 specimens for the untreated belt, with the vulcanization temperature fixed at 145 °C. According to ISO 37, the specimens were cut according to the bow tie apparatus [16]. The cutting process was carried out using the B Type template in the TS EN ISO 283 standard. Specimens were cut from the inside of the belt lengthwise, 50 mm from the edges. All specimens were subjected to tensile testing until rupture occurred. Type B bow tie specimen apparatus is shown in Figure 3.

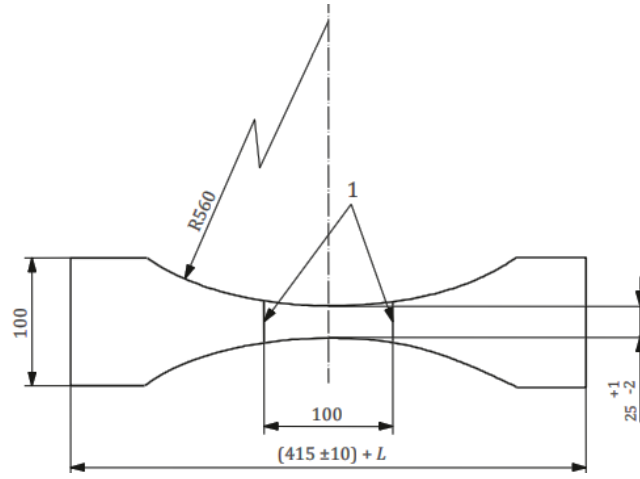


Figure 3. Type B bow tie apparatus [10].

Table 1. Vulcanization time and number of prepared specimens (Vulkanizasyon süresi ve hazırlanan numune sayısı).

Specimen Name	Number of Specimens	Vulcanization Time	Vulcanization Temperature
Untreated Belt Specimens			
N-1,2,3	3 specimens	Original Unspliced Belt	Original Unspliced Belt
Specimens Prepared by Water Cooled Welding Machine			
S-15-1,2,3	3 specimens	15 Minutes	145 °C
S-30-1,2,3	3 specimens	30 Minutes	145 °C
S-30-1,2,3	3 specimens	45 Minutes	145 °C

Specimen pictures prepared by cutting according to Type B bow tie apparatus at different vulcanized welding times are as follows (Figure 4, Figure 5, Figure 6, Figure 7).

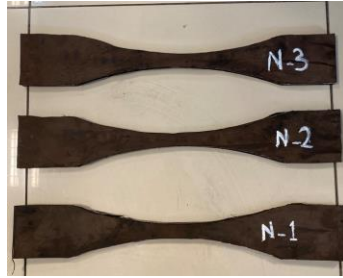


Figure 4. Untreated belt specimens (İşlenmemiş bant numuneleri).



Figure 5. Specimens prepared according to the vulcanization time of 15 minutes (15 dakikalık vulkanizasyon süresine göre hazırlanan numuneler).



Figure 6. Specimens prepared according to the vulcanization time of 30 minutes (30 dakikalık vulkanizasyon süresine göre hazırlanan numuneler).



Figure 7. Specimens prepared according to the vulcanization time of 45 minutes (45 dakikalık vulkanizasyon süresine göre hazırlanan numuneler).

2.2. Tensile Test (Çekme Testi)

In the tensile test, jaw positions for Type B template were adjusted according to the size of 415 ± 10 mm. Width for each specimen is 1000 mm, number of cloth coatings is 5, top coating thickness is 6 mm, bottom coating thickness is 3 mm, total thickness is 16 mm. The test specimen was fixed by placing it between the jaws. The dimensions required to start the tensile test (diameter of the specimen, thickness and width) are defined. After the finished test, all the detected test results were obtained in the test software program. Likewise, these processes were repeated for all other specimens and separate data were obtained for each specimen. The sample specimens picture of the experiments performed is shown in Figure 8.

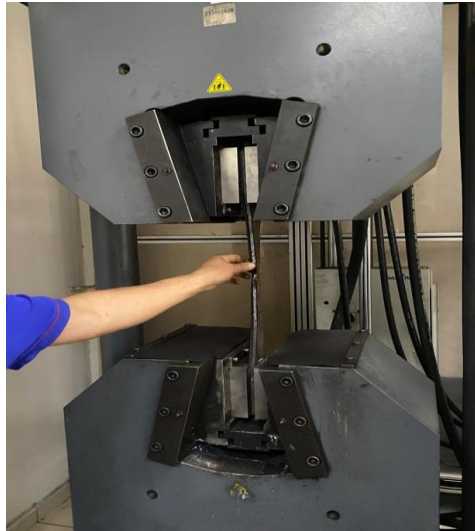


Figure 8. Tensile test applied to a vulcanized welded specimen (Vulkanize kaynaklı numunesine uygulanan çekme testi).

3. EXPERIMENTAL RESULTS AND DISCUSSION (DENEYSSEL SONUÇLAR VE TARTIŞMA)

The maximum force generated during the tensile test is divided by the width of the test specimens. The arithmetic average of these values, which were found for a total of 12 belt specimens, of which 3 original unspliced belt specimens and 3 each prepared according to the

vulcanization time of 15, 30, 45 minutes with a water-cooled vulcanized welding machine, were taken. Accordingly, the breaking strength of the belt is expressed as Eq.1, with F_{max} breaking strength being the narrowest width of the belt D_0 .

$$\sigma_T = \frac{F}{A_0} \left(\frac{N}{mm^2} \right) \quad (1)$$

The tensile strength test results of untreated belt specimens are shown in Table 2, the rupture-elongation diagram in Figure 9, and the rupture photograph of specimen N-1 as an example in Figure 10.

Table 2. Tensile strength values of untreated specimens (İşlem görmemiş numunelerinin çekme dayanımı değerleri).

Specimen No.	Thickness (mm)	Width (mm)	Area A_0 (mm ²)	Pulling Force F_{max} (N)	Tensile Strength (N/mm ²)	Average Tensile Strength (N/mm ²)
N-1	16	27.8	444.80	20098	45.18	46.57 ± 2.38
N-2	16	25.8	412.80	18665	45.22	
N-3	16	25.8	412.80	20361	49.32	

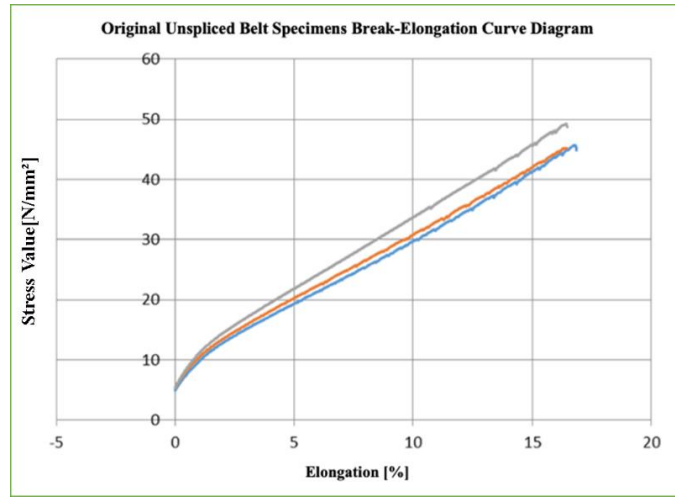


Figure 9. Break-elongation curve diagram of original unspliced belt specimens (Orijinal eklenmemiş kayış numunelerinin kopma-uzama eğrisi diyagramı).



Figure 10. Breaking of specimen N-1 after tensile test.

According to these results, the average breaking strength of the untreated belt specimen is 46.57 N/mm². Evaluations of the specimens that were combined with a water-cooled welding machine, applied with a vulcanization time of 15 minutes are shown in Table 3, Figure 11, Figure 12.

Table 3. Tensile strength values of specimens numbered S-15 (S-15 numaralı numunelerin çekme dayanımı değerleri).

Specimen No.	Thickness (mm)	Width (mm)	Area A_0 (mm ²)	Pulling Force F_{max} (N)	Tensile Strength (N/mm ²)	Average Tensile Strength (N/mm ²)	% Power Value in Terms
S15-1	16	25	400.00	8464	25.00		
S15-2	16	23,6	377.60	7613	20.16	22.48 ± 2.42	% 48.27
S15-3	16	25	400.00	8910	22.28		

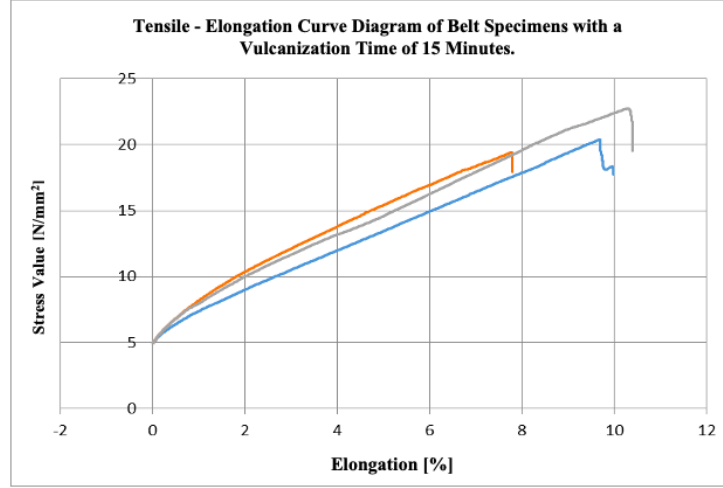


Figure 11. Tensile-elongation curve diagram of belt specimens with a vulcanization time of 15 minutes.



Figure 12. Breaking of specimen S-15-3 after tensile test (S-15-3 numunesinin çekme testinden sonra kırılması).

It was observed that the belt specimens, which were applied with a vulcanization time of 15 minutes, lost 51.72 % of their strength compared to the untreated belt.

Evaluations of the specimens with a vulcanization time of 30 minutes given in Table 4, Figure 13 and Figure 14.

Table 4. Tensile strength values of specimens numbered S-30 (S-30 numaralı numunelerin çekme dayanımı değerleri).

Specimen No.	Thickness (mm)	Width (mm)	Area A_0 (mm ²)	Pulling Force F_{max} (N)	Tensile Strength (N/mm ²)	Average Tensile Strength (N/mm ²)	% Power Value in Terms
S30-1	16	25	400.00	9349	23.37		
S30-2	16	26.2	419.20	9562	22.81	22.09 ± 1.75	% 47.74
S30-3	16	26	416.00	8362	20.10		

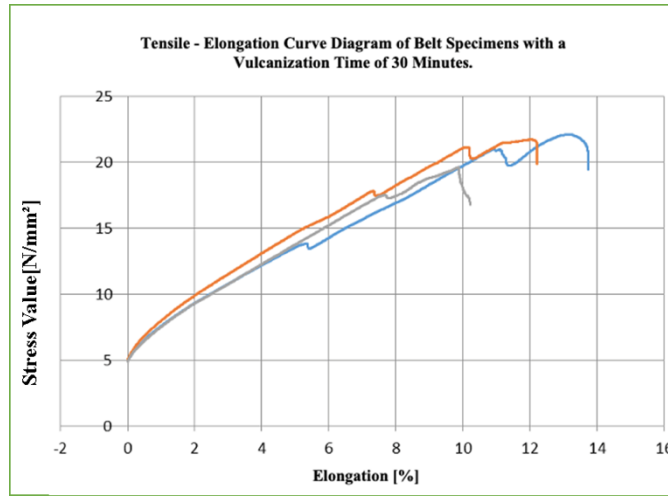


Figure 13. Tensile-elongation curve diagram of belt specimens with a vulcanization time of 30 minutes.



Figure 14. Breaking of specimen number S-30-3 after tensile test (S-30-3 numunesinin çekme testinden sonra kırılması).

It was observed that the belt specimens, which were applied 30 minutes of vulcanization time, lost 52.56 % of their strength compared to the untreated belt.

Evaluations of the specimens with a vulcanization time of 45 minutes are given in Table 5, Figure 15 and Figure 16.

Table 5. Tensile strength values of specimens numbered S-45.

Specimen No.	Thickness (mm)	Width (mm)	Area A_0 (mm ²)	Pulling Force F_{max} (N)	Tensile Strength (N/mm ²)	Average Tensile Strength (N/mm ²)	% Power Value in Terms
S45-1	16	25	400.00	10438	26.10		
S45-2	16	27	432.00	10552	24.43	24.95 ± 0.99	% 53.57
S45-3	16	20	320.00	7787	24.33		



Figure 15. Breaking of specimen number S-45-2 after tensile test (S-45-2 numaralı numunenin çekme testinden sonra kırılması).

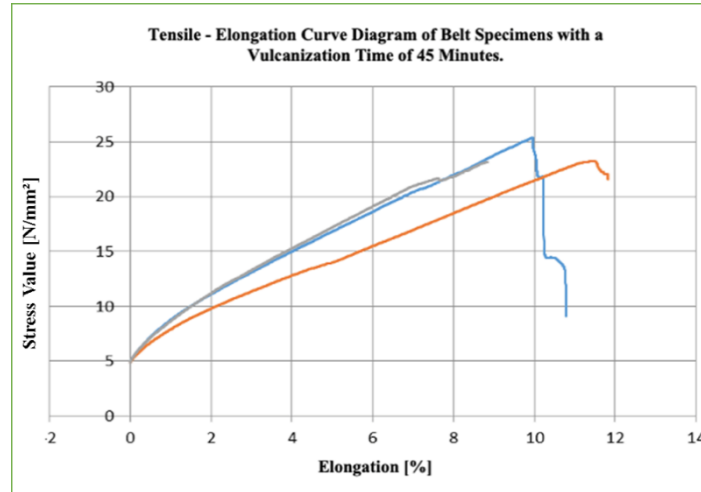


Figure 16. Tensile-elongation curve diagram of belt specimens with a vulcanization time of 45 minutes.

It was observed that the belt specimens, which were applied with a vulcanization time of 45 minutes, lost 46.42 % of their strength compared to the original unspliced belt.

In Figure 17 below, the rupture-elongation curves of 9 and 3 original unspliced belt specimens prepared with a water-cooled welding machine are shown.

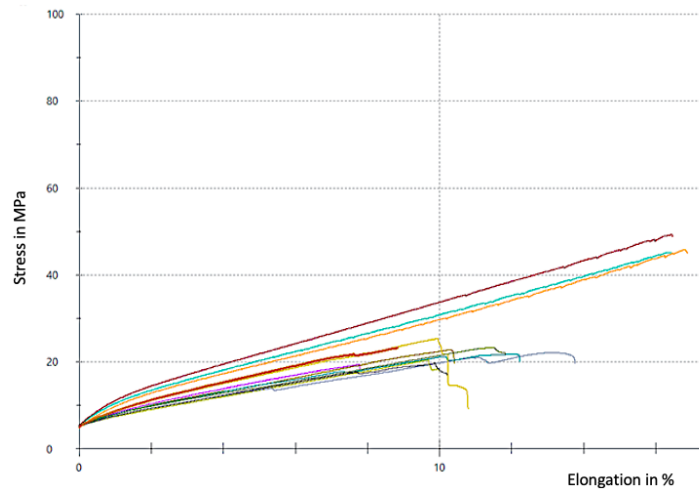


Figure 17. Break-elongation curve diagram of 12 specimens (12 numunenin kopma-uzama eğrisi diyagramı).

The strengths of belt specimens that underwent vulcanization process for 15, 30, and 45 minutes were compared with the untreated specimen. It was observed that there wasn't much difference in strength between the 15-minute and 30-minute specimens, whereas an improvement of approximately 11% in strength was seen when the process was extended to 45 minutes. It was concluded that an optimal increase in vulcanization time leads to an increase in strength [17, 18]. The tensile strengths of 12 specimens were compared in Figure 18.

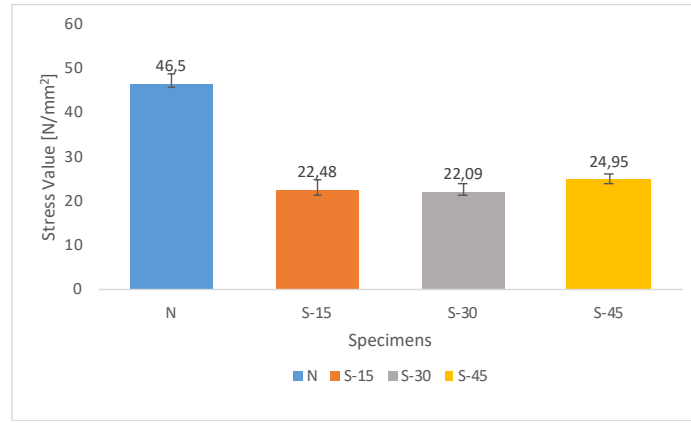


Figure 18. Comparison of tensile strength of specimens (Numunelerin çekme mukavemetinin karşılaştırılması)

4. CONCLUSIONS AND RECOMANDATIONS (SONUÇLAR VE ÖNERİLER)

In this study, EP800-1000-5-6/3-A type wear-resistant belt were used, and splicing was made with a water-cooled vulcanized welding machine at a constant temperature of 145 °C for 15, 30, 45 minutes.

In addition, 3 untreated belt specimens were also prepared. The tensile strengths of the prepared specimens were examined and as a result of the experiments;

- According to the tensile test results of the normal untreated belt, the breaking strength of the belt was calculated as $46.57 \text{ N/mm}^2 \pm 2.38 \text{ N/mm}^2$. This value is lower than 50 N/mm^2 , which is the minimum breaking strength according to the TS EN ISO 14890 standard. It is thought that the factors such as the fact that the used belt has been waiting in stocks for around 1-2 years and whether the company from which the belt is supplied has sent in accordance with the desired conditions is considered to be a factor.

- Using a water-cooled welding machine, when the curing temperature is constant at 145 °C, the average breaking strength of 3 specimens with a vulcanization time of 15 minutes was $22.48 \text{ N/mm}^2 \pm 2.42 \text{ N/mm}^2$, the strength value compared to the untreated belt is 48.27 %, the average breaking strength of 3 specimens with a vulcanization time of 30 minutes was $22.09 \text{ N/mm}^2 \pm 1.75 \text{ N/mm}^2$, the strength value compared to the untreated belt is 47.74 %, the average breaking strength of 3 specimens with a vulcanization time of 45 minutes was $24.95 \text{ N/mm}^2 \pm 0.99 \text{ N/mm}^2$, the strength value compared to the untreated belt was found to be 53.57 %. According to this comparison, it was observed that the belt strength increased as the vulcanization time increased. The strength value of the belt specimen, which had a vulcanization time of 45 minutes, exceeded 50 %.

- One of the most important issues in vulcanized belt welding is that there is no dust and moisture on the surface of the belt, that is, the belt is dry. In addition, factors such as unintentional knife blows or leaks on the surface of the belt and the poor quality of the material from which the belt is made play an important role in opening the splice of the belt.

ACKNOWLEDGMENTS (TEŞEKKÜR)

The authors gratefully thank KARDEMİR Karabük Iron Steel Industry Trade & Co. Inc. for their valuable support for this study.

REFERENCES (KAYNAKLAR)

1. T. Er, Bantlı konveyörlerde basınçlı hava risklerini önleme çalışması, Ohs Academy, 2(2): 53-57, 2019.
2. V. Govindan, E. Palaniswamy, M. Sambathkumar, R. Vijayakumar, T. Sakthimuruga, Conveyor belt troubles (bulk material handling), Int. J. Emerg. Eng. Res. Technol., 2: 21–30, 2014.
3. S. Zamarano, Surface ore movement, storage, and recovery systems, SME Mining Eng. Handbook, Darling P. (Ed.), Third Edition, USA, 2011.
4. C. Can, Bir bantlı konveyörün sonlu eleman yöntemiyle dinamik analizi, Yüksek Lisans Tezi, İstanbul Teknik Üniversitesi Fen Bilimleri Enstitüsü, İstanbul, Türkiye, 2012.

5. M. Bajda, R. Błażej, L. Jurdziak, Analysis of changes in the length of belt sections and the number of splices in the belt loops on conveyors in an underground mine, *Engineering Failure Analysis*, 101: 436-446, 2019.
6. M. Hardygóra, M. Bajda, R. Błażej, Laboratory testing of conveyor textile belt joints used in underground mines, *Mining Science*, 22: 161-169, 2015.
7. L. Xie, Z. Wenqi, Z. Hao, Y. Aibing, Q. Yujun, S. Yougong, Wear process during granular flow transportation in conveyor transfer, *Powder Technology*, 288: 65-75, 2016.
8. T. Kozłowski, J. Wodecki, R. Zimroz, R. Błażej, M. Hardygóra, A diagnostics of conveyor belt splices. *Applied Sciences*, 10: 6259, 2020.
9. D. Zaremba, P. Heitzmann, L. Overmeyer, L. Hillerns, T. Hassel, Automatable splicing method for steel cord conveyor belts – evaluation of water jetting as a preparation process, *Strojníški vestnik - Journal of Mechanical Engineering*, 63(10): 590-596, 2017.
10. L.P. Alviari, M.A. Chiron, I.P. Tama, Optimization of cold splicing parameters in conveyor belt joints on shear strength using taguchi method, *Journal of Engineering and Management in Industrial System*, 1: 1-10, 2022.
11. B. Soyubel, Elastomerlerin statik ve dinamik özelliklerinin incelenmesi, Yüksek Lisans Tezi, Uludağ Üniversitesi Fen Bilimleri Enstitüsü, Bursa, Türkiye, 2006.
12. D.A. Şahbaz, Soğuk vulkanize yapıştırıcı üretimi ve uygulama koşullarının değerlendirilmesi, Doktora Tezi, Bilecik Şeyh Edebali Üniversitesi Fen Bilimleri Enstitüsü, Bilecik, Türkiye, 2017.
13. Z. Zhaoxiang, G. Fei, K. Yuchao, X. Chong, J. Xiaohong, Effect of vulcanization on deformation behavior of rubber seals: Thermal–mechanical–chemical coupling model, numerical studies, and experimental validation, *Materials and Design*, 224: 111314, 2022.
14. S. Chen, Y. Runsheng, S. Ligang, Z. Rengang, C. Xingzhong, W. Baoyi, Z. Peng, Effect of low temperature vulcanization time on the structure and optical properties of ZnS thin films, *Applied Surface Science*, 498: 143876, 2019.
15. TS EN ISO 14890, Konveyör bantları - Genel amaçlar için - Kauçuk veya plâstik kaplanmış tekstil karkaslı konveyör bantlarının özellikleri, T.S.E., Ankara, 2013.
16. TS ISO 37, Lastikler ve Termoplastikler – Çekme gerilmesi-uzama özelliklerinin tayini, T.S.E., Ankara, 2017.
17. K.K. Sasidharan, R. Joseph, S. Palaty, K.S. Gopalakrishnan, G. Rajammal, P.V. Pillai, Effect of the vulcanization time and storage on the stability and physical properties of sulfur-prevulcanized natural rubber latex, *Journal of Applied Polymer Science*, 97: 1804-1811, 2005.
18. M. Wu, L. Yang, Q. Shen, Z. Zheng, C. Xu, Endeavour to balance mechanical properties and self-healing of nature rubber by increasing covalent crosslinks via a controlled vulcanization, *European Polymer Journal*, 161, 110823, 2021.

Investigation of The Effect of Reduced Shank Thickness of Friction Welded Yoke Shaft on Strength

Onur ŞEN¹ , Mert Can KAHYALAR¹ 

¹Tirsan Kardan A.Ş., Ar-Ge Merkezi, Manisa, Turkey

ARTICLE INFORMATION

Received: 29.03.2023

Accepted: 27.04.2023

Keywords:

Rotary friction welding

Yoke shaft

Wall thickness

FEA

ABSTRACT

Usage of friction welding method on the joints provides many advantages such as cost reduction, weight reduction and higher quality. The yoke shaft produced by rotary friction welding (RFW) involves a yoked part and a hollow round bar which are welded to each other. And so, no additional drilling method used in the way of removing material from the centre of the yoke shaft, is required to reduce the weight. The weight is inherently reduced thanks to hollow round bar used in RFW method. It is possible to use a friction welded yoke shaft in a wide range of wall thickness by removing material from the shank diameter for different applications. At this point, the key factor is strength of the friction welded yoke shaft with reduced wall thickness on the shank diameter. The aim of this study is investigation the effect of the reduced wall thickness of a yoke shaft produced by RFW on the strength. For this purpose, yoke shafts were manufactured by using RFW and consecutive processes such as turning and millings to reduce the wall thickness. The specimens in different wall thickness were tested to determine the strength. Additionally finite element analyses (FEAs) were implemented for each variation of the specimens and compared with the test results. As a result, it was determined that yoke shafts with reduced wall thicknesses, which were produced by RFW and then consecutively machining operations to obtain a specific wall thickness, can be used in drive shaft manufacturing securely.

Sürtünme Kaynaklı Çatallı Milin Boğaz Cidar Kalınlığındaki Azaltmanın Dayanım Üzerindeki Etkisinin İncelenmesi

MAKALE BİLGİSİ

Alınma: 29.03.2023

Kabul: 27.04.2023

Anahtar Kelimeler:

Dönel sürtünme kaynağı

Çatallı Mil

Cidar kalınlığı

FEA

ÖZET

Sürtünme kaynağı yönteminin birleştirmelerde kullanılması, maliyet düşürme, ağırlık azaltma ve daha yüksek kalite gibi birçok avantaj sağlar. Dönel sürtünme kaynağı (RFW) ile üretilen çatallı mil birbirine kaynaklanmış çatallı bir parça ve içi boş yuvarlak çubuk içerir. Ve bu nedenle, ağırlığı azaltmak için çatallı milin merkezinden malzeme azaltmak için kullanılan ek bir delme yöntemi gerekmez. RFW yönteminde kullanılan içi boş yuvarlak çubuk sayesinde ağırlık kendiliğinden azaltılmıştır. Farklı uygulamalar için boğaz çapından malzeme kaldırılarak çok çeşitli cidar kalınlıklarında sürtünme kaynaklı çatallı mil kullanmak mümkündür. Bu noktada kilit faktör, boğaz çapında azaltılmış cidar kalınlığına sahip sürtünme kaynaklı çatallı milin dayanımıdır. Bu çalışmanın amacı, RFW ile üretilen çatallı milin azaltılmış cidar kalınlığının parçanın dayanımı üzerindeki etkisinin araştırılmasıdır. Bu amaçla, RFW ve cidar kalınlığını azaltmak için tornalama ve frezeleme gibi ardışık işlemler kullanılarak çatallı miller üretilmiştir. Dayanımı belirlemek için farklı cidar kalınlıklarındaki numuneler test edilmiştir. Ek olarak, numunelerin her varyasyonu için sonlu eleman analizleri (FEA) uygulanmış ve test sonuçlarıyla karşılaştırılmıştır. Sonuç olarak RFW ve ardından belirli bir cidar kalınlığı elde etmek için ardışık talaşlı imalat işlemleri ile üretilen azaltılmış cidar kalınlığına sahip çatallı millerin kardan mili imalatında güvenle kullanılabileceği belirlenmiştir.

* Corresponding author, E-mail: senonurmail@gmail.com

1. INTRODUCTION (GİRİŞ)

Friction welding technique has become one of the major joining methods with its rising usage ratio in various industries such as automotive and aerospace where high-quality joints are needed. Difficulty of the joining of special materials used in automotive and aerospace requires using friction welding methods such as friction stir welding (FSW), linear friction welding (LFW) and rotary friction welding (RFW) [1]. Ferrous and non-ferrous alloys of various geometrical shapes can be joined with the same or different alloys by friction welding methods. Basically, friction welding method is a solid-state joining process in which heat is emerged during transformation of mechanical energy to thermal energy at the faying surface of the workpiece couple due to the rotation under exerted pressure. As a result of the said process, a metallic bonding is generated at lower temperatures compared to the melting point of the base material. Parameters effecting the friction and forging, and rotation speed are dominant on the product quality [2].

It is possible to handle FW in three ways depending on the relative movement of the workpieces: rotary, linear and orbital (Fig. 1). Rotary friction welding (RFW) is the most common type of friction welding in industry. In this method, one of the workpieces rotates about its axis while the other workpiece is stationary, and the workpieces are joined to each other under a friction pressure. RFW can be addressed in two different types in which rotation converted to friction heat is determinant: direct drive also known as continuous drive (CDFW) and inertia drive (IDFW) in which the energy is stored [3-5].

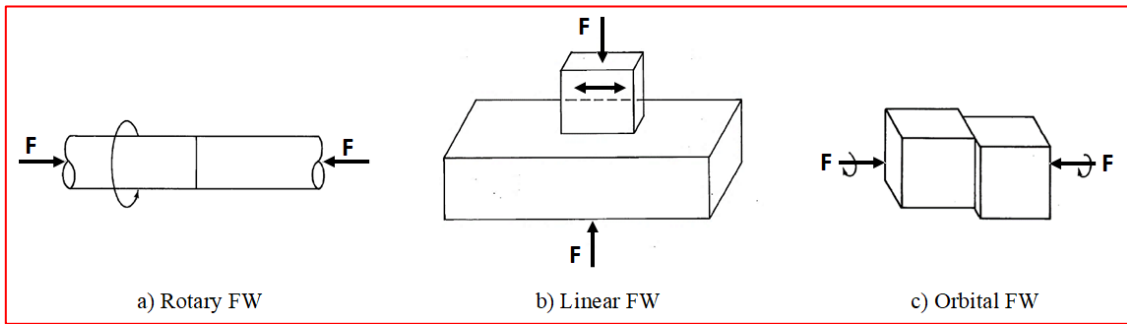


Figure 1. Relative movements of the workpieces in friction welding [6].

CDFW, which is the subject of the paper, is an extensively used friction welding method from the 1940's to the present. In this process whose steps and their relationships are illustrated in Fig. 2, one of the workpieces is stationary under an axial pressure while the other rotates at a constant speed [5-11]. Each workpiece contacts to each other and comes closer by axial pressure during a certain friction time. Right after, rotating workpiece is stopped within the braking time and the pressure on the stationary part is increased in a predetermined upset time. During the welding process, the narrow regions near the welding interface are rapidly heated by friction until they exhibit a steady state of high strain rate plastic flow. The welding process is then terminated with a forging stage to reinforce the joint [11,12]. Although CDFW has been experimentally proven to be a rapid and reliable method for joining the material pair which can be similar and dissimilar materials [13-17], a simple and accurate analytical thermo-mechanical model is still required to better understand heat generation and material flow during the process [11,18,19].

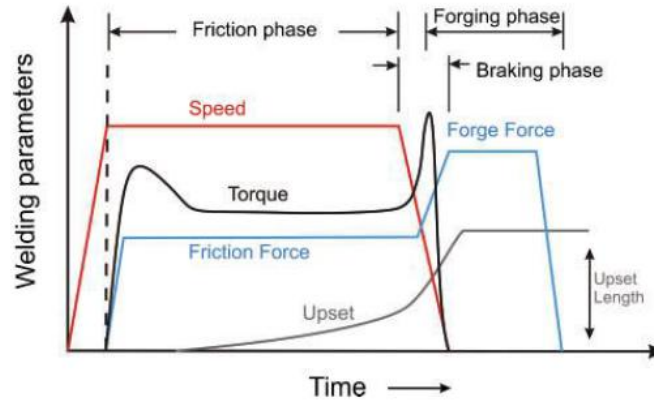


Figure 2. Critical welding parameters and their relationship for direct drive friction welding process [5].

When the literature is reviewed, it has been seen that the joining of the different materials together was the common subject handled in most of the studies. These studies addresses that the challenges encountered during the joining of dissimilar materials by friction welding, process parameters and mechanical properties of the final product as well. Some of the studies are about 6063 aluminum alloy and AISI 304 austenitic stainless-steel by Kimura et al. [20], YSZ–alumina composite and 6061 aluminium alloy by Uday et al. [21], AA1050 aluminum with AISI 304 stainless steel by Alves [22].

On the other hand, analytical models and literature review are the other main idea of the rest of the studies in literature. In one of these studies implemented by Xiong et al. [23], it was focused on an analytical model for continuous drive friction welding (CDFW). The results from analytical model and experiments were compared considering plastic region thickness, welding power, and average temperature. As a results, it was indicated that the analytical model could provide reliable descriptions during steady state CDFW. Maalekian [5] reviewed and investigated the literature.

Unlike these studies, this study handles the effect of the reduced shank thickness of friction welded yoke shaft on strength. In this context, different shank thicknesses were considered and examined with FEA software and tests under laboratory conditions.

2. MATERIAL AND METHOD (MATERYAL VE YÖNTEM)

The study basically includes two verification methods, finite element analyses (FEAs) and laboratory tests also known as bench test. Finite element analyses (FEAs) were applied on 3D data of yoke shaft specimens while the laboratory tests conducted with drive shaft specimens which are prepared for evaluation of the yoke shaft specimens.

The yoke shaft specimens were produced by respectively forging, implementing CDFW and machining processes applied as a finish operation. Following specimen production of yoke shafts, the specimens were examined for checking welding quality by using various inspection methods. Finally, drive shaft specimens were produced for laboratory tests conducted to check the performance of the yoke shaft with various wall thickness.

2.1. Specimen Preparation (Numune Hazırlama)

The production of the sub-components to be welded each other, which compose the welded yoke shaft, is the first step of the specimen production of yoke shaft. In this context, tube yokes with chemical composition defined in Table 1 were produced by the processes respectively close die hot forging, heat treatment and machining. Beside tube yokes, hollow round bars were prepared for FW by cutting and machining processes on the raw material with chemical composition defined in Table 1. The sub-components (tube yoke and hollow round bar) and welded yoke shaft were given in Figure 3.

Table 1. Chemical composition of sub-components in %mass: tube yoke and hollow round bar

	C	Si	Mn	P	S	Cr	Mo
Tube yoke	0.38-0.45	0.10-0.40	0.60-0.90	max 0.025	max 0.035	0.90-1.20	0.15-0.30
Hollow round bar	0.38-0.45	max 0.40	0.60-0.90	max 0.035	max 0.035	0.90-1.20	0.15-0.30



Figure 3. 3D data of tube yokes, hollow round bar and welded yoke shaft (Çatal, içi boş yuvarlak çubuk ve kaynaklı çatalı milin 3B verileri)

Sub-components were joined together by CDFW method as given in Figure 4. The picture of welded yoke shaft before and after finish operations, which are such as splining, turning, etc., was given by the Figure 5.



Figure 4. The yoke shaft during CDFW operation (CDFW işlemi sırasında çatalı mil)

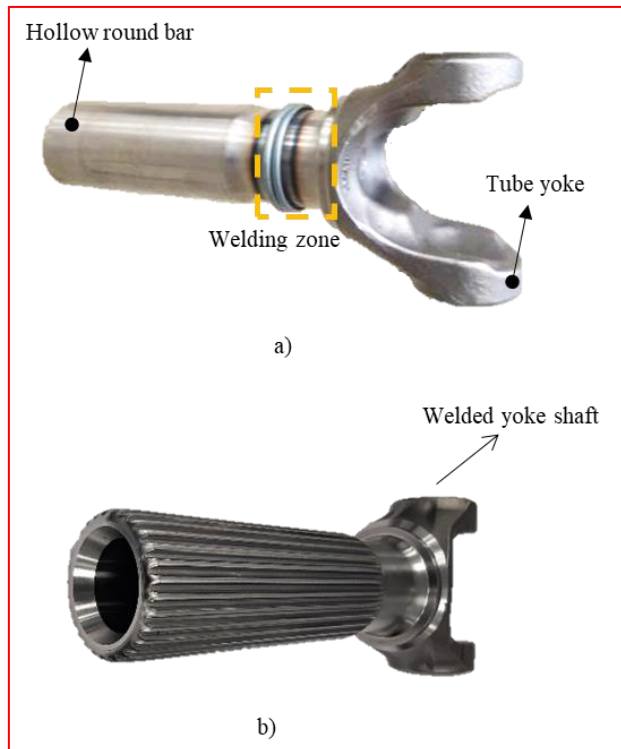


Figure 5. A welded yoke shaft specimen, a) before finish operations (splining, turning, etc.), b) after finish operations (splining, machining, etc.)

Mechanical and metallurgical properties of specimens were evaluated for checking the weld performance. And so, following testes and analyses were respectively performed on the weld cross-section for each of the specimens in different wall thickness.

- Hardness scan
- Bending test
- Macroscopic/microscopic inspection

Hardness scan

The main purpose of the hardness scan is to determine the distribution of hardness, and evaluation. A specimen was prepared by cutting in such a way that including the welded cross-section. And then, hardness scan was carried out along the cross-section of welded joint in Vickers scale at room temperature. The way of Vickers hardness scan and its result were shared in Figure 6. As a result of the hardness scans, it was observed that faying surface is harder through the weld zone as expected. Besides, the hardness values both on the faying surface and adjacent zone pointed out that the welding zone was suitable.

According to the weld zone hardness distribution seen in Figure 6b, the yield strength here corresponds to 940 MPa by converting the lowest hardness value to 300 HV to yield stress guided by ISO 18265 [24].

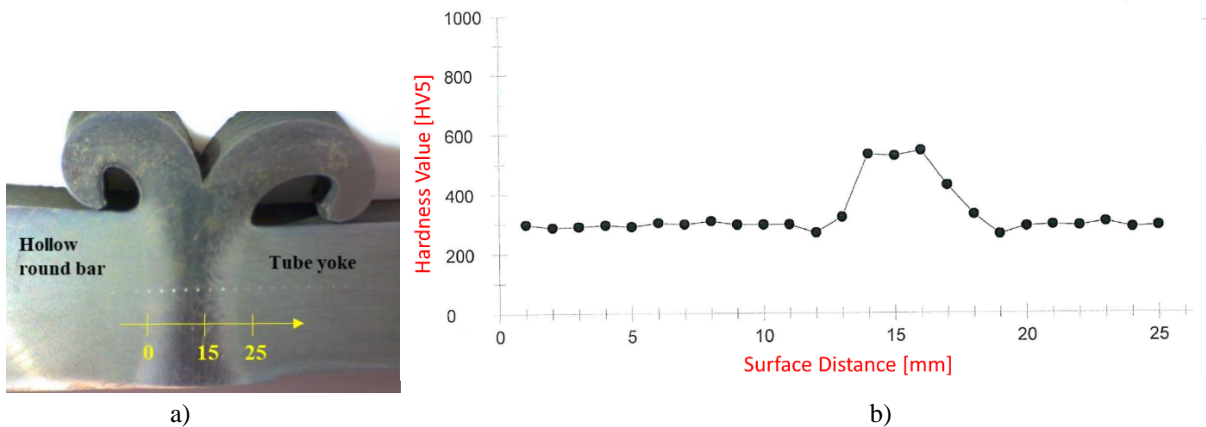


Figure 6. Hardness scan of the cross-section of welded joint, a) hardness scan direction, b) hardness profile

Bending Test

The bending test was performed to investigate the joint quality and performance. And so, the joint area was inspected against possible linear discontinuity along the welding line.

The specimens were prepared in such a way of that covering the weld zone as having a size of 5x120 mm (thickness x length) from the cross-section of the welded joint. The specimen was supported with a vice, leaving the weld zone free to bend. Afterwards a force was applied to the free end of the specimen until it bended with 90 degrees. As seen in Fig. 7 no tearing was observed along the weld section.



Figure 7. A bended specimen during the bending test to investigate the cross-section of welded joint in terms of the welding quality and performance.

Macroscopic/Microscopic Inspection

A specimen was cut from the welded yoke shaft for macro inspection. Respectively the specimen was polished and etched to reveal the weld and heat affected zone (HAZ). The specimen was taken under inspection to take macroscopic images. Macroscopic inspection of the longitudinal section of the welded joint showed us that there was no lack of fusion or cracking. Macrographs of the welded specimens were shown in Figure 8.



Figure 8. A specimen under macroscopic inspections, a) welded yoke shaft, b) specimen sectioned from welded yoke shaft (Makroskopik incelemeler altındaki bir numune, a) kaynaklı çatallı mil, b) kaynaklı çatallı milden kesit numune).

Specimen for microscopic inspection were prepared by respectively sectioning, mounting, fine grinding, polishing, and etching (nital usage of 2%). Specimen was inspected with two separate magnifications as 10x and 50x. Microscopic inspection on the weld line of specimen revealed that there was no micro crack or any defects on the weld zone for both 10x and 50x magnification as in Figure 9.



Figure 9. A specimen under microscopic inspections, a) 10x magnification on weld line, b) 50x magnification on weld line

After inspections, the welded yoke shafts were machined to reach the wall thickness defined in Table 2. And so, the final yoke shaft specimens were prepared in 3 groups; Group-1 doesn't involve any reduction of wall thickness while Group-2 and Group-3 involve. Driveshafts to be used in laboratory tests, an example of which is given in the Figure 10, were produced as 3 pieces for each group.

Table 2. The values of wall thickness of the specimens (Numunelerin et kalınlık değerleri)

Specimen ID	Wall Thickness A [mm]	
Group-1 (no reduction)	12	
Group-2 (2 mm reduction)	10	
Group-3 (3 mm reduction)	9	



Figure 10. A drive shaft specimen produced for laboratory tests

2.2. Finite Element Analyses

Finite element analyses were applied on the 3D models which are prepared by considering the wall thicknesses reduced by machining the shank of welded yoke shaft. The yoke shaft 3D models designed with CatiaV5 R62020 computer aided design program was transferred to the HyperWorks-2021.2 computer aided finite element analysis program. For meshing, which is the first step of finite element analysis, necessary geometric arrangements were performed on the 3D model. Afterwards, a mesh structure on which the boundary conditions and external loads would be defined was established by using 3D tetra elements proper to size of the yoke shaft. The mesh structure was created by using the element size that has been proven by tests within the scope of one of our previous studies [25].

In the next step, two opposing yoke holes are connected to each other by rigid elements, and moment of 17.000 Nm is defined at the midpoint of the rigid member as in Fig. 11.

Like the yoke holes, the spline tooth faces are connected by rigid members and, assigned fixing elements to the midpoints of these rigid elements in such a way that there is no freedom in rotational and translational movements as in Fig. 11.

FEA models with the various wall thickness, which is prepared under the same conditions, was compared with each other. In addition, evaluating the models were not conducted by only FEA results but also laboratory testing. Considering all these, FEA model was prepared as one part due to the difficulty and uncertainty of the realization of the weld zone as a model.

The pre-processing for FEA were completed by defining respectively elasticity module and poisson ratio as 210 GPa and 0.3. After these preparations analysis was carried out under structurally linear static condition.

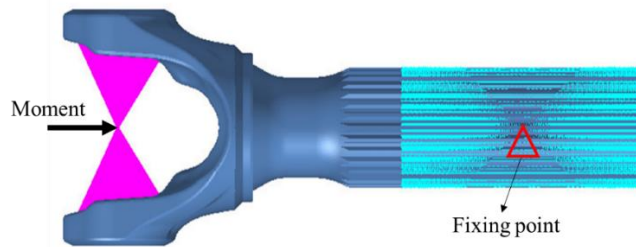


Figure 11. The FEA model after the pre-processing (Ön işlemeden sonraki FEA modeli)

2.3. Laboratory tests of the specimens

In the experimental studies, torsional tests were implemented on the drive shafts composed of welded yoke shafts produced by reducing the outer diameters of the welded components. Torsional tests were conducted for three groups of specimens, each containing two drive shafts, as defined in the Table 2. The test bench is specific for the drive shafts, and it is a custom production. The layout of the test bench was illustrated in the Figure 12. One end of the drive shaft was driven by the driven unit of the test machine while the other end of the drive shaft was fixed on the machine. The torque was applied in one direction defined in figure below.

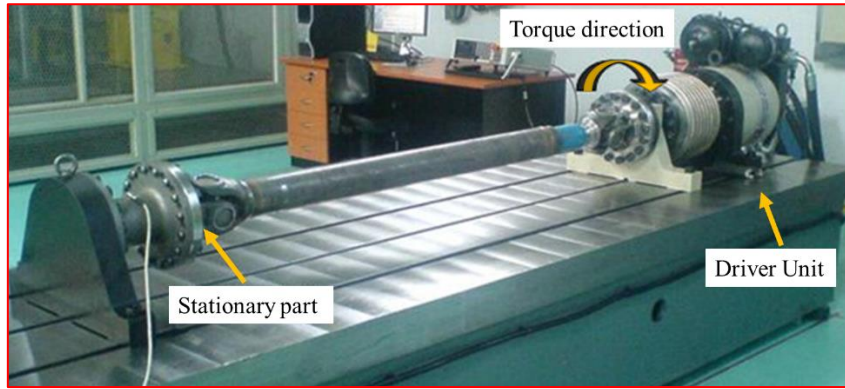


Figure 12. An illustration of the test bench (Test tezgahının bir örneği)

Each test was continued until any deformation was detected. Johnson's Apparent Elastic Limit (JAEL) values of the specimens were determined at the end of the tests.

3. EXPERIMENT AND OPTIMIZATION RESULTS (DENEY VE OPTİMİZASYON SONUÇLARI)

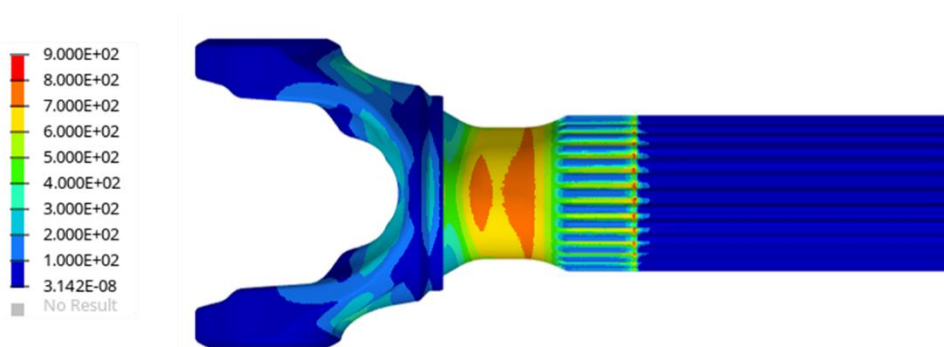
Johnson's Apparent Elastic Limit (JAEL) values of the specimens were determined at the end of the tests as given in Table 3. JEAL values of the specimens are compliant with the wall thickness, as expected. So, JEAL decreases as the wall thickness decreases.

Von Mises stress values on the shank, which are obtained from FEA, have been taken into consideration for comparison of three Group of specimens and they were listed in Figure 13. The stress values on the spline, which is in red, has been ignored because they occur due to lack of freedom.

The values of the hardness scan were considered to evaluate the stress obtained by FEA, which is corresponding to the weld zone.

Table 3. Torsional test results

Specimen ID	Wall Thickness [mm]	JAEL [kNm]	
Group-1	12	18.0	19.4
Group-2	10	17.5	17.1
Group-3	9	17.0	17.3



Specimen ID	Wall Thickness on Shank [mm]	Stress on Shank [MPa]
Group-1	12	606
Group-2	10	695
Group-3	9	763

Figure 13. FEA results for three group of specimens

4. CONCLUSIONS (SONUÇLAR)

In the study, tube yoke and hollow yoke bar were joined successfully by using CDFW method. Welded yoke shafts were subjected to consecutive machining processes to reduce the wall thickness. Finally, the effect of reduced shank thickness of friction welded yoke shaft on strength was investigated by FEA and laboratory tests. Important outputs of the study are as follows:

1. While the yield strength for tube yoke material is 820 MPa, it is 700 MPa for hollow round bar material. The yield strength of the weld zone obtained as 940 MPa by converting the lowest hardness value (300 HV) to yield stress guided by ISO 18265.
2. It is possible to use the product with reduced wall thickness which is obtained in a way of removing material from the outer surface of the shank as long as the machined product serves for the desired torque capacity.
3. Product with 9 mm wall thickness of shank, which is obtained after machining operation of product with 12 mm wall thickness of shank, produced by rotary friction welding method, can be used instead of product with 12 mm of wall thickness when considered the desired torque capacity of 17 kNm.
4. A comprehensive study is required to realize the friction weld zone in finite element analysis. Because uncertainties and difficulties prevail in friction welding modelling.

ACKNOWLEDGMENTS (TEŞEKKÜR)

This study was carried out with the facilities and support of Tirsan Kardan A.Ş. R&D Center.

REFERENCES (KAYNAKLAR)

1. S.W. Kallee, E.D. Nicholas, M.J. Russell, Friction welding of aero engine components, 10th World Conference on Titanium Ti-2003, 2003, Hamburg, Germany.
2. V. I. Vill, Friction Welding of Metals, American Welding Society, New York, 1962.
3. W. Kinley, Inertia welding: simple in principle and application, *Welding and Metal Fabrication*, 585–589, 1979.
4. N. Fomichev, The friction welding of new high-speed tool steels to structural steels, *Weld Prod*, 27(4): 31-34, 1980.
5. M. Maalekian, Friction welding critical assessment of literature, *Science and Technology of Welding and Joining*, 12(8): 738-759, 2007.
6. ANSI/AWS C6.1-89, Recommended Practices for Friction Welding, American National Standards Institute, 1989.
7. T. Lienert, W.A. Baeslack, J. Ringnalda, H.L. Fraser, Inertia-friction welding of SiC-reinforced 8009 aluminium, *J Mater Sci*, 31(8): 2149–2157, 1996.
8. V.V. Satyanarayana, G.M. Reddy, T.J. Mohandas, Dissimilar metal friction welding of austenitic–ferritic stainless steels, *Journal of Materials Processing Technology*, 160: 128–137, 2005.
9. A. Ambroziak, Friction welding of titanium–tungsten pseudoalloy joints, *Journal of Alloys and Compounds*, 506(2): 761–765, 2010.
10. H.C. Dey, M. Ashfaq, A.K. Bhaduri, K.R. Prasad, Joining of titanium to 304L stainless steel by friction welding, *Journal of Materials Processing Technology*, 209(18-19):5862–5870, 2009.
11. G.J. Bendzsak, T.H. North, Z. Li, Numerical model for steady-state flow in friction welding, *Acta Materialia*, 45(4): 1735–1745, 1997.
12. M. Kimura, M. Kusaka, K. Seo, A. Fuji, Improving Joint Properties of Friction Welded Joint of High Tensile Steel, *JSME Int J Ser A*, 48(4): 399–405, 2005.
13. Z.W. Huang, H.Y.Li, M. Preuss, M. Karadge, P. Bowen, S. Bray, G. Baxter, Inertia friction welding dissimilar nickel-based superalloys alloy 720Li to IN718, *Metallurgical and Materials Transactions A*, 38(7): 1608-1620, 2007.
14. W.B. Lee, M.G. Kim, J.M. Koo, K.K. Kim, D.J. Quesnel, Y.J. Kim, S.B. Jung, Friction welding of TiAl and AISI4140, *Journal of Materials Science*, 39(3):1125–1128, 2004.
15. P. Sathiya, S. Aravindan, A.N. Haq, Some experimental investigations on friction welded stainless steel joints, *Materials & Design*, 29(6): 1099-1109, 2008.
16. B. Uday, M. N. Ahmad Fauzi, H. Zuhailawat i, A. B. Ismail, Advances in friction welding process: A review, *Science and Technology of Welding and Joining*, 15(7): 534-558, 2010.

17. İ. Çelikyürek, O. Torun, B. Baksan, Microstructure and strength of friction-welded Fe-28Al and 316 L stainless steel, *Materials Science and Engineering: A*, 528(29): 8530-8536, 2011.
18. M. Maalekian, Thermal modelling of friction welding, *ISIJ International*, 10: 1429–1433, 2008.
19. O.T. Midling, Ø. Grong, A process model for friction welding of Al-Mg-Si alloys and Al-SiC metal matrix composites, *Acta Metallurgica et Materialia*, 42(5): 1595-1622, 1994.
20. M. Kimura, M. Kusaka, K. Kaizu, et al., Friction welding technique and joint properties of thin-walled pipe friction-welded joint between type 6063 aluminum alloy and AISI 304 austenitic stainless steel, *Int J Adv Manuf Technol* 82: 489–499, 2016.
21. M.B. Uday, M.N. Ahmad Fauzi, H. Zuhailawati, A.B. Ismail, Effect of welding speed on mechanical strength of friction welded joint of YSZ–alumina composite and 6061 aluminum alloy. *Materials Science and Engineering: A*, 528(13–14): 4753-4760, 2011.
22. E. P. Alves, F. P. Neto, C.Y. An., Welding of AA1050 aluminum with AISI 304 stainless steel by rotary friction welding process, *Journal of Aerospace Technology and Management*, 2(3): 301-306, 2010.
23. J.T. Xiong, J.L. Li, Y.N. Wei, F.S. Zhang, W.D. Huang, An analytical model of steady-state continuous drive friction welding, *Acta Materialia*, 61(5): 1662-1675, 2013.
24. ISO 18265:2013, Metallic materials-Conversion of hardness values, International Organization for Standardization, 2013.
25. O. Şen, M.C. Kahyalar, Structural analysis of yoke part in design of driveshaft, *International Journal Of Automotive Science and Technology*, 4(4): 248-252, 2020.